Summer 8-13-2010

Enhanced High-Resolution Imaging through Multiple-Frequency Coarray Augmentation

Jeannie L. Moulton
University of Pennsylvania, ljeannie@seas.upenn.edu

Enhanced High-Resolution Imaging through Multiple-Frequency Coarray Augmentation

Abstract
In imaging, much attention is paid to increasing the resolution capabilities of a system. Increasing resolution allows for high-accuracy source location and the ability to discriminate between two closely-spaced objects. In conventional narrowband techniques, resolution is fundamentally limited by the size of the aperture. For apertures consisting of individual elements, direction-of-arrival techniques allow for high-resolution images of point sources. The main limiting factor on conventional high-resolution imaging is the number of elements in the aperture. For both passive and active imaging, to resolve K point sources/targets, there must be at least K+1 elements receiving radiation. In active imaging, when these targets reflect coherently - the more difficult case in imaging - an additional constraint is that at least K of the elements must also be transmitting radiation to illuminate the targets. For small arrays consisting of only a few elements, this constraint can be problematic.

In this dissertation, we focus on improving resolution by using multiple frequencies in both passive and active imaging, especially for small arrays. Using multiple frequencies increases the size of the coarray, which is the true limiting factor for resolution of an imaging system when virtual arrays are considered. For passive imaging, we show that the number of sources that can be resolved is limited only by the bandwidth available for certain types of sources. In active imaging, we develop a frequency-averaging method that permits resolution of K coherent point targets with fewer than K transmitting and receiving elements. These methods are investigated primarily for linear arrays, but planar arrays are also briefly examined.

Another resolution improvement method researched in this work is a retransmission scheme for active imaging using classical beamforming techniques. In this method, the coarray is extended not by using multiple frequencies, but by retransmitting the received data back into the scene as a second transmission and processing the returns. It is known that when this method is used to image multiple targets, the resulting image is contaminated by crossterms. We investigate methods to reduce the crossterms.

Degree Type
Dissertation

Degree Name
Doctor of Philosophy (PhD)

Graduate Group
Electrical & Systems Engineering

First Advisor
Saleem A. Kassam

Keywords
High-resolution imaging, Direction-of-arrival estimation, Wideband imaging, Coarray, Virtual arrays, Multiple Signal Classification

ENHANCED HIGH-RESOLUTION IMAGING THROUGH MULTIPLE-FREQUENCY COARRAY AUGMENTATION

Jeannie L. Moulton

A DISSERTATION

in

ELECTRICAL AND SYSTEMS ENGINEERING

Presented to the Faculties of the University of Pennsylvania in Partial Fullfillment of the Requirements for the Degree of Doctor of Philosophy

2010

Supervisor of Dissertation

_____

Saleem A. Kassam, Professor of Electrical Engineering

Graduate Group Chair

_____

Roch Guerin, Professor of Telecommunications Networks

Dissertation Committee

Ali Jadbabaie, Professor of Electrical Engineering

Alejandro Ribeiro, Professor of Electrical Engineering

Fauzia Ahmad, Research Associate Professor at Villanova University

ENHANCED HIGH-RESOLUTION IMAGING THROUGH MULTIPLE-FREQUENCY COARRAY AUGMENTATION

Jeannie L. Moulton

2010

Dedicated to my family, whose hard work made it easier for me to get here.

ACKNOWLEDGMENT

This dissertation would absolutely not be possible without the unwavering support of my advisor, Dr. Saleem Kassam. I am truly thankful for his wisdom, patience and dedication throughout my graduate career. I enjoyed having an advisor who was also a friend. Thank you.

Many sincere thanks are due to my committee members from Penn, Dr. Ali Jadbabaie, Dr. Alejandro Riberio and Dr. Santosh Venkatesh, for taking the time to evaluate my work. I am grateful to the group at the Center for Advanced Communication at Villanova University for helping me get my first paper published and specifically to Dr. Fauzia Ahmad, for serving on my committee and also being a good role model.

Thank you to my office mate, Yang, for being a friend, supporting my work and keeping me company. I am grateful to my Penn State friends in the Philadelphia area and my friends I made while living in Delaware, who have all made my time in graduate school more enjoyable. I am especially grateful to Pam and Doug, who let me live with them while in limbo between Philadelphia and Tucson.

I am incredibly indebted to my parents and step-parents, who have helped me emotionally and financially throughout all of my schooling. They have always made every effort to make my life easier in anyway they could.

Words cannot truly express how thankful I am for my husband, Derek, who has put up with me for the last five years. Thank you for picking me up when I was down and helping me make it through.

ABSTRACT

ENHANCED HIGH-RESOLUTION IMAGING THROUGH
MULTIPLE-FREQUENCY COARRAY AUGMENTATION

Jeannie L. Moulton

Advisor: Saleem A. Kassam

In imaging, much attention is paid to increasing the resolution capabilities of a system. Increasing resolution allows for high-accuracy source location and the ability to discriminate between two closely-spaced objects. In conventional narrowband techniques, resolution is fundamentally limited by the size of the aperture. For apertures consisting of individual elements, direction-of-arrival techniques allow for high-resolution images of point sources. The main limiting factor on conventional high-resolution imaging is the number of elements in the aperture. For both passive and active imaging, to resolve K point sources/targets, there must be at least $K+1$ elements receiving radiation. In active imaging, when these targets reflect coherently - the more difficult case in imaging - an additional constraint is that at least K of the elements must also be transmitting radiation to illuminate the targets. For small arrays consisting of only a few elements, this constraint can be problematic.

In this dissertation, we focus on improving resolution by using multiple frequencies in both passive and active imaging, especially for small arrays. Using multiple frequencies increases the size of the *coarray*, which is the true limiting factor for resolution of an imaging system when *virtual arrays* are considered. For passive imaging, we show that the number of sources that can be resolved is limited only by the bandwidth available for certain types of sources. In active imaging, we develop a frequency-averaging method that permits resolution of K *coherent* point targets with

fewer than K transmitting and receiving elements. These methods are investigated primarily for linear arrays, but planar arrays are also briefly examined.

Another resolution improvement method researched in this work is a retransmission scheme for active imaging using classical beamforming techniques. In this method, the coarray is extended not by using multiple frequencies, but by retransmitting the received data back into the scene as a second transmission and processing the returns. It is known that when this method is used to image multiple targets, the resulting image is contaminated by crossterms. We investigate methods to reduce the crossterms.

Contents

List of Tables

List of Figures

Chapter 1

Introduction

The primary focus of this dissertation is on high-resolution imaging using multiple frequencies, particularly with small arrays. Small arrays are loosely defined as arrays consisting of an order less than tens of individual elements [1]. We take a natural progression from passive line arrays to active line arrays and then extend to planar arrays for high-resolution imaging. We also examine a retransmission beamforming active imaging technique as another high-resolution technique.

High resolution passive imaging with line arrays has been studied intensively since some early work in [2, 3, 4, 5]. It is intended to image scenes with sources that are emitting their own radiation or objects that are already being illuminated by a separate source. Examples include astronomy, where the stars emit their own radiation [6], passive SONAR [7], which uses the noise and vibrations from propellors or engines, and seismic imaging [8]. An advantage of passive imaging is that no radiation is being transmitted by the observer, so a scene can be observed without giving away that it is being imaged. For this reason, it is attractive in military-type applications. A disadvantage of passive imaging is that coherent sources - sources that emit radiation completely correlated with each other - cannot be resolved without

additional processing. Coherent sources may arise as natural phenomena between two coupled sources or as man-made interference such as signal jamming. Special techniques, such as spatial smoothing [9] or pattern diversity [10], must be used to process the data for coherent target imaging. Spatial smoothing and pattern diversity can possibly lead to a reduction in the effective number of receiving elements. For small arrays, this reduction may not be acceptable because it reduces the already small number of sources that can be resolved.

To image a scene containing objects that do not emit their own radiation or do not have a reliable outside illumination source, active imaging is used. Instead of just observing radiation, radiation is transmitted into the scene, reflected, and then the returns are received by the array. Examples of this include active SONAR [11], and RADAR [12]. This type of imaging has distinct advantages over passive imaging. First, we can choose the radiation that is transmitting into the scene. Second, we can transmit from multiple antennas to direct the radiation by constructive interference. Also, by transmitting from each antenna individually, we can store the returns in such a way that we know which transmitting element leads to which return. This storage capability is the idea given in [13], which allows for high-resolution location of coherent targets without techniques such as spatial smoothing.

There are two main ideas we will use in the development of this work: the coarray formalism and the virtual array. The coarray is a concept for both passive and active arrays. For passive narrowband arrays, the coarray is the *difference coarray* and it is defined as the set of all pairwise differences between receive array element positions:

$$\{y_l^D\} = \{y_l^D | y_l^D = x_{Rm} - x_{Rn}, m = 1, 2, ..., M, n = 1, 2, ..., M\}, \tag{1.1}$$

where x_{Rm} is the position of the m^{th} receive array element. For active imaging, the

coarray is the *sum coarray*, which is defined as:

$$\{y_l^S\} = \{y_l^S | y_l^S = x_{Rm} + x_{Tn}, m = 1, 2, ..., M, n = 1, 2, ..., N\}, \tag{1.2}$$

where x_{Tn} is the position of the n^{th} transmit array element.

This difference in the coarray between active and passive imaging arises because the operations used to form images are different in passive versus active imaging. However, the central result is the same for both: the coarray determines imaging capabilities of the system. For beamforming, the coarray determines the resolution and sidelobes characteristics. This is well-studied and summarized in [14]. For high-resolution techniques, the coarray determines the total number of sources that can be resolved. This has been studied in [15, 13, 16], but not always from the point of view of the coarray formalism.

A key extension of the coarray formalism obtained when multiple frequencies are available for imaging. When multiple frequencies are used, the wideband coarray contains more points than the narrowband (single frequency) coarray alone [17]. This yields possibly better resolution and sidelobe characteristics in beamforming. For high-resolution imaging, the effects of using multiple frequencies have been studied in [18, 19, 20]. Multiple frequencies here were used mainly for increased robustness and improved statistical properties of source location estimates. However, what appears to have remained unstudied is whether the additional coarray points created by using multiple frequencies can allow for the location of additional sources beyond the conventional narrowband limit. This is the crux of this dissertation.

The second central idea utilized in this dissertation is the virtual array. A *virtual array* is an array whose effect is synthesized by the physical array. Related work has been done with virtual arrays and coarray augmentation in [15, 21]. The conclusion

in these works was that, for passive line arrays, if the coarray is filled and uniformly-spaced, the number of coarray points determines the number of sources that can be resolved using high-resolution techniques. By using the idea of virtual arrays, additional sources can be resolved above the conventional limit. The work done in [13] extends these ideas to active imaging and planar arrays. In [22], the work in [21] is extended to non-filled uniformly spaced coarrays using a convex optimization technique.

By using multiple frequencies, in this work we extend the coarray and make use of virtual arrays to enable location of additional point sources in both active and passive imaging. The result is that for passive imaging of sources with spectra meeting certain requirements, the number of sources that can be resolved is only limited by the bandwidth available. For active imaging, we combine what was done in [13], which cannot successfully resolve coherent targets when the largest virtual array is used, with existing coherent subspace techniques [19] to yield an elegant alternative to coherent target location without reduction in the number of targets that can be successfully resolved.

From there, we extend the idea to planar arrays. This is desirable since with line arrays only elevation angle can be determined, so a one-dimensional image is obtained. If planar arrays are used, both elevation and azimuthal angle can be resolved and the resulting image is two-dimensional. Such two-dimensional high-resolution techniques have been studied in [23]. The problem with imaging with planar arrays is that it is very computationally complex. The trend in the literature is to use search-free techniques such as root-MUSIC [24]. However, root-MUSIC, for example, relies on the fact that the array is a uniformly-spaced line array, which obviously is not true for planar arrays, so techniques such as array interpolation [19] and manifold separation [25] are often used. In this dissertation, we do not consider search-free techniques.

We assume that the time can be taken to process the signals for 2-D high-resolution imaging, and we examine extending the techniques we develop for line arrays to planar arrays. However, we will see that the idea of array interpolation plays a central part in our work for both linear and planar arrays.

The final ideas in this dissertation switch focus from model-based high-resolution techniques to a beamforming retransmission technique. This technique was originally proposed in [26], but not studied in depth. The motivating idea behind it is to use retransmission to increase the length of the coarray, since it is known that the length of the coarray determines the resolution capabilities of the imaging system. Other retransmission techniques exist, such as time reversal imaging [27], but do not increase the diameter of the coarray in the way that we propose. It will be shown that while this idea does indeed extend the coarray for the point spread function, for multiple targets the gain in resolution is thwarted by "crossterms" - artifactual peaks in the image - which arise because retransmission is a non-linear operation.

This dissertation does not directly deal with how to choose the best array element locations or the best frequencies to use. However, these problems would make for interesting future research in terms of minimum redundancy arrays [28, 29] when multiple frequencies are being used.

1.1 Organization of the Dissertation

This dissertation is organized into four chapters. Chapters 2 and 3 are the main contributions and are self-contained. Chapter 4 is an extension of Chapters 2 and 3 to planar arrays. To avoid unnecessary redundancy, it is assumed the reader has read the previous chapters. Chapter 5 is a separate, though related, idea from the previous chapters and is also self-contained.

Chapter 2 focuses on high-resolution passive imaging using multiple frequencies and is restricted to line arrays. It is reviewed how the narrowband difference coarray relates to high-resolution imaging. The main contribution is the extension of the coarray relationship from narrowband to wideband (multi-frequency operation) for high-resolution imaging. It is shown that by using multiple frequencies, under certain conditions on the sources' spectra, we can synthesize the effect of a larger coarray and thus resolve additional point sources beyond conventional limits. Methods are also examined for use when the conditions on the sources' spectra are not satisfied.

In Chapter 3, we consider using multiple frequencies to increase the number of coherent targets that can be resolved using high-resolution techniques in active imaging with line arrays. It is not a direct extension of Chapter 2 to active imaging. This technique uses multiple frequencies to, in effect, average out the phase coherence between targets. It is similar in spirit to spatial smoothing or pattern diversity, except there is no reduction in the effective size of the array. The restriction here is that only a small sector of the scene can be imaged successfully, though techniques to overcome this are suggested.

We extend the ideas of Chapters 2 and 3 to planar arrays in Chapter 4. For passive imaging, the extension does not directly follow the work for line arrays. We will see that it is much more difficult. In the active imaging technique, the extension follows nicely from line arrays.

Chapter 5 further investigates a previously proposed technique involving retransmission for active imaging [26], which was not studied in depth. Instead of a single transmit and receive step, the received signals are retransmitted into the scene and the returns are processed by beamforming to form an image. This is not a high-resolution technique like direction-of-arrival estimation is, but the idea is to increase resolution on an existing array by augmenting the coarray through retransmission. It is shown

that because this is not a linear technique, when linear beamforming processing is used, an artifactual crossterm appears as a false peak in the image. This thwarts any higher-resolution gained. This idea is also connected to a popular retransmission scheme called time-reversal imaging, by the coarray concept.

The dissertation is concluded and directions for future research are suggested in Chapter 6.

1.2 Contributions and Publications

The main contributions of this dissertation are on resolution improvement with small arrays - that is arrays consisting of only a few elements. Small arrays are limited in resolution when using high-resolution techniques, because the number of sources/targets that can be resolved is limited by the number of elements in the array. We show that by using multiple frequencies in ways that have not been done before, the number of sources/targets that can be resolved in passive and active imaging with line arrays can be increased above conventional limits. This idea is also extended to planar arrays. An alternative method to increase resolution with small arrays using classical beamforming is explored using a retransmission scheme.

For high-resolution techniques applied to passive imaging with line arrays, we show that by using multiple frequencies, additional targets can be resolved under certain conditions on the sources' spectra. By using multiple frequencies, the coarray is augmented [17], which synthesizes the effect of a larger, virtual array, effectively increasing the total number of sources that can be resolved. In [15, 21], similar techniques using virtual arrays for passive imaging have been studied, though not through use of multiple frequencies. These techniques rely on a uniformly spaced coarray. Our work does not rely on a uniformly spaced coarray, as missing coarray

points can be filled in by using multiple frequencies. Though the case of a non-uniformly spaced coarray was studied in [30, 22], the coarray was completed by using a convex optimization technique, yielding an approximation to the desired virtual correlation matrix. In our work, under certain conditions on the sources' spectra, this step is not necessary.

While the techniques for passive imaging do not appear to be directly extendable to active imaging, some significant improvements on the number of coherent targets that can be resolved can be made for active imaging. Here, we do not augment the coarray by using multiple frequencies, but we use the idea of a virtual array to resolve additional targets. The starting point for this work is in [13], where it was shown that additional incoherent targets can be resolved above conventional limits by using virtual arrays. However, no approach was considered there to resolve additional coherent targets. Our method allows for resolution of additional coherent targets. It has a similar effect as spatial smoothing [9, 31] and pattern diversity [10]. However, the problem with spatial smoothing, and possibly pattern diversity, with small arrays is that the number of effective array elements is reduced, and thus the number of targets that can be resolved is also reduced. An advantage of our method is that it has no such reduction; it actually increases the number of coherent targets that can be resolved.

We also explore extending these methods to planar arrays. This is desirable since with planar arrays, both azimuthal and elevation angle can be resolved. Use of high resolution techniques with planar arrays has been studied intensively in recent work [32, 25, 33], and it is clearly useful if our methods can be extended in this direction.

As a different approach to the small array problem, a retransmission scheme that was originally suggested in [26] is studied in further detail. In [26], it was suggested that retransmission may be a viable way to increase the resolution in beamforming.

The retransmission step, for a single target, creates a wider coarray and thus increases the resolution in terms of main beamwidth. However, when there are multiple targets present, it is known that false peaks appear in the image. In our work, we attempt several methods to mitigate these false peaks.

This and related work has led to several conference and journal papers [34, 35, 36, 37, 38, 39]:

- J.L. Moulton, S.A. Kassam, "Resolving more sources with multi-frequency coarrays in high-resolution direction-of-arrival estimation," *43rd Annual Conference on Information Sciences and Systems, 2009,* March 18-20, 2009, pp. 772 – 777.

- J.L. Moulton, S.A. Kassam, "High-resolution spectrum estimation for non-coherent source location using the multi-frequency virtual correlation matrix," *IEEE Pacific Rim Conference on Communications, Computers and Signal Processing, 2009,* Aug. 23-26, 2009, pp. 843 – 848.

- J.L. Moulton, S.A. Kassam, "High-resolution coherent reflector location with multi-frequency active virtual arrays," *44th Annual Conference on Information Sciences and Systems, 2010,* Marc. 17-19, 2010, pp. 1 – 5.

- J. Moulton, S. Kassam, F. Ahmad, M. Amin, K. Yemelyanov, "Target and change detection in synthetic aperture radar sensing of urban structures," *IEEE Radar Conference, 2008,* Aug. 26-30, 2008 pp. 1 – 6.

- J.L. Moulton, S.A. Kassam, "Multi-frequency MUSIC for passive imaging with line arrays," *in preparation.*

- J.L. Moulton, S.A. Kassam, "Frequency smoothing with virtual arrays for active imaging," *in preparation.*

Chapter 2

Passive Multi-frequency High-Resolution Techniques

2.1 Introduction

In high-resolution imaging, the objective is to be able to resolve sources which are much closer together than can be resolved with linear beamforming (Fourier) methods. Many high-resolution techniques exist, but are generally limited by the number of sensors observing the scene. To resolve a number of distinct point sources, the number of sensors must be greater than the number of point sources. In situations where the number of point sources is greater than or equal to the number of receiving elements, the otherwise powerful high-resolution techniques are rendered useless.

Work has been done for narrowband passive arrays, [21, 15], showing that the number of point sources that can be resolved is not necessarily directly dependent on the size of the array, but on the size and configuration of what is called the *coarray* - or the set of correlation lags between the array elements. The application of this idea in these previous studies is contingent on producing a full, uniformly spaced coarray.

Under this condition, more point sources can be resolved.

In this chapter, we propose a method to resolve additional sources without the need for a full, uniformly spaced coarray at a *single* frequency. We will show that multiple frequencies can be used to expand the size of the coarray, fill in missing coarray points, and produce the *effect* of a larger, uniformly spaced array at a single frequency under certain assumptions. The proposed method will be most useful in situations where there are many point sources, but not many available physical array elements. Such situations may arise, for example, when the available real estate for antennas is limited or very expensive, or where the antennas themselves are very expensive or large. The method could be useful in a situation where an array is already deployed, but needs additional imaging capabilities without changing the array configuration. It will be shown that under the conditions necessary, for any array, the number of sources which can be resolved is limited only by the bandwidth available - the band need not necessarily be a continuous band, it can, in fact, be quite sparse, perhaps making this approach attractive for multi-band applications.

Section 2.2 will provide a brief overview of passive imaging of incoherent sources including the data model, narrow- and wideband coarrays, the spatial correlation matrix, and some well-known high-resolution imaging techniques. Section 2.3 will introduce the "virtual correlation matrix" - a matrix constructed from narrowband correlation matrices at different frequencies that synthesizes the effect of a larger array. Section 2.4 will simulate a simple but relevant example that explores the properties of the virtual correlation matrix and the conditions under which it is valid. The effect of noise on the virtual correlation matrix is discussed in Section 2.6. Additional examples are included in Section 2.7 and the chapter is concluded in Section 2.8.

2.2 Incoherent Imaging

Incoherent imaging, or passive imaging, is an imaging scenario in which an array of sensor elements measures incident radiation from a distribution of incoherent sources. The object of the passive imaging system is to provide an estimate of the angular distribution of source power from sources that are emitting their own radiation. This is in contrast to active imaging in which sources are reflecting transmitted radiation.

The arrays considered in this chapter will consist of sensing elements in a line, called line arrays, receiving radiation from the sources. The positions of these elements are denoted by $\{x_{Rm}|m = 1, 2, ..., M\}$ with respect to an arbitrary origin, which is often taken to be the midpoint of the array. The origin may or may not be an element position. The array diameter, D_A, is defined as the distance between the two array elements furthest away from each other.

The sources are assumed to emit independently of each other in a narrow frequency band, and they are assumed to be far enough away from the array and small enough that they can be viewed as far-field point sources, thus producing plane waves at the receive array. For now, we will consider that the array is receiving radiation at a frequency ω_0 with corresponding wavelength λ_0. A widely accepted condition for far-field imaging is that the sources must be at a distance of at least $\frac{D_A^2}{\lambda_0}$ from the array [40]. When sources are emitting narrowband radiation or the received radiation is filtered by a narrowband filter, the received phase is the quantity of interest. The assumption of source independence in a narrow band of frequencies means that the sources are phase incoherent with each other - the phases with which the plane waves from each source arrives at the array do not depend on each other. The variation in phase may arise when the sources are not fixed in space with respect to each other. Mathematically, the random complex amplitudes of each source, $S_k(\omega_0), k =$

$1, 2, ..., K$ have the following relationship between them at a frequency ω_0:

$$\mathbb{E}[S_k(\omega_0)S_n^*(\omega_0)] = \begin{cases} P_k(\omega_0) & \text{for } k = n \\ 0 & \text{for } k \neq n \end{cases} \tag{2.1}$$

Here $P_k(\omega_0)$ is the power of the k^{th} source at frequency ω_0.

The line array can be thought of as being contained in the intersection of two particular planes - the ground plane and the vertical plane which is orthogonal to the ground plane. The sources are assumed to lie in the vertical plane. For a source located in this plane, since we are considering far-field imaging, the position of the source is given by the angle that the line between the source and the origin makes with the array. This is illustrated in Figure 2.1. The direction in the vertical plane normal to the array is referred to as broadside of the array and this will be the reference direction from which the source directions are measured. The K sources are located in the directions $\{\theta_k\}, k = 1, 2, ..., K$ measured from broadside, and we denote $u_k = \sin\theta_k$.

The array is generally capable of receiving wideband radiation, but we say that the *reference frequency* is ω_0 when the spacing of the array elements is specified on the basis of λ_0, the wavelength corresponding to ω_0. For example, in linear beamforming, the Nyquist sampling spacing is elements spaced at $\frac{\lambda_0}{2}$ [40]. For a 5 element array, the elements could be at locations $\{-\lambda_0, -\frac{\lambda_0}{2}, 0, \frac{\lambda_0}{2}, \lambda_0\} = \{-2, -1, 0, 1, 2\}\frac{\lambda_0}{2}$. This type of array which contains all integer multiples of $\frac{\lambda_0}{2}$ between two integers is called a uniformly spaced array and will play a central part in this chapter.

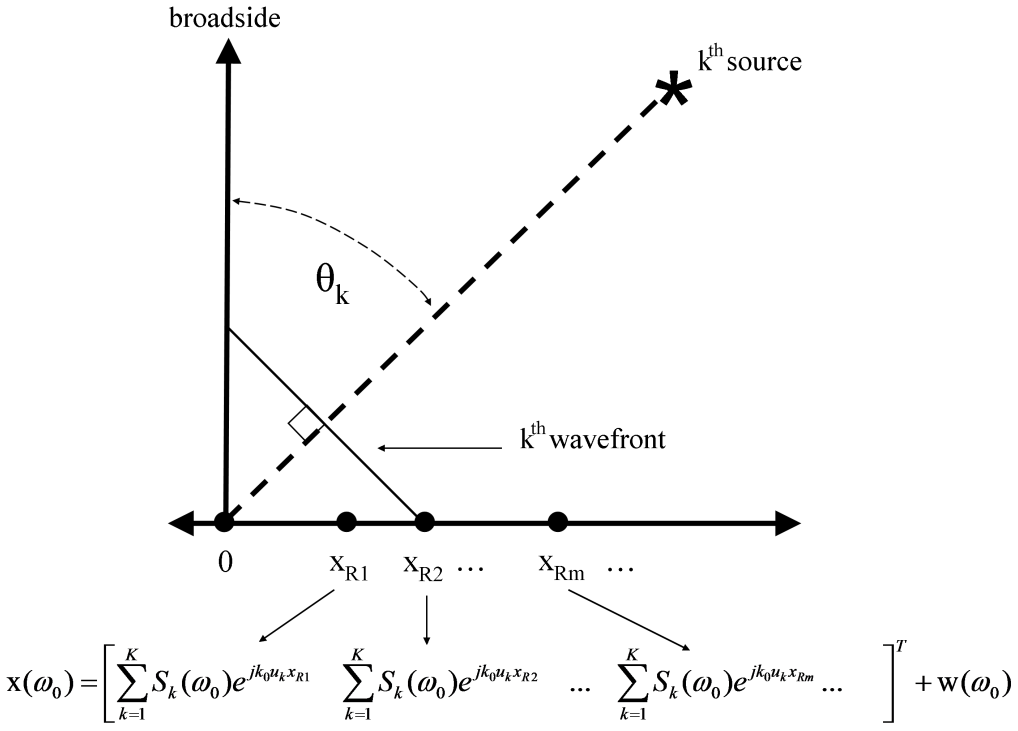

Figure 2.1: Array Geometry

2.2.1 Data Collection

Suppose an array of M co-linear elements with positions $\{x_{Rm}|m = 1, 2, ..., M\}$ is receiving narrowband radiation at frequency ω_0 from K farfield sources. As is illustrated in Figure 2.1, the complex amplitudes received at the set of array elements is stored in the data vector $\mathbf{x}(\omega_0)$, given by

$$\mathbf{x}(\omega_0) = \mathbf{A_R}(\omega_0)\mathbf{s}(\omega_0) + \mathbf{w}(\omega_0) = \begin{bmatrix} \sum_k S_k(\omega_0) e^{jk_0 u_k x_{R1}} \\ \sum_k S_k(\omega_0) e^{jk_0 u_k x_{R2}} \\ \vdots \\ \sum_k S_k(\omega_0) e^{jk_0 u_k x_{RM}} \end{bmatrix} + \begin{bmatrix} w_1(\omega_0) \\ w_2(\omega_0) \\ \vdots \\ w_M(\omega_0) \end{bmatrix}, \quad (2.2)$$

where $k_0 = \frac{2\pi}{\lambda_0}$ is the wavenumber associated with the reference frequency. The receive array manifold matrix at frequency ω_0, $\mathbf{A_R}(\omega_0)$, is given by

$$\mathbf{A_R}(\omega_0) = \begin{bmatrix} e^{jk_0u_1x_{R1}} & e^{jk_0u_2x_{R1}} & ... & e^{jk_0u_Kx_{R1}} \\ e^{jk_0u_1x_{R2}} & e^{jk_0u_2x_{R2}} & ... & e^{jk_0u_Kx_{R2}} \\ \vdots & \vdots & \vdots & \vdots \\ e^{jk_0u_1x_{RM}} & e^{jk_0u_2x_{RM}} & ... & e^{jk_0u_Kx_{RM}} \end{bmatrix}, \tag{2.3}$$

$\mathbf{s}(\omega_0) = [S_1(\omega_0), S_2(\omega_0), ..., S_K(\omega_0)]^T$ is the vector of the complex amplitudes of each source, and $\mathbf{w}(\omega_0) = [w_1(\omega_0), w_2(\omega_0), ..., w_M(\omega_0)]^T$ is the complex vector of observation noise associated with the each element at frequency ω_0. The noise observed at the elements in the narrow band at frequency ω_0 is assumed to be zero-mean, circular, independent, Gaussian noise with variance $\sigma^2(\omega_0)$. Note that because the source radiation is incoherent, we do not need to account for the exact path lengths from the sources to the elements. The path length differences are sufficient and are captured in the $\{u_k x_{Rm}\}$ products in the argument of the exponentials in the array manifold matrix.

2.2.2 Correlation, Beamforming and the Coarray

In incoherent imaging, the correlation between the data collected at each of the elements is used to form an image (i.e. the angular power density). The normalized

correlation between the m and n^{th} element is given by

$$\begin{aligned}
\mathbf{R}(\omega_0)_{m,n} &= \frac{\mathbb{E}[\mathbf{x}_m(\omega_0)\mathbf{x}_n^*(\omega_0)]}{\frac{1}{M}\mathbb{E}[\mathbf{x}^H(\omega_0)\mathbf{x}(\omega_0)]} \\
&= \sum_{k=1}^{K}\sum_{r=1}^{K} \frac{\mathbb{E}[S_k(\omega_0)S_r(\omega_0)^*]}{\frac{1}{M}\mathbb{E}[\mathbf{x}^H(\omega_0)\mathbf{x}(\omega_0)]} e^{jk_0u_kx_{Rm}}e^{-jk_0u_rx_{Rn}} + \frac{\sigma^2(\omega_0)}{\frac{1}{M}\mathbb{E}[\mathbf{x}^H(\omega_0)\mathbf{x}(\omega_0)]}\delta(m-n) \\
&= \sum_{k=1}^{K} \frac{P_k(\omega_0)}{\sum_{l=1}^{K} P_l(\omega_0) + \sigma^2(\omega_0)} e^{jk_0u_k(x_{Rm}-x_{Rn})} + \frac{\sigma^2(\omega_0)}{\sum_{l=1}^{K} P_l(\omega_0) + \sigma^2(\omega_0)}\delta(m-n) \\
&= \sum_{k=1}^{K} \bar{P}_k(\omega_0)e^{jk_0u_k(x_{Rm}-x_{Rn})} + \bar{\sigma}^2(\omega_0)\delta(m-n),
\end{aligned} \tag{2.4}$$

where $\mathbf{x}_m(\omega_0)$ is the m^{th} element of the data vector and $\delta(m-n)$ is the Kronecker delta function. The bars over the source powers and noise variance denote normalized power (normalized by total power received at that frequency), so that

$$\begin{aligned}
\bar{P}_k(\omega_0) &= \frac{P_k(\omega_0)}{\sum_{l=1}^{K} P_l(\omega_0) + \sigma^2(\omega_0)} \\
\bar{\sigma}^2(\omega_0) &= \frac{\sigma^2(\omega_0)}{\sum_{l=1}^{K} P_l(\omega_0) + \sigma^2(\omega_0)}.
\end{aligned} \tag{2.5}$$

For high enough signal-to-noise ratio (SNR),

$$\begin{aligned}
\bar{P}_k(\omega_0) &\approx \frac{P_k(\omega_0)}{\sum_{l=1}^{K} P_l(\omega_0)} \\
\bar{\sigma}^2(\omega_0) &\approx \frac{\sigma^2(\omega_0)}{\sum_{l=1}^{K} P_l(\omega_0)}.
\end{aligned} \tag{2.6}$$

Note that the correlation between the m and n^{th} element is supported on the point $x_{Rm} - x_{Rn}$. This point is called a *coarray point*. The coarray is the support for the correlation operation. For incoherent narrowband imaging at the reference frequency, the coarray points are defined as the set of all possible pairwise differences between

the array element positions [14]:

$$\{y_l\} = \{y_l | y_l = x_{Rm} - x_{Rn} | m, n = 1, 2, ..., M\} \tag{2.7}$$

The coarray plays an important role in understanding the capabilities of an imaging system.

In linear beamforming, the image is formed by "looking" in the direction desired, u, by phase delaying the array elements so that if there were a source in the direction u, the radiation received at each of the elements would add constructively. The image at u is given by summing over all receive elements. Disregarding noise, is image is easily seen to be obtained as follows:

$$\begin{aligned} I(u) &= \sum_{m=1}^{M}\sum_{n=1}^{M} \mathbf{R}(\omega_0)_{m,n} e^{-jk_0 u x_{Rm}} e^{jk_0 u x_{Rn}} \\ &= \sum_{m=1}^{M}\sum_{n=1}^{M}\sum_{k=1}^{K} \bar{P}_k(\omega_0) e^{-jk_0(u-u_k)(x_{Rm}-x_{Rn})} \end{aligned} \tag{2.8}$$

If we consider a source with unit power at broadside, its image as a function of u is the *point spread function* (or impulse response) of the system:

$$PSF(u) = \sum_{m=1}^{M}\sum_{n=1}^{M} e^{-jk_0 u(x_{Rm}-x_{Rn})} = \sum_{l=1}^{L} \gamma_l e^{-jk_0 u y_l} \tag{2.9}$$

Here $\{y_l\}$ are the coarray points and γ_l is the coarray weight (number of distinct array element pairs) associated with the difference y_l. We refer to this point/weight combination collectively as the coarray. We see that the point spread function is the Fourier transform of the coarray. This is a central result given in [14], and the consequence of this relationship is that the coarray controls the beamwidth and sidelobe characteristics of the image. The resolution capabilities of an imaging system

are generally associated with the 3 dB beamwidth - the narrower the beam, the closer the two sources can be and still be resolved. Resolution in linear beamforming can be controlled by manipulating the coarray and its weighting [14, 41].

For example, if we consider a uniform linear array with spacing at the Nyquist spacing ($\frac{\lambda_0}{2}$), the coarray is also uniformly spaced with a Bartlett (triangular) weighting. Note that in general, array weights $\{w_{Rm}\}$ can be applied to the array elements when beamforming to change the coarray weighting, but we will only consider uniform weighting for simplicity. For the uniformly spaced and weighted array, the angular distance from the center of the mainbeam to the 3 dB point is given approximately by $\frac{.88}{M}$ [40], which means that two source must be approximately separated more than $\frac{1.76}{M}$ (in the units of u) in order to be resolved. Since the expression for beamwidth is inversely proportional to M, more elements in the array yields a better resolution.

We will illustrate this by example. For a 5 element $\frac{\lambda_0}{2}$ uniformly spaced array, the approximate minimum resolvable angular separation is $\frac{1.76}{5} = 0.352$. In Figure 2.2(a), the two point sources are separated by 0.35 and they appear as one peak in the image. They cannot be resolved. When the sources are separated slightly further apart by 0.39, they can be resolved, as is shown in Figure 2.2(b).

Wideband Coarray

It is possible to observe radiation at a frequency other than the reference frequency. When observing radiation at a frequency different from the reference frequency, the source powers and noise power may change. The phases received at the array sensors will also differ from those at the reference frequency. The array data obtained at a

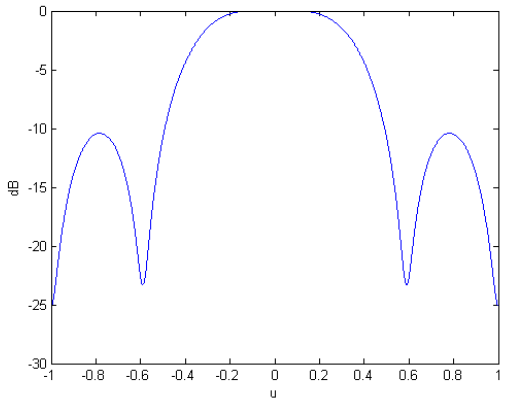

(a) Two sources separated by 0.35, unresolvable

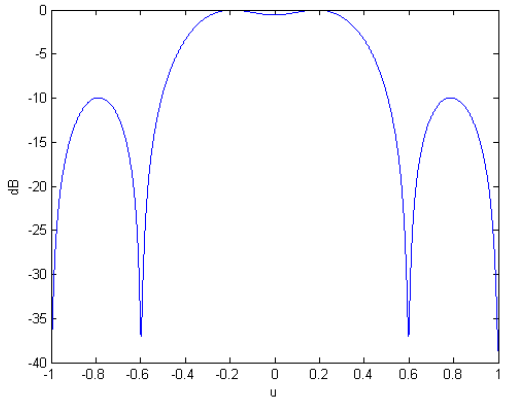

(b) Two sources separated by 0.39, resolvable

Figure 2.2: Linear Beamforming Example with Two Incoherent Point Sources and Five Array Elements

frequency $\omega_q = \alpha_q \omega_0$ is modeled as

$$\mathbf{x}(\omega_q) = \mathbf{A_R}(\omega_q)\mathbf{s}(\omega_q) + \mathbf{w}(\omega_q) = \begin{bmatrix} \sum_k S_k(\omega_q) e^{jk_q u_k x_{R1}} \\ \sum_k S_k(\omega_q) e^{jk_q u_k x_{R2}} \\ \vdots \\ \sum_k S_k(\omega_q) e^{jk_q u_k x_{RM}} \end{bmatrix} + \begin{bmatrix} w_1(\omega_q) \\ w_2(\omega_q) \\ \vdots \\ w_M(\omega_q) \end{bmatrix}, \quad (2.10)$$

where $k_q = \frac{2\pi}{\lambda_q} = \alpha_q k_0$ is the wavenumber associated with the frequency ω_q. The factor $\alpha_q = \frac{\omega_q}{\omega_0}$ is related to the fact that we are observing radiation of frequency ω_q when the array spacing is generally based on the reference frequency ω_0. The receive array manifold matrix at frequency ω_q, $\mathbf{A_R}(\omega_q)$, is given by

$$\begin{aligned} \mathbf{A_R}(\omega_q) &= \begin{bmatrix} e^{jk_q u_1 x_{R1}} & e^{jk_q u_2 x_{R1}} & ... & e^{jk_q u_K x_{R1}} \\ e^{jk_q u_1 x_{R2}} & e^{jk_q u_2 x_{R2}} & ... & e^{jk_q u_K x_{R2}} \\ \vdots & \vdots & \vdots & \vdots \\ e^{jk_q u_1 x_{RM}} & e^{jk_q u_2 x_{RM}} & ... & e^{jk_q u_K x_{RM}} \end{bmatrix} \\ &= \begin{bmatrix} e^{jk_0 u_1 \alpha_q x_{R1}} & e^{jk_0 u_2 \alpha_q x_{R1}} & ... & e^{jk_0 u_K \alpha_q x_{R1}} \\ e^{jk_0 u_1 \alpha_q x_{R2}} & e^{jk_0 u_2 \alpha_q x_{R2}} & ... & e^{jk_0 u_K \alpha_q x_{R2}} \\ \vdots & \vdots & \vdots & \vdots \\ e^{jk_0 u_1 \alpha_q x_{RM}} & e^{jk_0 u_2 \alpha_q x_{RM}} & ... & e^{jk_0 u_K \alpha_q x_{RM}} \end{bmatrix}. \end{aligned} \quad (2.11)$$

The vector $\mathbf{s}(\omega_q) = [S_1(\omega_q), S_2(\omega_q), ..., S_K(\omega_q)]^T$ is the vector of the complex amplitudes of each source and $\mathbf{w}(\omega_q) = [w_1(\omega_q), w_2(\omega_q), ..., w_M(\omega_q)]^T$ is the vector of observation noise associated with the each element at frequency ω_q. The noise observed at the elements in the narrow band at frequency ω_q is assumed to be zero-mean, independent, circular, Gaussian noise with variance $\sigma^2(\omega_q)$.

Just as in Equation 2.4, the normalized correlation between the m^{th} and n^{th}

element at frequency $\omega_q = \alpha_q \omega_0$ is given by

$$\begin{aligned}
\mathbf{R}(\omega_q)_{m,n} &= \frac{\mathbb{E}[\mathbf{x}_m(\omega_q)\mathbf{x}_n^*(\omega_q)]}{\frac{1}{M}\mathbb{E}[\mathbf{x}^H(\omega_q)\mathbf{x}(\omega_q)]} \\
&= \sum_{k=1}^{K}\sum_{r=1}^{K} \frac{\mathbb{E}[S_k(\omega_q)S_r(\omega_q)^*]}{\frac{1}{M}\mathbb{E}[\mathbf{x}^H(\omega_q)\mathbf{x}(\omega_q)]} e^{jk_q u_k x_{Rm}} e^{-jk_q u_r x_{Rn}} + \frac{\sigma^2(\omega_q)}{\frac{1}{M}\mathbb{E}[\mathbf{x}^H(\omega_q)\mathbf{x}(\omega_q)]}\delta(m-n) \\
&= \sum_{k=1}^{K} \frac{P_k(\omega_q)}{\sum_{l=1}^{K} P_l(\omega_q) + \sigma^2(\omega_q)} e^{jk_0 u_k \alpha_q (x_{Rm} - x_{Rn})} + \frac{\sigma^2(\omega_q)}{\sum_{l=1}^{K} P_l(\omega_q) + \sigma^2(\omega_q)}\delta(m-n) \\
&= \sum_{k=1}^{K} \bar{P}_k(\omega_q) e^{jk_0 u_k \alpha_q (x_{Rm} - x_{Rn})} + \bar{\sigma}^2(\omega_q)\delta(m-n)
\end{aligned} \tag{2.12}$$

where $\mathbf{x}_m(\omega_q)$ is the m^{th} element of the data vector and $\delta(m-n)$ is the Kronecker delta function. The bars over the source powers and noise variance denote normalized power (normalized by total power received at that frequency):

$$\begin{aligned}
\bar{P}_k(\omega_q) &= \frac{P_k(\omega_q)}{\sum_{l=1}^{K} P_l(\omega_q) + \sigma^2(\omega_q)} \\
\bar{\sigma}^2(\omega_q) &= \frac{\sigma^2(\omega_q)}{\sum_{l=1}^{K} P_l(\omega_q) + \sigma^2(\omega_q)}
\end{aligned} \tag{2.13}$$

For high enough signal-to-noise ratio (SNR),

$$\begin{aligned}
\bar{P}_k(\omega_q) &\approx \frac{P_k(\omega_q)}{\sum_{l=1}^{K} P_l(\omega_q)} \\
\bar{\sigma}^2(\omega_q) &\approx \frac{\sigma^2(\omega_q)}{\sum_{l=1}^{K} P_l(\omega_q)}
\end{aligned} \tag{2.14}$$

We see that the correlation between the m^{th} and n^{th} element at frequency ω_q is supported on the coarray point $\alpha_q(x_{Rm} - x_{Rn})$. Comparing this to Equation 2.4, using a frequency other than the reference frequency effectively dilates the coarray by the factor α_q [17]. When multiple frequencies are used, more coarray points are

generated than when using a single frequency. Using multiple frequencies is a way of manipulating the coarray.

The wideband beamformed image is given by phase aligning each element at each frequency in a direction u and then summing the beamformed data over all array elements and all frequencies. The point spread function for wideband imaging with Q frequencies is given by:

$$\begin{aligned} PSF_{\mathrm{WB}}(u) &= \sum_{m=1}^{M}\sum_{n=1}^{M}\sum_{q=0}^{Q-1} e^{-jk_q u(x_{Rm}-x_{Rn})} \\ &= \sum_{m=1}^{M}\sum_{n=1}^{M}\sum_{q=0}^{Q-1} e^{-jk_0 u\alpha_q(x_{Rm}-x_{Rn})} = \sum_{l=1}^{L}\zeta_l e^{-jk_0 u z_l}. \end{aligned} \tag{2.15}$$

For wideband imaging, the set of coarray points is

$$\{z_l\} = \{z_l | z_l = \alpha_q(x_{Rm} - x_{Rn}), q = 0, 1, ..., Q-1, m = 1, 2, ..., M, n = 1, 2, ..., M\}. \tag{2.16}$$

As used in Equation 2.15, the set $\{z_l\}$ is assumed to be indexed such that it is a set of distinct points. The possible redundancies arising from multiple (q, m, n) combinations contributing to the same coarray point z_l are accounted for by the coarray weight ζ_l.

The wideband coarray can also be viewed as a union of the narrowband coarray at the reference frequency dilated by various α_q:

$$\begin{aligned} \{z_l\} &= \bigcup_{q=0}^{Q-1} \alpha_q\{y_l\} \\ &\text{where} \\ \{y_l\} &= \{x_{Rm} - x_{Rn} | m = 1, 2, ..., M, n = 1, 2, ..., M\}. \end{aligned} \tag{2.17}$$

Using a frequency higher than the reference frequency causes an expansion of the coarray - the coarray points become further apart and the coarray has a larger diameter. Using a frequency lower than the reference frequency causes a contraction of the coarray - the coarray points become closer together and the coarray diameter decreases. This idea can be used to created desired coarray points. For example, if we have the array $\{0,1,2,6\}\frac{\lambda_0}{2}$, the corresponding narrowband coarray at the reference frequency is $\{0,\pm1,\pm2,\pm4,\pm5,\pm6\}\frac{\lambda_0}{2}$. This is a uniformly spaced coarray except that it is missing the coarray points $\pm3\frac{\lambda_0}{2}$. Suppose for the image we wish to produce, it is necessary to have the point $\pm3\frac{\lambda_0}{2}$ in the coarray. These points can be obtained by using an additional frequency, $\omega_q = \alpha_q\omega_0$. The coarray corresponding to ω_q is $\{0,\pm\alpha_q,\pm2\alpha_q,\pm4\alpha_q,\pm5\alpha_q,\pm6\alpha_q\}\frac{\lambda_0}{2}$ and values of α_q that yield the coarray point $\pm3\frac{\lambda_0}{2}$ are $3,\frac{3}{2},\frac{3}{4},\frac{3}{5},\frac{1}{2}$. The value of α_q that is chosen may be chosen to fit any bandwidth constraints, but often it is desirable to minimize the bandwidth used. In this case, choose α_q so that it minimizes $|\omega_q-\omega_0| = |\alpha_q-1|\omega_0$.

In our case, we would choose $\alpha_q = \frac{3}{4}$ to minimize bandwidth. The wideband coarray becomes

$$\begin{aligned}\{0,\pm1,\pm2,\pm4,\pm5,\pm6\}\frac{\lambda_0}{2} \cup \frac{3}{4}\{0,\pm1,\pm2,\pm4,\pm5,\pm6\}\frac{\lambda_0}{2} \\ \supset \{0,\pm1,\pm2,\pm3,\pm4,\pm5,\pm6\}\frac{\lambda_0}{2},\end{aligned} \tag{2.18}$$

and it contains the desired uniformly spaced coarray.

2.2.3 The Narrowband Correlation Matrix and High Resolution Techniques

When the coarray cannot be manipulated in a way to deliver the linear beamformer resolution necessary, non-linear high-resolution techniques may be used. Many high-

resolution techniques make use of the narrowband correlation matrix. The normalized narrowband correlation matrix at the reference frequency is found as follows:

$$\begin{aligned}\mathbf{R}(\omega_0) &= \frac{\mathbb{E}[\mathbf{x}(\omega_0)\mathbf{x}(\omega_0)^H]}{\frac{1}{M}\mathbb{E}[\mathbf{x}^H(\omega_0)\mathbf{x}(\omega_0)]} \\ &= \mathbf{A_R}(\omega_0)\bar{\mathbf{P}}(\omega_0)\mathbf{A_R}(\omega_0)^H + \bar{\sigma}^2(\omega_0)\mathbf{I},\end{aligned} \tag{2.19}$$

where

$$\bar{\mathbf{P}}(\omega_0) = \text{diag}[\bar{P_1}(\omega_0), \bar{P_2}(\omega_0), ..., \bar{P_K}(\omega_0)] \tag{2.20}$$

is the diagonal matrix of normalized source powers. The $(m,n)^{th}$ element is given by (same as Equation 2.4)

$$\mathbf{R}(\omega_0)_{m,n} = \sum_{k=1}^{K} \bar{P_k}(\omega_0)e^{jk_0u_k(x_{Rm}-x_{Rn})} + \bar{\sigma}^2(\omega_0)\delta(m-n). \tag{2.21}$$

The matrix possesses a special structure. From (2.21), we see that without noise the $(m,n)^{th}$ element of $\mathbf{R}(\omega_0)$ has support on the point $x_{Rm} - x_{Rn}$. As was addressed in Section 2.2, this point is called a coarray point. The coarray is useful in high-resolution imaging because it reveals the structure of the correlation matrix.

Narrowband correlation matrices can also be formed at frequencies different from the reference frequency. The narrowband spatial correlation matrix at frequency ω_q is given by

$$\begin{aligned}\mathbf{R}(\omega_q) &= \frac{\mathbb{E}[\mathbf{x}(\omega_q)\mathbf{x}(\omega_q)^H]}{\frac{1}{M}\mathbb{E}[\mathbf{x}^H(\omega_q)\mathbf{x}(\omega_q)]} \\ &= \mathbf{A_R}(\omega_q)\bar{\mathbf{P}}(\omega_q)\mathbf{A_R}(\omega_q)^H + \bar{\sigma}^2(\omega_q)\mathbf{I},\end{aligned} \tag{2.22}$$

where $\bar{\mathbf{P}}(\omega_q) = \text{diag}[\bar{P_1}(\omega_q), \bar{P_2}(\omega_q), ..., \bar{P_K}(\omega_q)]$ is the diagonal matrix of normalized

source powers at the q^{th} frequency. The $(m,n)^{th}$ element is given by

$$\mathbf{R}(\omega_q)_{m,n} = \sum_{k=1}^{K} \bar{P}_k(\omega_q) e^{jk_0 u_k \alpha_q (x_{Rm} - x_{Rn})} + \bar{\sigma}^2(\omega_q)\delta(m-n). \tag{2.23}$$

This matrix possesses a similar structure to that at the reference frequency, but the $(m,n)^{th}$ element is now supported on the point $\alpha_q(x_{Rm} - x_{Rn})$. This is consistent with the dilation of the coarray when using frequencies other than the reference frequency as shown in Section 2.2.1.

There exist many well-known narrowband (single-frequency of operation) high-resolution imaging techniques. In this chapter, we will use three of the most popular - Multiple Signal Classification (MUSIC), Capon's Minimum Variance method, and Autoregressive (AR) - for comparison.

Multiple Signal Classification (MUSIC)

The basis of MUltiple SIgnal Classification (MUSIC) is the eigen-decomposition of the narrowband correlation matrix. The eigenvalue decomposition of the $M \times M$ narrowband correlation matrix is

$$\mathbf{R}(\omega_0) = \mathbf{V}(\omega_0)\mathbf{\Lambda}(\omega_0)\mathbf{V}(\omega_0)^H, \tag{2.24}$$

where $\mathbf{V}(\omega_0)$ is the matrix of eigenvectors and $\mathbf{\Lambda}(\omega_0)$ is the diagonal matrix of eigenvalues of $\mathbf{R}(\omega_0)$. Assuming the noiseless case, if $K < M$ and $\mathbf{A_R}(\omega_0)$ has full column rank, it can be shown [41] that there are $M-K$ zero eigenvalues with corresponding eigenvectors $\mathbf{v^0}_i(\omega_0)$ each denoted by the subscript $i = 1, 2, ..., M-K$. The zero eigenvectors are orthogonal to the columns of the array manifold matrix, so that

$$\mathbf{A_R}(\omega_0)^H \mathbf{v^0}_i(\omega_0) = \mathbf{0}. \tag{2.25}$$

The MUSIC estimator exploits this orthogonality and is defined as

$$P_{\text{MUSIC}}(u) = \frac{1}{\sum_{i=1}^{M-K} |\mathbf{a_R}^H(u,\omega_0)\mathbf{v^0}_i(\omega_0)|^2}, \tag{2.26}$$

where $\mathbf{a_R}(u,\omega_0)$ is the array steering vector:

$$\mathbf{a_R}(u,\omega_0) = \begin{bmatrix} e^{jk_0ux_{R1}} & e^{jk_0ux_{R1}} & ... & e^{jk_0ux_{R1}} \end{bmatrix}^T. \tag{2.27}$$

When $\mathbf{a_R}(u,\omega_0)$ is evaluated at any of the source locations u_k, it is the k^{th} column of the array manifold matrix and thus is orthogonal to the $\{\mathbf{v^0}_i(\omega_0)\}$.

It can also be shown that $\mathbf{a_R}(u,\omega_0)$ is orthogonal to $\mathbf{v^0}_i(\omega_0)$ only when $u = u_k$. Thus, the peaks of $P_{\text{MUSIC}}(u)$ are uniquely the locations of the point targets.

In the presence of spatially white noise, the eigenvectors corresponding to the $M-K$ smallest eigenvalues are chosen as the $\{\mathbf{v^0}_i(\omega_0)\}$. The addition of a diagonal noise covariance matrix does not change the eigenvectors, so the analysis holds. For a more detailed derivation of MUSIC, see [42].

Auto-regressive (AR) Spectrum Estimation

In auto-regressive (AR) modeling, the field sampled by the array is assumed to form an AR process. This may be a reasonable model at least for the uniformly spaced line array. This model is expressed as

$$\mathbf{x}_m(\omega_0) = -\sum_{i=1}^{M-1} \mathbf{b}_i(\omega_0)\mathbf{x}_{m-i}(\omega_0) + w_m(\omega_0) \tag{2.28}$$

where $\mathbf{x}_m(\omega_0)$ denotes the m^{th} element of the data vector and the $\{\mathbf{b}_i(\omega_0)\}$ are the AR parameters.

The $\{\mathbf{b}_i(\omega_0)\}$ can be solved for by minimizing the prediction error power, given

below, with respect to the $\{\mathbf{b}_i(\omega_0)\}$:

$$\text{Prediction Error Power} = \mathbb{E}\left|\mathbf{x}_m(\omega_0) + \sum_{i=1}^{M-1} \mathbf{b}_i(\omega_0)\mathbf{x}_{m-i}(\omega_0)\right|^2 \tag{2.29}$$

Differentiating with respect to the $\{\mathbf{b}_i\}$ leads to the well-known Yule-Walker equations, [42]. The Yule-Walker equations can be written in terms of sub-matrices of $\mathbf{R}(\omega_0)$ as

$$\mathbf{R}(\omega_0)_{1:M-1,1:M-1}\mathbf{b}(\omega_0) = -\mathbf{R}(\omega_0)_{2:M,1} \tag{2.30}$$

where the subscripts on the block matrices represent, respectively, the range of rows and columns and $\mathbf{b}(\omega_0)$ is the vector of the $\{\mathbf{b}_i(\omega_0)\}$. $\mathbf{b}(\omega_0)$ can be found efficiently by the Levinson-Durbin algorithm [42].

The AR spectrum estimator is given as

$$P_{\text{AR}}(u) = \frac{1}{|1 + \sum_{i=1}^{M-1} \mathbf{b}_i(\omega_0)e^{-j2\pi u x_{Rm}}|^2}. \tag{2.31}$$

In the plot of $P_{\text{AR}}(u)$ for $u \in [-1, 1]$, the peaks reveal the source locations. Since there are up to $M-1$ poles in Equation (2.34), there can be up to $M-1$ peaks in the plot of $P_{\text{AR}}(u)$ over u representing the source locations.

Capon Minimum Variance Spectrum Estimator

The Capon minimum variance spectrum estimator comes from finding the maximum likelihood estimate of the unknown complex amplitude, $S_0(\omega_0)$, of source at a known direction u_0, which is observed by the array elements in additive, white, zero-mean, complex Gaussian noise.

The observation at the m^{th} array element due to a source at u_0 is modeled as

$$\mathbf{x}_m(\omega_0) = S_0(\omega_0)e^{jk_0u_0x_{Rm}} + w_m(\omega_0), \tag{2.32}$$

where the $\{w_m\}$ are zero-mean white Gaussian variates with variance $\sigma^2(\omega_0)$. The maximum likelihood estimate of $S_0(\omega_0)$ is shown to be [42]

$$\hat{S}_0(\omega_0) = \frac{\mathbf{a_R}(u_0,\omega_0)^H\mathbf{R}^{-1}(\omega_0)\mathbf{x}(\omega_0)}{\mathbf{a_R}(u_0,\omega_0)^H\mathbf{R}^{-1}(\omega_0)\mathbf{a_R}(u_0,\omega_0)}. \tag{2.33}$$

This is also the linear minimum variance unbiased estimate of $S_0(\omega_0)$.

The Capon minimum variance spectrum estimator is given by the power output of the linear minimum variance unbiased estimator:

$$P_{\text{Capon}}(u) = \mathbb{E}[\hat{S}_0(\omega_0)\hat{S}_0(\omega_0)^*] = \frac{1}{\mathbf{a_R}(u,\omega_0)^H\mathbf{R}^{-1}(\omega_0)\mathbf{a_R}(u,\omega_0)} \tag{2.34}$$

where $\mathbf{a_R}(u,\omega_0)$ is the array steering vector given in Equation (2.27).

Limit on the number of sources that can be resolved

The high-resolution techniques covered here provide superior resolution capabilities compared to linear beamforming. For specific resolution capabilities, see [42]. The main limiting factor in high-resolution is the number of point sources which can be resolved. For MUSIC, it is easy to see that only $M-1$ point sources can be resolved because of the rank condition necessary on the correlation matrix to ensure there are noise eigenvectors. AR cannot resolve more than $M-1$ sources, as this is the maximum number of poles that can occur. Capon's source limit is also $M-1$ which can be understood when it is viewed as an average of auto-regressive processes of different orders, the maximum order being $M-1$ [42]. This hard limit on the number

of sources which can be resolved can create problems from arrays that only have a few elements due to cost or size limitations.

2.3 The Virtual Array and Constructing the Virtual Correlation Matrix

A virtual array is an array whose effect we wish to synthesize. The concept of a virtual array is not new. It has been used in works to describe data which behaves as if it were coming from a different array [41, 19, 15]. Our intent in this chapter is to synthesize the *effect* of a $\frac{\lambda_0}{2}$-uniformly-spaced array operating at a single frequency with more elements than the actual array, by using multiple frequencies. A *virtual correlation matrix* corresponding to the virtual array is constructed in order to resolve more point sources using high-resolution techniques. The virtual correlation matrix will be constructed from the narrowband correlation matrices at different frequencies but will be larger in dimension than the component narrowband correlation matrices. It will appear to be generated by narrowband sources being observed by the virtual array. Since the virtual correlation matrix will appear to have come from a single frequency, the high-resolution techniques covered in Section 2.2.3 can used without modification, but will be able to resolve more sources than just using a narrowband correlation matrix.

The main questions to be addressed are how to construct the virtual correlation matrix and under what assumptions is this matrix useful. We will see that the coarray helps us understand how to construct the virtual correlation matrix.

2.3.1 Coarray Support Matrix

The coarray support matrix is a different way of expressing the coarray. Instead of representing the coarray in the usual point/weight form, the coarray is represented as a matrix. Since high-resolution imaging is based on the spatial correlation matrix, representing the coarray in matrix form reveals its underlying structure.

For an array of M elements with elements at positions $\{x_{Rm}\}$, let the $M \times M$ matrix $\mathbf{C}(\omega_0)$, called the coarray support matrix for ω_0, be defined such that the $(m,n)^{th}$ element is

$$\mathbf{C}(\omega_0)_{m,n} = x_{Rm} - x_{Rn}. \tag{2.35}$$

Comparing this to Equation (2.21), we see that this is the supporting coarray point of the $(m,n)^{th}$ element of the narrowband correlation matrix at the reference frequency.

Since uniform linear arrays will be of great interest in this chapter, we will use a uniform linear array of 5 elements with spacing of $\frac{\lambda_0}{2}$ operating at the reference frequency, ω_0, as an example. The array is $\{-\lambda_0, -\frac{\lambda_0}{2}, 0, \frac{\lambda_0}{2}, \lambda_0\}$. The coarray support matrix at the reference frequency is given by

$$\mathbf{C}(\omega_0) = \begin{bmatrix} 0 & -\frac{\lambda_0}{2} & -\lambda_0 & -\frac{3\lambda_0}{2} & -2\lambda_0 \\ \frac{\lambda_0}{2} & 0 & -\frac{\lambda_0}{2} & -\lambda_0 & -\frac{3\lambda_0}{2} \\ \lambda_0 & \frac{\lambda_0}{2} & 0 & -\frac{\lambda_0}{2} & -\lambda_0 \\ \frac{3\lambda_0}{2} & \lambda_0 & \frac{\lambda_0}{2} & 0 & -\frac{\lambda_0}{2} \\ 2\lambda_0 & \frac{3\lambda_0}{2} & \lambda_0 & \frac{\lambda_0}{2} & 0 \end{bmatrix}. \tag{2.36}$$

Notice that the coarray point 0 appears on every element on the main diagonal giving it weight 5. The other coarray points appear on the other diagonals, the weight decreasing by one all the way out to the last coarray point $2\lambda_0$ with weight 1. This is the triangular weighting as expected. The coarray weight information is contained

within the coarray support matrix. The number of times a coarray point appears in the coarray support matrix is the weight of that coarray point.

In general, the coarray support matrix is always skew-symmetric since

$$\mathbf{C}_{m,n}(\omega_0) = x_{Rm} - x_{Rn} = -(x_{Rn} - x_{Rm}) = -\mathbf{C}_{n,m}(\omega_0) \tag{2.37}$$

The coarray support matrix for a uniform linear array always has a Toeplitz structure since

$$\mathbf{C}_{m,n}(\omega_0) = x_{Rm} - x_{Rn} = (m-n)\frac{\lambda_0}{2} = ((m+i)-(n+i))\frac{\lambda_0}{2} = \mathbf{C}_{m+i,n+i}(\omega_0) \tag{2.38}$$

The coarray support matrix for frequency $\omega_q = \alpha_q\omega_0$ is similarly defined as

$$\mathbf{C}(\omega_q)_{m,n} = \alpha_q(x_{Rm} - x_{Rn}) = \alpha_q\mathbf{C}(\omega_0)_{m,n}. \tag{2.39}$$

Comparing this with equation (2.23), this is consistent with the frequencies dilating the coarray. Using frequencies different from the reference frequency also dilates the coarray support matrix. For our example from (2.36) for a frequency $\omega_q = \alpha_q\omega_0$ the coarray support matrix is

$$\mathbf{C}(\omega_q) = \begin{bmatrix} 0 & -\alpha_q\frac{\lambda_0}{2} & -\alpha_q\lambda_0 & -\alpha_q\frac{3\lambda_0}{2} & -2\alpha_q\lambda_0 \\ \alpha_q\frac{\lambda_0}{2} & 0 & -\alpha_q\frac{\lambda_0}{2} & -\alpha_q\lambda_0 & -\alpha_q\frac{3\lambda_0}{2} \\ \alpha_q\lambda_0 & \alpha_q\frac{\lambda_0}{2} & 0 & -\alpha_q\frac{\lambda_0}{2} & -\alpha_q\lambda_0 \\ \alpha_q\frac{3\lambda_0}{2} & \alpha_q\lambda_0 & \alpha_q\frac{\lambda_0}{2} & 0 & -\alpha_q\frac{\lambda_0}{2} \\ 2\alpha_q\lambda_0 & \alpha_q\frac{3\lambda_0}{2} & \alpha_q\lambda_0 & \alpha_q\frac{\lambda_0}{2} & 0 \end{bmatrix} = \alpha_q\mathbf{C}(\omega_0). \tag{2.40}$$

The coarray support matrix is a useful tool to understand the underlying structure of the narrowband correlation matrices as well as the virtual correlation matrix we

wish to construct. By knowing this structure, we can construct the virtual correlation matrix in a way that allows it to be used for high-resolution imaging.

2.3.2 Virtual Correlation Matrix

The virtual correlation matrix is a correlation matrix constructed from a number of narrowband correlation matrices which appears, under certain conditions to be explored in this section, to have been generated by a virtual array with more elements than the actual array at a single frequency. Since the virtual array has more elements than the actual array, the virtual correlation matrix will have a dimension larger than the component narrowband correlation matrices from which it is constructed, and more point sources can be resolved. The virtual correlation matrix is constructed from the narrowband correlation matrices so that it is *coarray equivalent* to a correlation matrix that would be generated by the virtual array at a single frequency observing the same sources.

We will only consider virtual arrays which are uniformly spaced with spacing $\frac{\lambda_0}{2}$. This is because we know that a uniform linear array always produces a uniform linear coarray and then we know exactly what coarray we need to synthesize. Also, for a uniformly spaced coarray of a given diameter, the uniform linear array is the array with the most elements that produces this coarray. It makes sense to use the coarray we have synthesized in a way that allows us to resolve as many sources as possible.

Suppose we want to synthesize the effect of a virtual array, with elements at positions $\{\tilde{x}_{Rm}\}, m = 1, 2, ..., \tilde{M}$, whose coarray support matrix is given by $\tilde{\mathbf{C}}(\omega_0)$, i.e.

$$\tilde{\mathbf{C}}(\omega_0)_{m,n} = \tilde{x}_{Rm} - \tilde{x}_{Rn}. \tag{2.41}$$

To synthesize the effect of this array we need to generate data at all of the coarray

points contained in $\tilde{\mathbf{C}}(\omega_0)$. This is done by using multiple frequencies to dilate the narrowband coarray support matrix $\mathbf{C}(\omega_0)$. In order to cover all of the coarray points in $\tilde{\mathbf{C}}(\omega_0)$, the frequencies should be chosen so that

$$\tilde{\mathbf{C}}(\omega_0)_{i,j} = \mathbf{C}(\omega_q)_{m,n}, \text{ for some } q, m, n, \text{ for all } i, j. \tag{2.42}$$

The subscripts represent the row and column of the matrices.

If bandwidth is an issue, to minimize the bandwidth used, the α_q chosen to satisfy Equation 2.42 can be picked such that

$$\max_q\{\alpha_q\} - \min_q\{\alpha_q\} \tag{2.43}$$

is minimized with $\alpha_0 = 1$ corresponding to the reference frequency.

2.3.3 Condition for a Valid Virtual Correlation Matrix

For the virtual correlation matrix to be useable in the high-resolution techniques in Section 2.2.3 without modification, the virtual correlation matrix must have the same structure as a narrowband correlation matrix generated by the virtual array observing the scene. That is,

$$\tilde{\mathbf{R}}(\omega_0) = \tilde{\mathbf{A}}_{\mathbf{R}}(\omega_0)\bar{\mathbf{P}}\tilde{\mathbf{A}}_{\mathbf{R}}(\omega_0)^H \tag{2.44}$$

where $\bar{\mathbf{P}} = \text{diag}[\bar{P}_1, \bar{P}_2, ..., \bar{P}_K]$ is some positive-definite diagonal matrix that does not depend on frequency and $\tilde{\mathbf{A}}_{\mathbf{R}}(\omega_0)$ is the virtual array manifold,

$$\tilde{\mathbf{A}}_{\mathbf{R}}(\omega_0) = \begin{bmatrix} e^{jk_0u_1\tilde{x}_{R1}} & e^{jk_0u_2\tilde{x}_{R1}} & ... & e^{jk_0u_K\tilde{x}_{R1}} \\ e^{jk_0u_1\tilde{x}_{R2}} & e^{jk_0u_2\tilde{x}_{R2}} & ... & e^{jk_0u_K\tilde{x}_{R2}} \\ \vdots & \vdots & \vdots & \vdots \\ e^{jk_0u_1\tilde{x}_{R\tilde{M}}} & e^{jk_0u_2\tilde{x}_{R\tilde{M}}} & ... & e^{jk_0u_K\tilde{x}_{R\tilde{M}}} \end{bmatrix}. \tag{2.45}$$

All virtual coarray points in $\tilde{\mathbf{C}}(\omega_0)$ are generated from differences between two array positions, x_{Rm} and x_{Rn}, and some frequency, ω_q, i.e., for every virtual coarray point $\tilde{y}_p$, there exists a combination of (m, n, q) such that $\tilde{y}_p = \alpha_q(x_{Rm} - x_{Rn})$. When piecing together the virtual correlation matrix, the coarray point $\tilde{y}_p$ may come from the $(m_p, n_p)^{th}$ element of the correlation matrix at frequency ω_q, and the coarray point $\tilde{y}_l$ may come from the $(m_l, n_l)^{th}$ element of a different correlation matrix at frequency ω_r. Thus, each coarray point may come from different virtual correlation matrix at a different frequency, but we need to ensure that when the virtual correlation matrix is constructed that it has the structure given in Equation 2.44. Comparing the noiseless version of Equations 2.19 and 2.44, we see this is because the high-resolution techniques depend on the correlation matrix having this structure. This condition is satisfied when the following equalities are satisfied for some set $\{\bar{P}_k\}$:

$$\sum_k \bar{P}_k(\omega_q)e^{jk_0u_k\tilde{y}_p} = \sum_k \bar{P}_k e^{jk_0u_k\tilde{y}_p} \text{ for all } q, p \tag{2.46}$$

These equations can be satisfied if

$$\bar{P}_k(\omega_q) = \bar{P}_k(\omega_0) \text{ for all } k, q, \tag{2.47}$$

in which case we can take the $\{\bar{P}_k\}$ to be $\{\bar{P}_k(\omega_0)\}$ Recall that the *source-normalized* source power ("source-normalized" because it is normalized by the power of all sources at that frequuency)is defined as:

$$\bar{P}_k(\omega_q) \approx \frac{P_k(\omega_q)}{\sum_l P_l(\omega_q)} \tag{2.48}$$

for high SNR. This arises naturally in normalizing the narrowband correlation matrices. Equation 2.47 states that the normalized source powers at each frequency must be equal. While is may not be obvious, it is true that condition 2.47 is equivalent to the condition that the sources have *proportional spectra* - or equal *frequency-normalized* source powers - i.e.,

$$\frac{P_k(\omega_q)}{P_l(\omega_q)} = D_{k,l} \text{ for all } q, k, l, \tag{2.49}$$

where $D_{k,l}$ is a constant that depends only on the targets, not the frequency. This means the sources have essentially the same normalized power spectrum as a function of frequency. This examined in detail in the Appendix.

This is an intuitive condition because if the normalized source powers are not identical, effectively, a different scene is being observed at each frequency and then the virtual correlation matrix will be constructed from many different scenes. This would not happen in conventional narrowband imaging.

Note on Power Normalization

There are two ways to consider the normalized power of a source.

When forming the correlation matrix, we normalize all of the diagonals to be unity. This is a *source-normalized* power normalization because we divide the narrowband correlation matrix at frequency ω_q by $\sum_{k=1}^{K} P_k(\omega_q)$. The power is normalized with respect to other source power at that particular frequency.

The other way, which may be more intuitive to think about but is not directly calculable since we do not know the individual source powers, is a *frequency-normalized* power normalization. The power of a source at a particular frequency is normalized by the sum of the powers at all frequencies considered for that source. We divide the power of a source at frequency ω_q by $\sum_{p=0}^{Q-1} P_k(\omega_p)$. This type of normalization allow us to compare the emission characteristics among individual sources.

It is shown in the Appendix that sources have equal source-normalized powers is equivalent to sources have equal frequency-normalized source powers for high enough signal-to-ratios. If two sources have equal frequency-normalized source powers, their sampled power spectra are proportional. From this point forward, we use the term *proportional spectra* to denote the conditions in Equations 2.47 and 2.49.

This condition will be explored in an example in Section 2.4.

2.4 Example Illustrating Virtual Correlation Matrix Construction and Performance

This example will illustrate the most basic problem in high-resolution imaging - resolving two targets which are closer than can be resolved with linear beamforming. In conventional narrowband high-resolution imaging, there must be three receiving elements in order to resolve the two sources. This example will show that this can be done with only two elements using two frequencies, given that the sources have proportional spectra. We will also illustrate how this method behaves when the sources have non-proportional spectra.

The array for this example has elements at $\{\pm\frac{\lambda_0}{4}\}$. Operating at the reference

frequency, the coarray support matrix is given by

$$\mathbf{C}(\omega_0) = \begin{bmatrix} 0 & -\frac{\lambda_0}{2} \\ \frac{\lambda_0}{2} & 0 \end{bmatrix}. \tag{2.50}$$

In order to resolve the two sources, we need to have a virtual array which has three elements. The virtual array will be constructed with elements at $\{-\frac{\lambda_0}{2}, 0, \frac{\lambda_0}{2}\}$, and the virtual coarray support matrix for this is given by

$$\tilde{\mathbf{C}}(\omega_0) = \begin{bmatrix} 0 & -\frac{\lambda_0}{2} & -\lambda_0 \\ \frac{\lambda_0}{2} & 0 & -\frac{\lambda_0}{2} \\ \lambda_0 & \frac{\lambda_0}{2} & 0 \end{bmatrix}. \tag{2.51}$$

To synthesize the effect of this matrix with the array we have, we need to generate the coarray points $\pm\lambda_0$. For this we will need a second frequency ω_1 to have $\alpha_1 = \frac{\lambda_0}{\frac{\lambda_0}{2}} = 2$, that is, $\omega_1 = 2\omega_0$. The coarray support matrix for frequency ω_1 is

$$\mathbf{C}(\omega_1) = \begin{bmatrix} 0 & -\lambda_0 \\ \lambda_0 & 0 \end{bmatrix}. \tag{2.52}$$

To construct the virtual correlation matrix, a map from the elements of $\mathbf{C}(\omega_0)$ and $\mathbf{C}(\omega_1)$ to the elements of $\tilde{\mathbf{C}}(\omega_0)$ needs to be found. The map is not unique, but one possible map is given by

$$\tilde{\mathbf{C}}(\omega_0) = \begin{bmatrix} \mathbf{C}(\omega_0)_{1,1} & \mathbf{C}(\omega_0)_{1,2} & \mathbf{C}(\omega_1)_{1,2} \\ \mathbf{C}(\omega_0)_{2,1} & \mathbf{C}(\omega_0)_{1,1} & \mathbf{C}(\omega_0)_{1,2} \\ \mathbf{C}(\omega_1)_{2,1} & \mathbf{C}(\omega_0)_{2,1} & \mathbf{C}(\omega_0)_{1,1} \end{bmatrix}, \tag{2.53}$$

where $\mathbf{C}(\omega_q)_{i,j}$ represents the $(i,j)^{th}$ element from the coarray support matrix corre-

sponding to the q^{th} frequency. Other possible maps include using any of the following in the zero coarray point positions (on the diagonal): $\mathbf{C}(\omega_0)_{1,1}$, $\mathbf{C}(\omega_0)_{2,2}$, $\mathbf{C}(\omega_1)_{1,1}$, $\mathbf{C}(\omega_1)_{2,2}$ or an average of these points [41].

Applying this map to the narrowband correlation matrices, $\mathbf{R}(\omega_0)$ and $\mathbf{R}(\omega_1)$, we get the virtual correlation matrix $\tilde{\mathbf{R}}(\omega_0)$

$$\tilde{\mathbf{R}}(\omega_0) = \begin{bmatrix} \mathbf{R}(\omega_0)_{1,1} & \mathbf{R}(\omega_0)_{1,2} & \mathbf{R}(\omega_1)_{1,2} \\ \mathbf{R}(\omega_0)_{2,1} & \mathbf{R}(\omega_0)_{1,1} & \mathbf{R}(\omega_0)_{1,2} \\ \mathbf{R}(\omega_1)_{2,1} & \mathbf{R}(\omega_0)_{2,1} & \mathbf{R}(\omega_0)_{1,1} \end{bmatrix}, \tag{2.54}$$

where $\mathbf{R}(\omega_q)_{i,j}$ represents the $(i,j)^{th}$ element from the narrowband correlation matrix at frequency ω_q.

To understand why proportional spectra is a requirement for the virtual correlation matrix to be useful, it is helpful to look at the virtual correlation matrix fully written out for the noiseless case:

$$\tilde{\mathbf{R}}(\omega_0) = \begin{bmatrix} 1 & \sum_k \bar{P}_k(\omega_0) e^{-jk_0 u_k \frac{\lambda_0}{2}} & \sum_k \bar{P}_k(\omega_1) e^{-jk_0 u_k \lambda_0} \\ \sum_k \bar{P}_k(\omega_0) e^{jk_0 u_k \frac{\lambda_0}{2}} & 1 & \sum_k \bar{P}_k(\omega_0) e^{-jk_0 u_k \frac{\lambda_0}{2}} \\ \sum_k \bar{P}_k(\omega_1) e^{jk_0 u_k \lambda_0} & \sum_k \bar{P}_k(\omega_0) e^{jk_0 u_k \frac{\lambda_0}{2}} & 1 \end{bmatrix} \tag{2.55}$$

where the sum is over $k = \{1, 2\}$. Note that the $(3,1)$ and the $(1,3)$ elements have the terms $\bar{P}_k(\omega_1)$ while the other elements have $\bar{P}_k(\omega_0)$. Recall that the $\{\bar{P}_k(\omega_q)\}$ are the normalized source powers. Had this correlation matrix been generated by a receive array with three elements at a single frequency ω_0, all of the elements would have contained only the $\{\bar{P}_k(\omega_0)\}$. Hence, $\tilde{\mathbf{R}}(\omega_0)$ will appear to have been generated by receiving narrowband radiation at the frequency ω_0 at the virtual array as if it

were the actual array, provided that

$$\sum_{k=1}^{2} \bar{P}_k(\omega_1) e^{jk_0 u_k \lambda_0} = \sum_{k=1}^{2} \bar{P}_k(\omega_0) e^{jk_0 u_k \lambda_0}, \tag{2.56}$$

which is the condition we derived more generally in Equations 2.46 and 2.47. The condition in Equation 2.56 is satisfied when

$$\bar{P}_1(\omega_0) = \bar{P}_1(\omega_1) \text{ and } \bar{P}_2(\omega_0) = \bar{P}_2(\omega_1) \tag{2.57}$$

or

$$\bar{P}_1(\omega_0) = \bar{P}_2(\omega_0) \text{ and } \bar{P}_1(\omega_1) = \bar{P}_2(\omega_1). \tag{2.58}$$

Equation 2.57 states that when the source-normalized source powers are equal, we can construct a valid virtual correlation matrix. Equation 2.58 states that when the actual source spectra are proportional, we also can construct a valid virtual correlation matrix. While it is not obvious that these conditions are equivalent, we have already discussed why they are equilvalent, see Appendix. This is simply an illustration of the condition derived for the general problem in Section 2.3.3.

Provided that the spectra of the sources are proportional, the virtual correlation matrix will appear to have come from a single frequency and as was shown in Section 2.2.3, it can be used in the high-resolution techniques.

2.4.1 Simulations

In this section, we will simulate two point sources in a noiseless environment. While a noiseless environment is not practical, it ensures that if a simulation fails, it is not due to noise, but to the imaging method used. The effect of noise will be discussed in a later section.

First we will illustrate how using just the narrowband correlation matrices does not work. Then we will simulate imaging when the sources have proportional spectra and use the virtual correlation matrix in a few different high-resolution techniques. Then it will be shown that when the spectra are not proportional, using the virtual correlation matrix yields incorrect results.

Spectral Estimate Using only a Narrowband Correlation Matrix

In this example, we are simulating two point sources at $u_1 = .3$ and $u_2 = .5$ with proportional spectra given by

$$\begin{aligned} P_1(\omega_0) = 0.5, \quad P_2(\omega_0) = 0.5 \\ P_1(\omega_1) = 0.5, \quad P_2(\omega_1) = 0.5. \end{aligned} \tag{2.59}$$

.

Using the narrowband correlation matrices in MUSIC, the results for each of the two frequencies, ω_0 and ω_1, are shown in Figure 2.3. In these figures, the peaks represent the estimated source locations and the stars represent the actual source locations. Figure 2.3(a) shows the results of MUSIC applied to the narrowband correlation matrix at ω_0. We see that only one source location is estimated and it is incorrect. Figure 2.3(b) shows the results of MUSIC applied to the narrowband correlation matrix at ω_1 and this estimates that there are two sources, both at incorrect locations. The source at $u = -.6$ is actually due to aliasing of the source incorrectly located at $u = 0.4$ since the array elements are spaced further than the Nyquist rate for frequency ω_1.

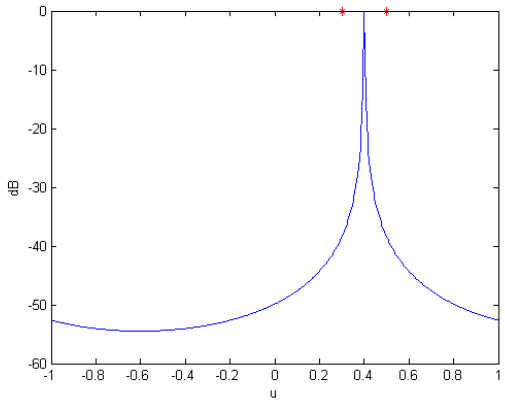

(a) Frequency ω_0, noiseless

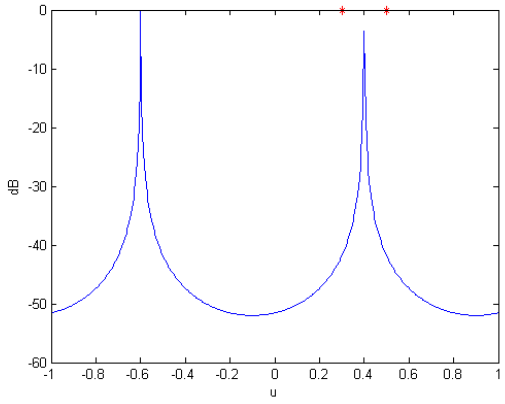

(b) Frequency ω_1, noiseless

Figure 2.3: MUSIC applied to the Narrowband Correlation Matrices

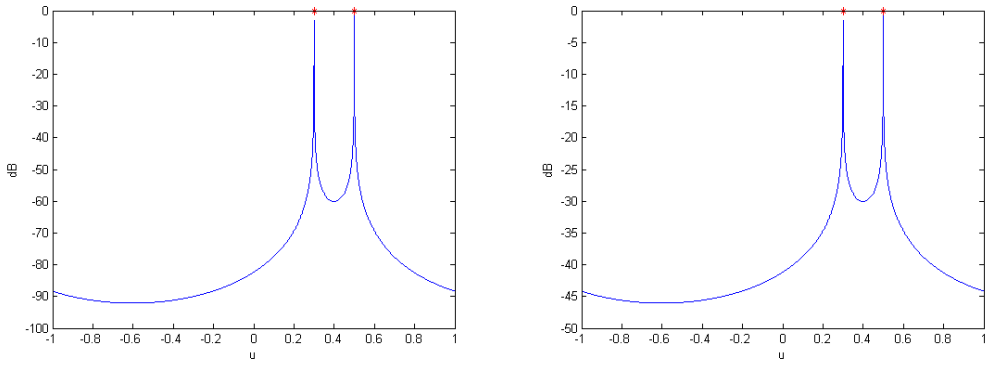

(a) Multiple Signal Classification (MUSIC), noiseless

(b) Auto-regressive (AR) spectral estimator, noiseless

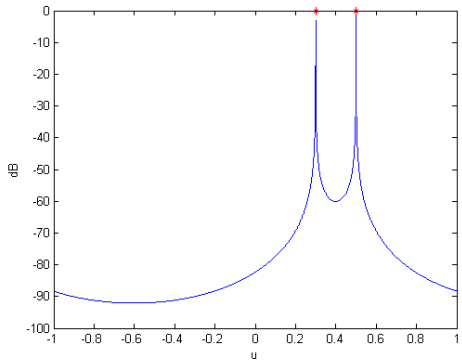

(c) Capon's minimum variance spectral estimator, noiseless

Figure 2.4: High-resolution Techniques applied to the Virtual Correlation Matrix - Proportional Spectra

Spectral Estimate Using the Virtual Correlation Matrix - Proportional Spectra

Keeping the proportional spectra given in Equation (2.59), in this example, we use the virtual correlation matrix in various high-resolution techniques. Shown in Figure 2.4 is the simulation of this example where MUSIC, AR spectrum estimation and Capon's minimum variance estimator are applied to the virtual correlation matrix. The dots represent the actual source locations.

For proportional spectra, the sources are located with accuracy according to the

expectations for the estimators used (see [42] for details on the performance of each estimator). This is expected since the virtual correlation matrix is identical to a narrowband correlation matrix that would have been formed by the virtual array.

Non-Proportional Spectra

When the spectra are not proportional, problems arise as the virtual correlation matrix does not have the structure necessary for high-resolution imaging. We now briefly examine the effects of non-proportional spectra for this example.

The same example is now simulated, but the source powers are changed so that the sources have non-proportional spectra. The source powers are

$$\begin{aligned} P_1(\omega_0) = 0.5, \quad P_2(\omega_0) = 0.5 \\ P_1(\omega_1) = 0.4, \quad P_2(\omega_1) = 0.6. \end{aligned} \tag{2.60}$$

None of the high-resolution methods are able to locate the two sources correctly as seen in Figure 2.5. MUSIC and AR behave similarly. They locate two sources, although in the wrong directions. Capon displays quite different behavior. It locates three sources, where two are approximately in the correct directions, and there is one extraneous source.

Possible ways to mitigate the effect of non-proportional spectra will be considered later in Section 2.5.

2.4.2 Relevance of the Two Source Scenario

The intent of this section was to clarify the method for constructing the virtual correlation matrix, how the virtual correlation matrix can be used successfully when the sources' spectra are proportional and to understand how it fails when they are

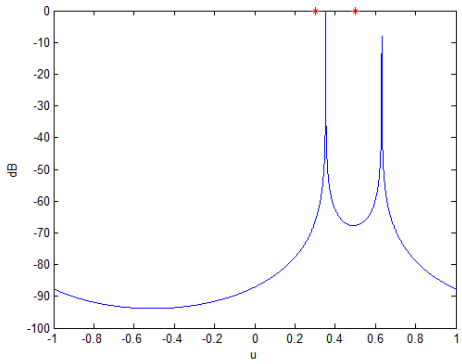

(a) Multiple Signal Classification (MUSIC), noiseless

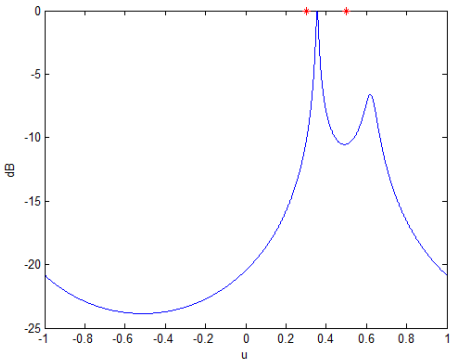

(b) Auto-regressive (AR) spectral estimator, noiseless

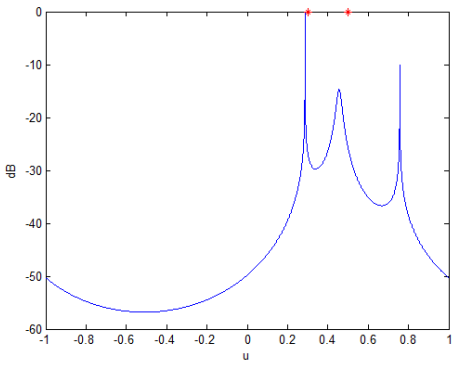

(c) Capon's minimum variance spectral estimator, noiseless

Figure 2.5: High-resolution Techniques applied to the Virtual Correlation Matrix - Non-Proportional Spectra

not proportional.

Since high-resolution estimators are non-linear, it is difficult to examine the effect of non-proportional spectra. This two-source, two-element example will also serve as a springboard to investigate possible ways to mitigate the effect of non-proportional spectra.

2.5 Working with Non-Proportional Spectra

It is difficult to analyze the effect of non-proportional spectra on the virtual correlation matrix. For example in MUSIC the peaks of the estimator are buried in the eigenvectors of the virtual correlation matrix. This is highly non-linear. In this section, starting within the context of the two-source, two-element example of Section 2.4, we first examine by simulation the sensitivity of the virtual correlation matrix to non-proportional spectra. Then we investigate possible ways to mitigate the effect of non-proportional spectra.

2.5.1 The Effect of Source Spacing and Non-proportionality on Estimation Error

In this simulation, we will examine the effect of source separation and amount of non-proportionality on the accuracy of source location. We will continue with the example of two sources and two elements in this section and vary the angle and the amount of non-proportionality between the sources. Consider two sources which are centered around broadside, $u_2 = -u_1$. The angular separation between the sources is $2u_1$. The amount of non-proportionality can be measured by the quantity δ where

$0 \leq \delta \leq 1$ and is defined as follows:

$$\begin{aligned} P_1(\omega_0) = .5, \quad P_2(\omega_0) = .5 \\ P_1(\omega_1) = .5(1-\delta), \quad P_2(\omega_1) = .5(1+\delta) \end{aligned} \tag{2.61}$$

If $\delta = 0$, the spectra are proportional. As δ increases to 1 the spectra become less proportional.

We will examine the total normalized error, which is defined as

$$\frac{|u_1 - \tilde{u}_1| + |u_2 - \tilde{u}_2|}{|u_1 - u_2|}, \tag{2.62}$$

where $\tilde{u}_k$ is the estimated location closest to the k^{th} source and u_k is the actual source location.

Figure 2.6 shows the total normalized error magnitude for the MUSIC estimator plotted against actual source separation and measure of non-proportionality. As expected, when the spectra are proportional ($\delta = 0$), there is no error in the estimates. However, we see that as the non-proportionality between the spectra , δ, increases, MUSIC with the virtual correlation matrix does not perform well. For sources that are very close together, the error is large. As sources get further apart, the error generally decreases. However, an interesting observation is that when sources are spaced exactly at an angular separation of 1, the error is zero. This occurs because the virtual correlation matrix that results from this spacing does not depend on the proportionality at all. For general δ, the virtual correlation matrix in this example

takes the form

$$\tilde{\mathbf{R}}(\omega_0) = \begin{bmatrix} 1 & \cos(\pi u_1) & \cos(2\pi u_1) + .5j\delta \sin(2\pi u_1) \\ \cos(\pi u_1) & 1 & \cos(\pi u_1) \\ \cos(2\pi u_1) - .5j\delta \sin(2\pi u_1) & \cos(\pi u_1) & 1 \end{bmatrix} \tag{2.63}$$

When $\sin(2\pi u_1) = 0$, δ is eliminated from the virtual correlation matrix, and thus has the effect of $\delta = 0$, or proportionality. This occurs when $u_1 = \frac{n}{2}$ for integer n.

For sources with proportional (or very close to proportional) spectra, MUSIC performs reasonably. Also if the sources are close to 1 angular unit apart, MUSIC performs reasonably, however, high-resolution imaging is generally not needed in this case to resolve the sources at this distance apart.

2.5.2 Forcing the Determinant of the Virtual Correlation Matrix to Zero

In this section, within the context of the two-source, two-element example, we will modify the virtual correlation matrix by a Hadamard (Schur or element-wise) product. The sources are assumed to have non-proportional spectra at the two frequencies, thus the virtual correlation matrix is not rank deficient. We are going to examine how we can use the Hadamard product on the virtual correlation matrix so that it becomes rank deficient, a necessary condition for a proper (noiseless) virtual correlation matrix.

We have narrowband correlation matrices $\mathbf{R}(\omega_0)$ and $\mathbf{R}(\omega_1)$ and from these have formed the virtual correlation matrix $\tilde{\mathbf{R}}(\omega_0)$. Since the $(3,1)$ and $(1,3)$ elements of the virtual correlation matrix in Equation (2.55) come from a different frequency, ω_1, compared to the other matrix elements, we will use a multiplicative scalar, $\beta = \beta_r + j\beta_i$

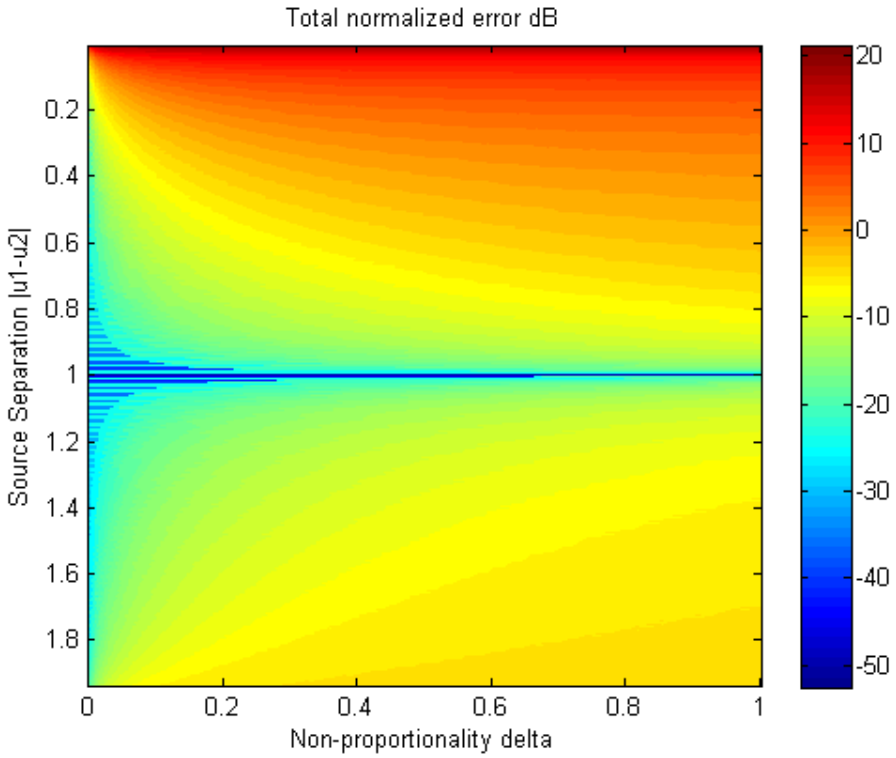

Figure 2.6: Total Normalized Error for MUSIC applied to the Virtual Correlation Matrix

and its conjugate $\beta^* = \beta_r - j\beta_i$, on these elements of the virtual correlation matrix, vary β and observe where the determinant of this new matrix is 0. The idea is to try to modify the ω_1 frequency contributions to make the virtual correlation matrix have the requisite zero-determinant. Let

$$\mathbf{T}(\beta) = \tilde{\mathbf{R}}(\omega_0) \odot (\mathbf{E_r} + \mathbf{E_i}), \tag{2.64}$$

where

$$\begin{aligned} \mathbf{E_r} &= \begin{bmatrix} \frac{1}{2} & \frac{1}{2} & \beta_r \\ \frac{1}{2} & \frac{1}{2} & \frac{1}{2} \\ \beta_r & \frac{1}{2} & \frac{1}{2} \end{bmatrix} \\ \mathbf{E_i} &= \begin{bmatrix} \frac{1}{2} & \frac{1}{2} & -j\beta_i \\ \frac{1}{2} & \frac{1}{2} & \frac{1}{2} \\ j\beta_i & \frac{1}{2} & \frac{1}{2} \end{bmatrix}. \end{aligned} \tag{2.65}$$

Here, the ω_0 frequency contributions are not modified (they are multiplied by unity) and the ω_1 frequency contributions are multiplied by $\beta = \beta_r + j\beta_i$ or $\beta^* = \beta_r - j\beta_i$. For simplification of notation, let $\tilde{\mathbf{R}}(\omega_0)_{2,1} = \tilde{\mathbf{R}}(\omega_0)_{3,2} = a$, $\tilde{\mathbf{R}}(\omega_0)_{3,1} = b$, then the determinant of $T(\beta)$ is given as

$$\det \mathbf{T}(\beta) = \det \begin{bmatrix} 1 & a^* & \beta^* b^* \\ a & 1 & a^* \\ \beta b & a & 1 \end{bmatrix} = 1 - 2|a|^2 + a^{*2} b\beta + a^2 b^* \beta^* - |\beta|^2 |b|^2. \tag{2.66}$$

Taking derivatives with respect to β_r and β_i, we get [43],

$$\begin{aligned}
\frac{\partial \det \mathbf{T}(\beta)}{\partial \beta_r} &= a^{*2}b + a^2 b^* - 2\beta_r^* |b|^2 \\
\frac{\partial \det \mathbf{T}(\beta)}{\partial \beta_i} &= ja^{*2}b - ja^2 b^* - 2\beta_i^* |b|^2 \\
\frac{\partial^2 \det \mathbf{T}(\beta)}{\partial \beta_r^2} &= -2|b|^2 \\
\frac{\partial^2 \det \mathbf{T}(\beta)}{\partial \beta_i^2} &= -2|b|^2 \\
\frac{\partial^2 \det \mathbf{T}(\beta)}{\partial \beta_r \partial \beta_i} &= 0.
\end{aligned} \tag{2.67}$$

The Hessian matrix, H, is negative definite:

$$H = \begin{bmatrix} \frac{\partial^2 \det \mathbf{T}(\beta)}{\partial \beta_r^2} & \frac{\partial^2 \det \mathbf{T}(\beta)}{\partial \beta_i \partial \beta_r} \\ \frac{\partial^2 \det \mathbf{T}(\beta)}{\partial \beta_r \beta_i \partial \beta} & \frac{\partial^2 \det \mathbf{T}(\beta)}{\partial \beta_i^2} \end{bmatrix} = \begin{bmatrix} -2|b|^2 & 0 \\ 0 & -2|b|^2 \end{bmatrix} \preceq 0 \tag{2.68}$$

Thus, $\det T(\beta)$ is concave in β_r and β_i, and there exists a β_c for which $\det \mathbf{T}(\beta)$ is maximized, [44, 45]. Also note that the first derivatives of $\det T(\beta)$ decrease with equal rate in each radial direction away from β_c.

Setting the first derivatives to zero and solving for β, the maximum occurs at

$$\beta_c = \frac{a^2}{b} \tag{2.69}$$

giving maximum determinant of

$$\det \begin{bmatrix} 1 & a^* & \beta_c^* b^* \\ a & 1 & a^* \\ \beta_c b & a & 1 \end{bmatrix} = \det \begin{bmatrix} 1 & a^* & a^{*2} \\ a & 1 & a^* \\ a^2 & a & 1 \end{bmatrix} = 1 - 2|a|^2 + |a|^4 = (|a|^2 - 1)^2 \geq 0 \tag{2.70}$$

We are not actually looking for where the determinant is maximized, but where the determinant is zero, as this is a necessary condition for having zero eigenvalues. Since $\det T(\beta_c)$ is always greater than or equal to zero and the function is concave, at some point as we move radially away from β_c, we will reach a value of β (call it β_0) that lies on a circle for which $\det T(\beta_0) = 0$. Thus, we search for solutions of the form $\beta_0 = \beta_c + re^{jx}$, where $x \in [0, 2\pi]$ and $r \geq 0$. With β_0 in place of β in the expression for determinant given by Equation 2.66, setting it equal to 0 and solving for r we get

$$\begin{aligned} 1 - 2|a|^2 + a^{*2}b(\beta_c + re^{jx}) + a^2b^*(\beta_c^* + re^{-jx})... \\ - (|\beta_c|^2 + r^2 + \beta_c re^{-jx} + \beta_c^* re^{jx})|b|^2 = 0 \\ r = \pm\frac{1 - |a|^2}{|b|}\forall x \end{aligned} \tag{2.71}$$

This means that the values of β which force the determinant to zero are given by

$$\beta_0 = \beta_c + re^{jx} = \frac{a^2}{b} + \frac{1 - |a|^2}{|b|}e^{jx}, x \in [0, 2\pi] \tag{2.72}$$

The determinant is 0 for β on a circle about point $\frac{a^2}{b}$ with radius $\frac{1-|a|^2}{|b|}$.

The values of β which force the determinant to zero lie in a circle, but which one of these points corresponds to the correct β giving us the correct source location? In Figure 2.7, 16 simulations are run for different values of x. These simulations suggest that the correct value of x corresponds to the x which estimates the sources to be the *least separated*. We see that the estimated source locations are the closest in angular distance to each other in, Figure 2.7(h), and this gives the correct source locations. The stars denote the actual source locations. This is supported by Figure 2.8 which plots the estimated source location separation versus x. Another observation is that the correct value of x minimizes the maximum eigenvalue of $\mathbf{T}(\beta_0)$ as is shown in Figure 2.9. Both Figures 2.8 and 2.9 are minimized at $x = 2.9829$.

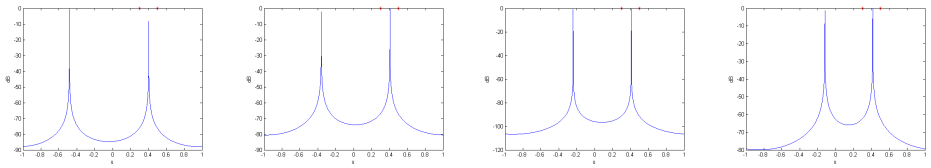

(a) $x = 0.2340$ (b) $x = 0.6267$ (c) $x = 1.0194$ (d) $x = 1.4121$

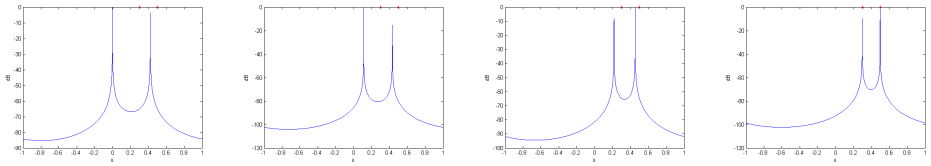

(e) $x = 1.8048$ (f) $x = 2.1975$ (g) $x = 2.5902$ (h) $x = 2.9829$

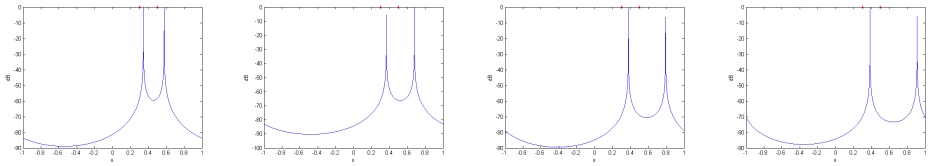

(i) $x = 3.3756$ (j) $x = 3.7683$ (k) $x = 4.1610$ (l) $x = 4.5537$

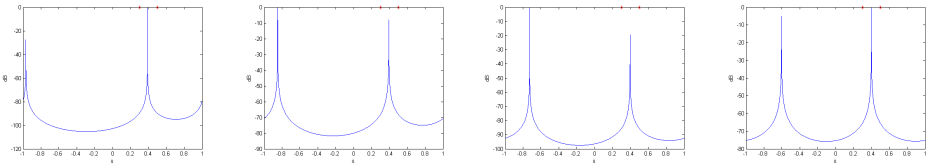

(m) $x = 4.9464$ (n) $x = 5.3391$ (o) $x = 5.7318$ (p) $x = 6.1245$

Figure 2.7: MUSIC applied to $T(\beta_0)$ for different e^{jx}

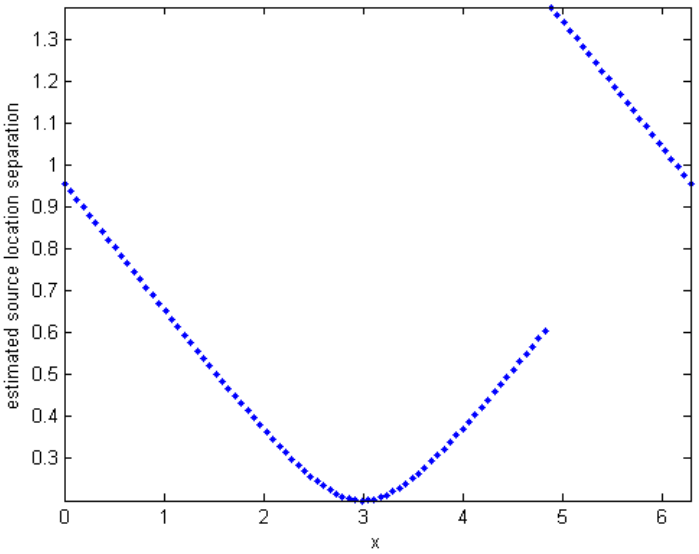

Figure 2.8: Separation of Estimated Source Locations vs. x

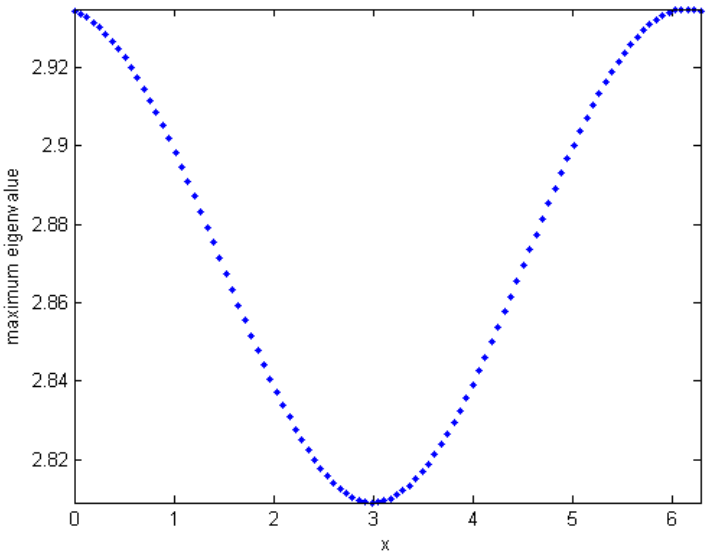

Figure 2.9: Maximum Eigenvalue of $\mathbf{T}(\beta_0)$ vs. x

This approach works well for this 3×3 virtual correlation matrix; however, as the dimension of the virtual correlation matrix increases, so does the number of variables such as β. The search for where the determinant is zero becomes more complicated, as the higher dimension surface $\det \mathbf{T}(\beta)$ may no longer be concave or convex. It is also unclear what the search criterion becomes on the subset where the determinant is zero.

2.5.3 Using Array Interpolation to Average Source Powers at Different Frequencies

In this part, we will investigate using an array interpolation method [19] which can help equalize non-proportional source spectra by averaging. This is first done for the two-element, two-source example, then it is shown how this can be extended to larger examples.

Suppose we know the sources we are trying to locate lie within some sector $[u_s, u_f]$. This could be known from generating a lower resolution image using Fourier beamforming methods. Interpolation matrices $\mathbf{B}_1(\omega_0)$ and $\mathbf{B}_0(\omega_1)$ can be found such that

$$\begin{aligned} \mathbf{B}_1(\omega_0)\mathbf{A}_\mathbf{R}(\omega_0) &\approx \mathbf{A}_\mathbf{R}(\omega_1) \\ \mathbf{B}_0(\omega_1)\mathbf{A}_\mathbf{R}(\omega_1) &\approx \mathbf{A}_\mathbf{R}(\omega_0). \end{aligned} \tag{2.73}$$

We do not know the array manifold matrices because they involve source locations, but since we know the sources lie within a sector we can approximate the array interpolation matrices by a least squares fit over the sector $[u_s, u_f]$ [19]. $\mathbf{B}_1(\omega_0)$ is found by minimizing

$$\int_{u_s}^{u_f} ||\mathbf{a}_\mathbf{R}(u, \omega_1) - \mathbf{B}_1(\omega_0)\mathbf{a}_\mathbf{R}(u, \omega_0)||^2 du \tag{2.74}$$

with respect to $\mathbf{B}_1(\omega_0)$, where $\mathbf{a_R}(u, \omega_q)$ is the array steering vector at frequency ω_q:

$$\mathbf{a_R}(u, \omega_q) = [e^{jk_q u x_{R1}}, e^{jk_q u x_{R2}}, ..., e^{jk_q u x_{RM}}]^T \tag{2.75}$$

To find $\mathbf{B}_1(\omega_0)$, we approximate the integral in Equation 2.74 by a summation taken over points in the sector. The sector is sampled N times and the matrices $\mathbf{A}_q$, $q = 0, 1$ are constructed as follows:

$$\mathbf{A}_q = \begin{bmatrix} \mathbf{a_R}(u_1, \omega_q)^H \\ \mathbf{a_R}(u_2, \omega_q)^H \\ \vdots \\ \mathbf{a_R}(u_i, \omega_q)^H \\ \vdots \\ \mathbf{a_R}(u_N, \omega_q)^H \end{bmatrix} \tag{2.76}$$

Here u_i is the i^{th} sample of the sector.

Assuming that $N \geq 2$ and that the matrices $\mathbf{A}_q$ each have full column rank, the least squares solution is given by [44].

$$\mathbf{B}_1(\omega_0) = \mathbf{A}_1^H \mathbf{A}_0 [\mathbf{A}_0^H \mathbf{A}_0]^{-1}. \tag{2.77}$$

Similarly,

$$\mathbf{B}_0(\omega_1) = \mathbf{A}_0^H \mathbf{A}_1 [\mathbf{A}_1^H \mathbf{A}_1]^{-1}. \tag{2.78}$$

Since the columns of the array manifold matrices are the array steering vector eval-

uated at source locations,

$$\begin{aligned}\mathbf{A_R}(\omega_0) &\approx \mathbf{B}_0(\omega_1)\mathbf{A_R}(\omega_1)\\ \mathbf{A_R}(\omega_1) &\approx \mathbf{B}_1(\omega_0)\mathbf{A_R}(\omega_0)\end{aligned} \tag{2.79}$$

in the least square error sense.

Using this, we can define "averaged" narrowband correlation matrices:

$$\begin{aligned}\bar{\mathbf{R}}(\omega_0) &= \frac{1}{2}[\mathbf{R}(\omega_0) + \mathbf{B}_0(\omega_1)\mathbf{R}(\omega_1)\mathbf{B}_0(\omega_1)^H]\\ &= \frac{1}{2}[\mathbf{A_R}(\omega_0)\bar{\mathbf{P}}(\omega_0)\mathbf{A_R}(\omega_0)^H + \mathbf{B}_0(\omega_1)\mathbf{A_R}(\omega_1)\bar{\mathbf{P}}(\omega_1)\mathbf{A_R}(\omega_1)^H\mathbf{B}_0(\omega_1)^H]\\ &\approx \frac{1}{2}[\mathbf{A_R}(\omega_0)\bar{\mathbf{P}}(\omega_0)\mathbf{A_R}(\omega_0)^H + \mathbf{A_R}(\omega_0)\bar{\mathbf{P}}(\omega_1)\mathbf{A_R}(\omega_0)^H]\\ &= \mathbf{A_R}(\omega_0)\frac{1}{2}[\bar{\mathbf{P}}(\omega_0) + \bar{\mathbf{P}}(\omega_1)]\mathbf{A_R}(\omega_0)^H\\ &= \mathbf{A_R}(\omega_0)\bar{\mathbf{P}}\mathbf{A_R}(\omega_0)^H\\ \bar{\mathbf{R}}(\omega_1) &= \frac{1}{2}[\mathbf{R}(\omega_1) + \mathbf{B}_1(\omega_0)\mathbf{R}(\omega_0)\mathbf{B}_1(\omega_0)^H]\\ &= \frac{1}{2}[\mathbf{A_R}(\omega_1)\bar{\mathbf{P}}(\omega_1)\mathbf{A_R}(\omega_1)^H + \mathbf{B}_1(\omega_0)\mathbf{A_R}(\omega_0)\bar{\mathbf{P}}(\omega_0)\mathbf{A_R}(\omega_0)^H\mathbf{B}_1(\omega_0)^H]\\ &\approx \frac{1}{2}[\mathbf{A_R}(\omega_1)\bar{\mathbf{P}}(\omega_1)\mathbf{A_R}(\omega_1)^H + \mathbf{A_R}(\omega_1)\bar{\mathbf{P}}(\omega_0)\mathbf{A_R}(\omega_1)^H]\\ &= \mathbf{A_R}(\omega_1)\frac{1}{2}[\bar{\mathbf{P}}(\omega_1) + \bar{\mathbf{P}}(\omega_0)]\mathbf{A_R}(\omega_1)^H\\ &= \mathbf{A_R}(\omega_1)\bar{\mathbf{P}}\mathbf{A_R}(\omega_1)^H\end{aligned} \tag{2.80}$$

Since these equalities are only approximate, the $\bar{\mathbf{P}}$ matrices in Equation 2.80 may not be exactly the same. To partially account for this, we will assume a further normalization in which we normalize the averaged correlation matrices such that the diagonal elements are approximately unity. This is done by multiplying each matrix

by $M = 2$ and dividing by its trace:

$$\begin{aligned} \bar{\mathbf{R}}(\omega_0) &\Leftarrow \frac{\bar{\mathbf{R}}(\omega_0)}{\frac{1}{2}\mathrm{Tr}\bar{R}(\omega_0)} \\ \bar{\mathbf{R}}(\omega_1) &\Leftarrow \frac{\bar{\mathbf{R}}(\omega_1)}{\frac{1}{2}\mathrm{Tr}\bar{R}(\omega_1)} \end{aligned} \tag{2.81}$$

This is simply a power normalization since $\frac{1}{2}\mathrm{Tr}\bar{R}(\omega_q) \approx \sum_{k=1}^{K} \bar{P}_k$.

These averaged correlation matrices have approximately the same diagonal power matrix $\bar{\mathbf{P}} = \frac{1}{2}[\bar{\mathbf{P}}(\omega_0) + \bar{\mathbf{P}}(\omega_1)]$, but maintain approximately the structure of two narrowband correlation matrices at frequencies ω_0 and ω_1. Thus, they can be assumed to satisfy the criterion in Section 2.3.3 to construct a valid virtual correlation matrix.

To illustrate the potential of this method, we will simulate the case where we have two sources being observed by the array $\pm\frac{\lambda_0}{4}$ and use two frequencies ω_0 and $\omega_1 = 2\omega_0$. The sources are located at $u_1 = .2$ and $u_2 = .3$. The source powers are

$$\begin{aligned} P_1(\omega_0) = 0.5, \quad P_2(\omega_0) = 0.5 \\ P_1(\omega_1) = 0.4, \quad P_2(\omega_1) = 0.6. \end{aligned} \tag{2.82}$$

The sector is taken to be $[.1, .4]$ and we will take 100 uniformly spaced samples of the sector. The result using the virtual correlation matrix constructed from the averaged matrices is shown in Figure 2.10. The estimated source locations and very close to the actual source locations despite the non-proportional source spectra. The actual source locations are denoted by red stars.

This method appears to be sensitive to sector size. If a larger sector is chosen, it becomes more difficult to satisfy Equation 2.73 exactly. The same simulation is run in Figure 2.11, except the sector is increased to $[-.4, .9]$. The estimated source locations are not close to the actual source locations. However, they are still much

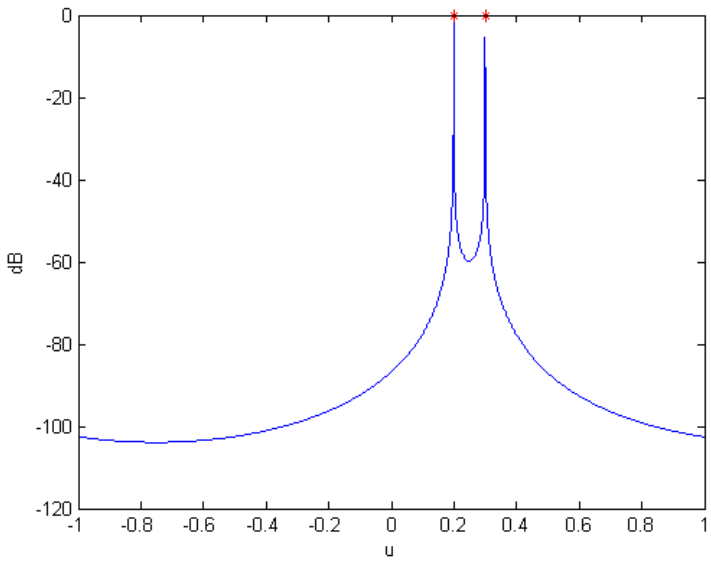

Figure 2.10: MUSIC using Virtual Correlation Matrix constructed from Array-Interpolated Correlation Matrices. Sector [0.1,0.4]

more accurate than without any sort of averaging, see Figure 2.12.

For a small enough sector, this may be a viable method for larger problems with more sources and elements. If Q frequencies are needed to construct the virtual correlation matrix, then $Q^2 - Q$ array interpolation matrices are found as in Equation 2.77:

$$\mathbf{B}_q(\omega_p) = \mathbf{A}_q^H \mathbf{A}_p [\mathbf{A}_p^H \mathbf{A}_p]^{-1}, \text{ for } p \neq q. \tag{2.83}$$

Then Q averaged correlation matrices can be formed,

$$\bar{\mathbf{R}}(\omega_q) = \frac{1}{Q}[\mathbf{R}(\omega_q) + \sum_{p \neq q} \mathbf{B}_q(\omega_p)\mathbf{R}(\omega_p)\mathbf{B}_q(\omega_p)^H], \tag{2.84}$$

and used to construct the virtual correlation matrix.

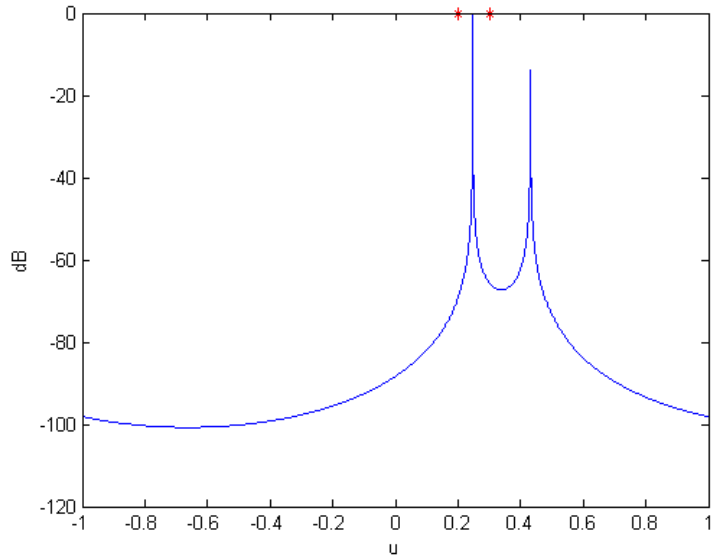

Figure 2.11: MUSIC using Virtual Correlation Matrix constructed from Array-Interpolated Correlation Matrices. Sector [-0.4,0.9]

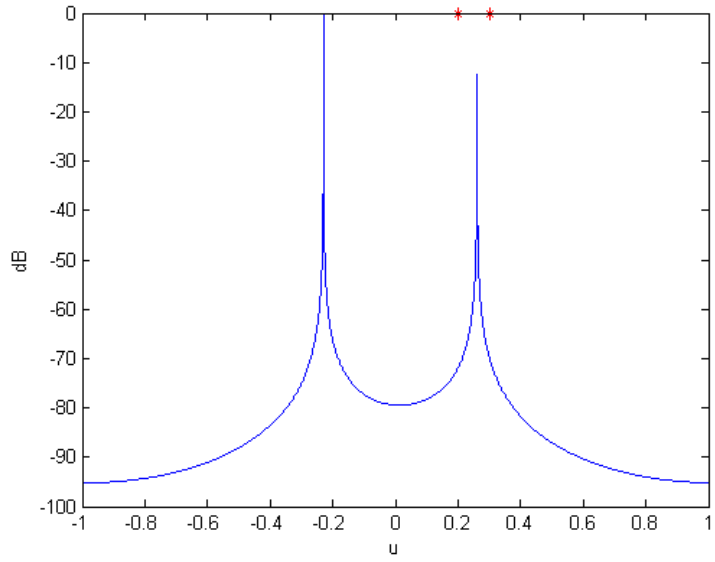

Figure 2.12: MUSIC using Virtual Correlation Matrix constructed from Original Narrowband Correlation Matrices

2.5.4 Weighting the Array Elements to Overcome the Effect of Non-proportional Spectra

We will now consider an alternative approach in which the array elements are weighted at frequency ω_1 in order to attempt to compensate for the non-proportional spectra in the two-element example. A weight w_1 is applied to one array element and w_2 is applied to the other. The element weight is applied to the received complex amplitude from that element.

This weighting can be expressed as multiplication of the array correlation matrices with a diagonal matrix $\mathbf{W} = \text{diag}[w_1, w_2]$. Recall that the actual correlation matrices for the unweighted elements in the absence of noise are

$$\begin{aligned} \mathbf{R}(\omega_0) &= \mathbf{A_R}(\omega_0)\bar{\mathbf{P}}(\omega_0)\mathbf{A_R}(\omega_0)^H \\ \mathbf{R}(\omega_1) &= \mathbf{A_R}(\omega_1)\bar{\mathbf{P}}(\omega_1)\mathbf{A_R}(\omega_1)^H. \end{aligned} \tag{2.85}$$

The weighted correlation matrix at frequency ω_1 is

$$\mathbf{R_w}(\omega_1) = \mathbf{W}\mathbf{A_R}(\omega_1)\bar{\mathbf{P}}(\omega_1)\mathbf{A_R}(\omega_1)^H\mathbf{W}^H = \mathbf{W}\mathbf{R}(\omega_1)\mathbf{W}^H. \tag{2.86}$$

Since our objective is to force $\mathbf{R_w}(\omega_1)$ to appear to have been generated by sources with the same powers at frequency ω_0, it is useful to know what our desired correlation matrix for frequency ω_1 is. We will call this matrix $\mathbf{R_{ref}}(\omega_1)$. Note that we do not actually have access to this matrix for this method because we do not know the source locations, it is simply for comparison in this study.

$$\mathbf{R_{ref}}(\omega_1) = \mathbf{A_R}(\omega_1)\bar{\mathbf{P}}(\omega_0)\mathbf{A_R}(\omega_1)^H \tag{2.87}$$

If the method works, $\mathbf{R_w}(\omega_1)$ should equal $\mathbf{R_{ref}}(\omega_1)$.

To study this proposed method, we will use specific numerical results. We assume there are receiving array elements at $\pm\frac{\lambda_0}{4}$, two sources at 0.2 and 0.3 with powers $P_1(\omega_0) = .5, P_2(\omega_0) = .5, P_1(\omega_1) = .4, P_2(\omega_0) = .6$, and the frequencies ω_0 and $\omega_1 = 2\omega_0$ are used.

The narrowband correlation matrix at ω_0 is given by

$$\mathbf{R}(\omega_0) = \begin{bmatrix} 1 & .6984 - .6984j \\ .6984 + .6984j & 1 \end{bmatrix}, \tag{2.88}$$

and for ω_1 is given by

$$\mathbf{R}(\omega_1) = \begin{bmatrix} 1 & .0618 - .9511j \\ .0618 + .9511j & 1 \end{bmatrix}. \tag{2.89}$$

Had we actually observed the narrowband correlation matrix at ω_1 with spectra $P_1(\omega_1) = .5, P_2(\omega_1) = .5$, the narrowband correlation matrix would have been

$$\mathbf{R_{ref}}(\omega_1) = \begin{bmatrix} 1 & .9511j \\ .9511j & 1 \end{bmatrix}. \tag{2.90}$$

Our goal is to find $\mathbf{W}$ such that $\mathbf{R_w}(\omega_1)$ appears to have been generated by sources of the same power as at frequency ω_0, i.e. $\mathbf{R_w}(\omega_1) = \mathbf{R_{ref}}(\omega_1)$.

Since the source locations and powers are not known, we cannot directly solve for $\mathbf{W}$. Therefore, we propose a method based on the observation in Section 2.5.2, that the virtual correlation matrix which yields least-separated source locations gives the correct virtual correlation matrix. This is simply an approach based on this observation, but it appears to work for this small example.

We restrict the weights to have unit power and to be complex conjugates of each

other. The unit power assumption is reasonable because we do not want to attenuate what is received at one element compared to the other. The complex conjugate assumption is reasonable because it reduces our search parameter from two (w_1 and w_2) to one (ϕ, where $w_1 = w_2^* = e^{j\pi\phi}$). Since the weights can be applied after the correlation matrix is formed, what matters is the phase between the weights, not their absolute phases, and this is why we can assume the weights are complex conjugates of each other.

We will use an iterative process. Starting from an initial ϕ_0, the virtual correlation matrix is constructed from $\mathbf{R}(\omega_0)$ and $\mathbf{R_w}(\omega_1)$. We measure the angular separation between the source location estimates using a high-resolution technique applied to the virtual correlation matrix. Call this separation δu_0.

For the first iteration, ϕ_0 is changed by a small amount to give $\phi_1 = \phi_0 + \delta\phi_0$. The virtual correlation matrix is constructed using ϕ_1, used in the high-resolution technique, and the angular separation is measured again. Call it δu_1.

For the second iteration, $\phi_2 = \phi_1 + \delta\phi_1$. The change in ϕ is based on the change in separation between the last two iterations. $\delta\phi_1 \propto \delta u_0 - \delta u_1$. ϕ_2 changes based on the change in separation. If the separation becomes smaller, we continue to increase ϕ. If it becomes larger, ϕ is decreased.

In general, for the i^{th} iteration, $\phi_i = \phi_{i-1} + a(\delta u_{i-2} - \delta u_{i-1})$, where a is a positive user-specified constant controlling the magnitude of change in ϕ from the previous iteration. The iterations continue until the change in separation is sufficiently small, i.e.,

$$|\delta u_i - \delta u_{i-1}| < \epsilon. \tag{2.91}$$

For our example, we start by plotting the MUSIC estimate when there is no weighting, $\phi = 0$. This is shown in Figure 2.13(a). Then a small change in the

i	ϕ_i	δu_i
0	0	.5760
1	.005	.3594
2	.01	.1014
3	.15	.3364
4	.0125	.1982
5	.01125	.1244
6	.010625	.1014
7	.0103125	.0967

Table 2.1: Iteration Results

angle of the weights is tried, $\delta\phi_0 = .005$. $w_1 = w_2^* = e^{j\pi.005}$, and the estimate using this virtual correlation matrix is shown in Figure 2.13(b). The iteration is continued until the separation from one iteration changes by less than some small number, say $\epsilon = 5 \times 10^{-3}$ for this example. The results are summarized in the Table 2.1 and the MUSIC estimates are plotted in Figure 2.13.

The weighting found is $w_1 = e^{j\pi.0103125}, w_2 = e^{-j\pi.0103125}$ and we see in Figure 2.13(h) that the estimated source locations are very close to the actual source locations.

The matrix $\mathbf{R_w}(\omega_1)$ corresponding to $\phi = .0103125$ is

$$\mathbf{R_w}(\omega_1) = \begin{bmatrix} 1 & -.0002 - .9531j \\ -.0002 + .9531j & 1 \end{bmatrix}. \tag{2.92}$$

This is quite close to $\mathbf{R_{ref}}(\omega_1)$ given in Equation 2.90.

This method may be a viable option for a two source example. Extending to more than two sources may be a problem since the search criterion is unclear. Also, as the number of array elements increases, the search space dimension would also increase.

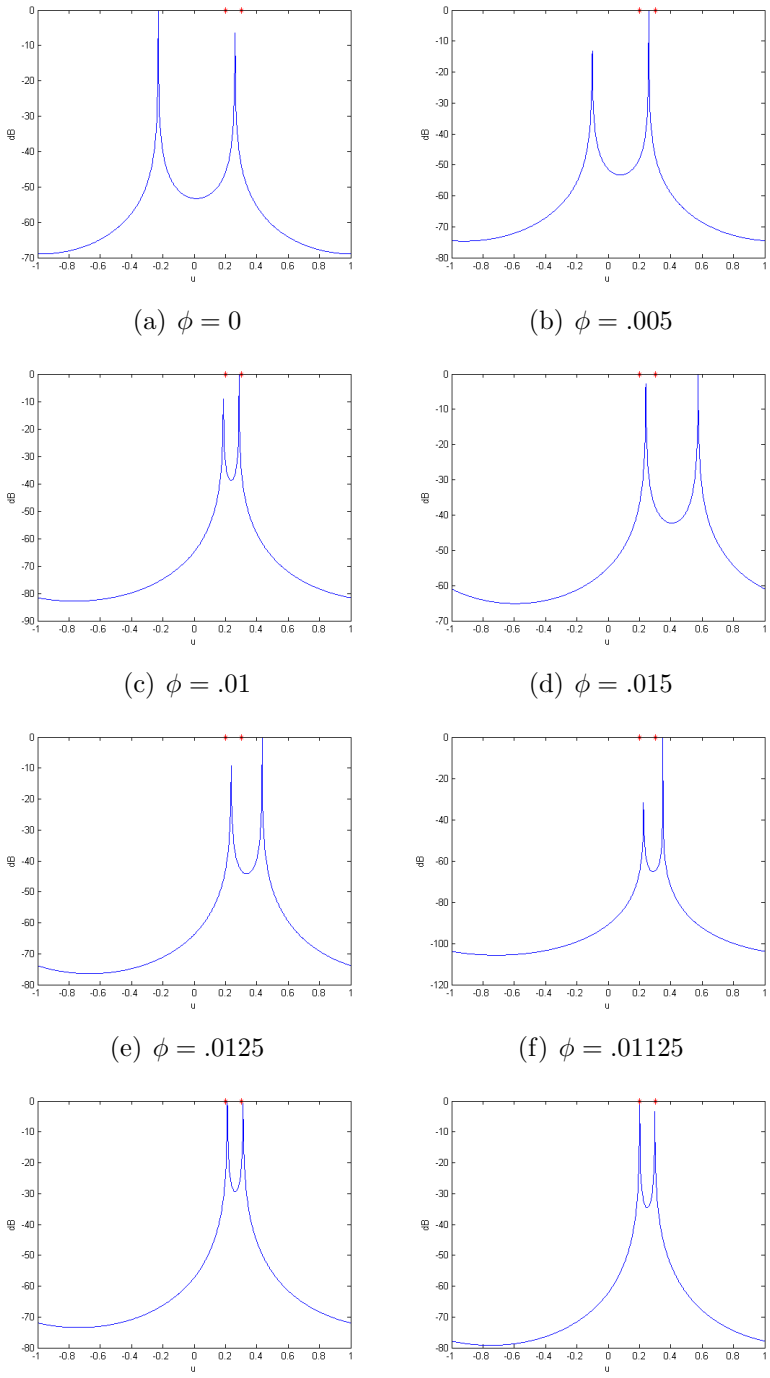

(a) $\phi = 0$ (b) $\phi = .005$

(c) $\phi = .01$ (d) $\phi = .015$

(e) $\phi = .0125$ (f) $\phi = .01125$

(g) $\phi = .010625$ (h) $\phi = .0103125$

Figure 2.13: MUSIC estimates for iterations

2.6 Effect of Noise on the Virtual Correlation Matrix

In the previous examples, the simulations were performed without noise to illustrate that the method ideally works, but in more realistic simulations, noise must be included as it is inevitable in practice.

As is shown in Equations 2.56-2.58, the condition for the virtual matrix to be useful is that the sources must satisfy

$$\bar{P}_k(\omega_q) = \bar{P}_k(\omega_0) \text{ for all } q, k. \tag{2.93}$$

When this equation is examined in detail, we find that the noise power plays a role in the normalized powers:

$$\begin{aligned} \bar{P}_k(\omega_q) &= \frac{P_k(\omega_q)}{\sum_{l=1}^{K} P_k(\omega_q) + \sigma^2(\omega_q)} \\ \bar{P}_k(\omega_0) &= \frac{P_k(\omega_0)}{\sum_{l=1}^{K} P_k(\omega_0) + \sigma^2(\omega_0)} \end{aligned} \tag{2.94}$$

For high SNR,

$$\begin{aligned} \bar{P}_k(\omega_q) &\approx \frac{P_k(\omega_q)}{\sum_{l=1}^{K} P_k(\omega_q)} \\ \bar{P}_k(\omega_0) &\approx \frac{P_k(\omega_0)}{\sum_{l=1}^{K} P_k(\omega_0)}. \end{aligned} \tag{2.95}$$

In the case of high SNR, provided that the sources' spectra are proportional, then Equation 2.93 is satisfied. Since both the source powers and noise powers may vary over frequency, a problem may occur when the noise power is significant and varies over frequency. If this occurs, even with proportional spectra, Equation 2.93 may

not be satisfied because the difference in noise power over frequency may cause the normalized spectra to be non-proportional. This will be examined in the example in Section 2.7.

Another issue with noise arises when constructing the virtual correlation matrix. Recall that the map from the narrowband correlation matrices to the virtual correlation matrix is not unique. In Equation 2.54 from the previous example, the zero-coarray points (on the diagonal) were all chosen to come from the same frequency. However, the diagonal elements could have been chosen to come from narrowband correlation matrices at a different frequencies. If the normalized noise powers varied over frequency, the effective noise matrix for the virtual correlation matrix would no longer be a scaled identity. This can cause problems with source location estimation since these estimators assume spatially white noise. Special care should be taken when choosing the map such that the effective noise correlation matrix is a scaled identity. This can be achieved by either choosing all of the zero coarray points in the virtual correlation matrix from the same narrowband correlation matrix at a single frequency or taking an average of correlation data at all zero coarray points over all frequencies and using this in the zero-coarray point positions in the virtual correlation matrix. The latter may yield better statistical results since more points are used, as is suggested in [41]. However, since we are dealing with normalized correlation matrices and ideally the diagonal of all of the narrowband and virtual correlation matrices should be unity, it may be reasonable to just set all of the diagonal elements to unity and avoid this problem all together.

If this step is taken with the zero coarray points, for high enough SNRs, then the effect of noise on the high-resolution techniques will have the same characteristics of the techniques applied in the traditional setting and we do not need extra consideration for noise using the virtual correlation matrix.

2.7 Additional Examples

In this section, we will give additional examples with different array configurations and available bandwidths. Noise will also be taken into consideration.

2.7.1 Example: Three-Element Uniform Linear Array

In this example, we will study a three-element uniform linear array. Using conventional high-resolution imaging methods, this array can resolve at most two point sources. The array elements are at positions $\{-1, 0, 1\}\frac{\lambda_0}{2}$ and the coarray is $\{-2, -1, 0, 1, 2\}\frac{\lambda_0}{2}$. This example will be similar to the example presented in the previous section as it also has a uniform linear coarray, so we do not need to fill in coarray points but we use additional frequencies to extend the coarray. The coarray points $\pm 3\frac{\lambda_0}{2}$ can be included by using the frequency $\omega_1 = 1.5\omega_0$.

Now the augmented coarray is $\{-3, -2, -1, 0, 1, 2, 3\}\frac{\lambda_0}{2}$ corresponding to the four element array $\{-1.5, -.5, .5, 1.5\}\frac{\lambda_0}{2}$. Up to three point sources with proportional spectra can be resolved with this virtual array.

Simulations were run for various signal-to-noise ratios and spacing between the sources. The following high-resolution techniques were applied to the resulting virtual correlation matrices: MUltiple SIgnal Classification (MUSIC), Auto-Regressive (AR) spectrum estimator and Capon's minimum variance spectrum estimator. The results are shown in Figures 2.14-2.19. The simulations were performed using 1000 snapshots to create the narrowband correlation matrices. Sources at both frequencies have equal powers.

In general, accuracy of the estimated location of the sources decreases as the sources becomes more closely spaced together (see the progression from Figure 2.14 to 2.19) and also as the signal-to-noise ratio (SNR) decreases (from top to bottom

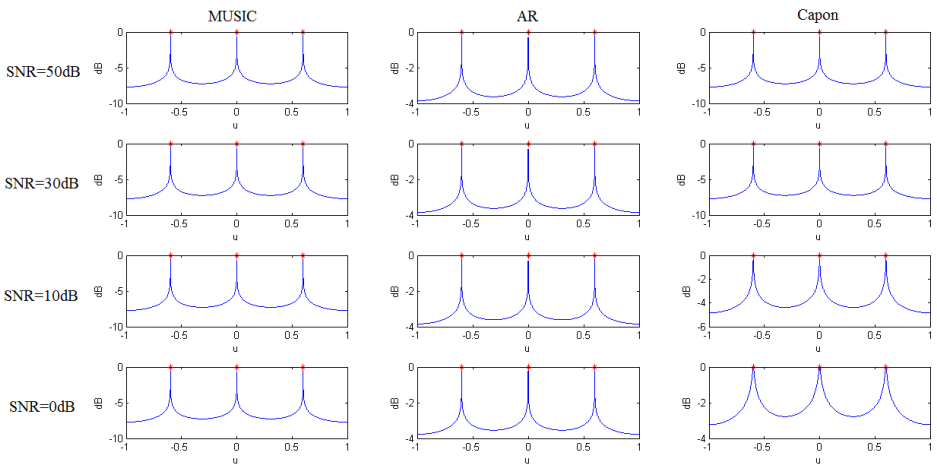

Figure 2.14: Three-element Uniform Linear Array - Source locations u = [-0.6 0 0.6]

of each figure). MUSIC performs the best of the estimators used here. It is the last to degrade with decreasing SNR and source separation. Capon's minimum variance estimator performs the worst as it is the first to degrade with both decreasing SNR and source separation. This is consistent with the performance given in the literature [42] and is expected because when the sources have proportional spectra, the virtual correlation matrix appears to have actually come from the virtual array at a single frequency.

It was stated in Section 2.6 that for low SNRs, problems may arise with normalization when the SNRs vary over frequency. We will examine this by simulation. In Figure 2.15 with equal SNRs at both frequencies, MUSIC has no problem resolving the sources at any of the SNRs. Figure 2.20 simulates the same example except the SNR at ω_0 is 40 dB and at ω_1 is 20 dB. Here, even though there is a large discrepancy in the SNRs, they are high enough that there is no problem with source location. Figure 2.21 shows the results of MUSIC when the SNR at ω_0 is 20 dB and at ω_1 is 10 dB. There is a small amount of error in the source location estimates. In Figure

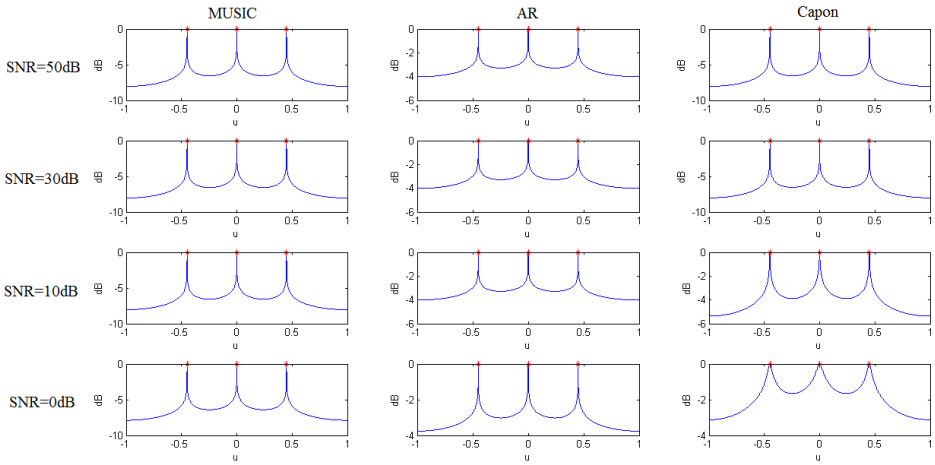

Figure 2.15: Three-element Uniform Linear Array - Source locations u = [-0.45 0 0.45]

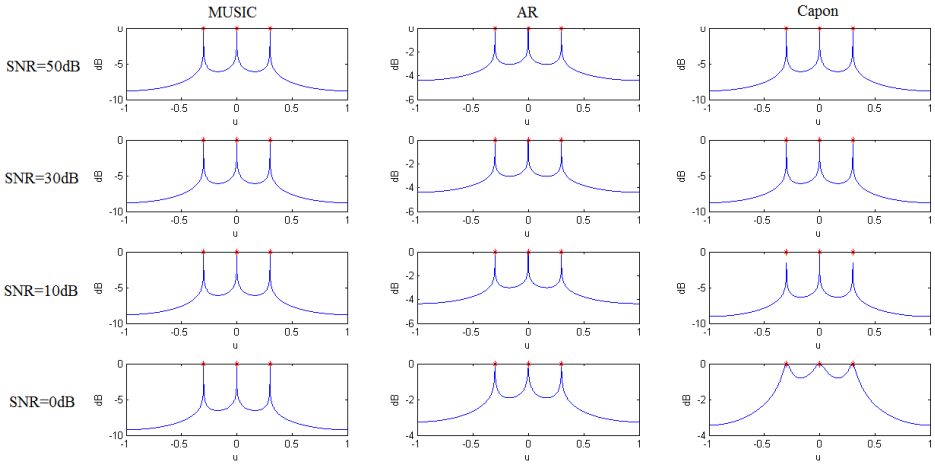

Figure 2.16: Three-element Uniform Linear Array - Source locations u = [-0.3 0 0.3]

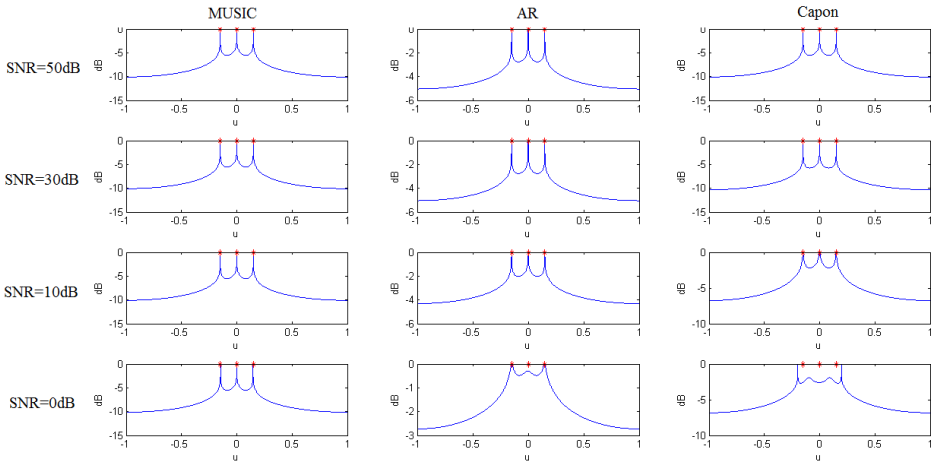

Figure 2.17: Three-element Uniform Linear Array - Source locations u = [-0.15 0 0.15]

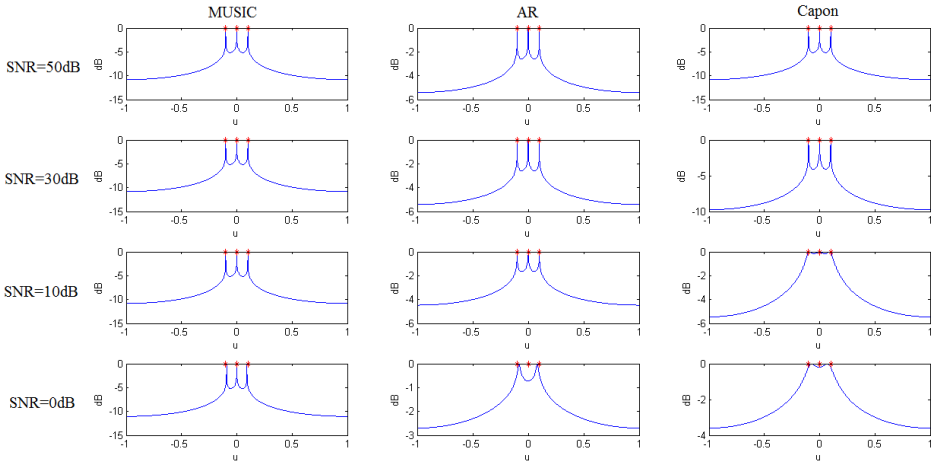

Figure 2.18: Three-element Uniform Linear Array - Source locations u = [-0.1 0 0.1]

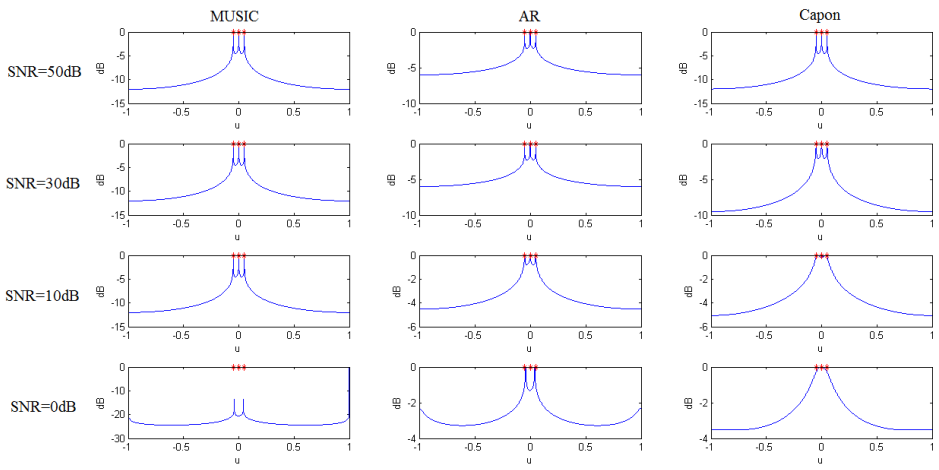

Figure 2.19: Three-element Uniform Linear Array - Source locations u = [-0.05 0 0.05]

2.22, the results are plotted for when the SNR at ω_0 is 0 dB and at ω_1 is 10 dB. There is significant error in the source location estimates. These problems arise at low SNRs because the assumption in Equation 2.14 can no longer be made. Even if the source spectra are proportional, the large noise variance skews the proportionality when normalized.

If the available bandwidth permitted, a third frequency, $\omega_2 = 2\omega_0$ could be used to give the augmented coarray $\{-4,-3,-2,-1,0,1,2,3,4\}\frac{\lambda_0}{2}$ and yield the virtual array $\{-2,-1,0,1,2\}\frac{\lambda_0}{2}$ with which up to four sources with proportional spectra could be resolved.

Comment on General Uniformly Spaced Arrays

In general, for a $\frac{\lambda_0}{2}$-uniformly-spaced linear array with M elements, the $2M-1$ element coarray at the reference frequency ranges from $-(M-1)\frac{\lambda_0}{2}$ to $(M-1)\frac{\lambda_0}{2}$. To extend the coarray by using multiple frequencies to include the points $\pm(M+l)\frac{\lambda_0}{2}$, $l = 1, 2, ...$, the bandwidth available needs to include the frequency $\omega_l = \alpha_l\omega_0$ where

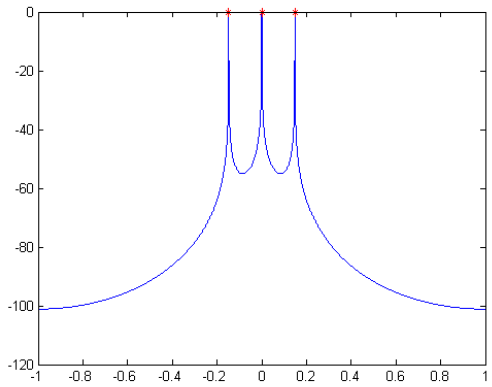

Figure 2.20: Three-element Uniform Linear Array - $\text{SNR}(\omega_0) = 40dB, \text{SNR}(\omega_1) = 20dB$

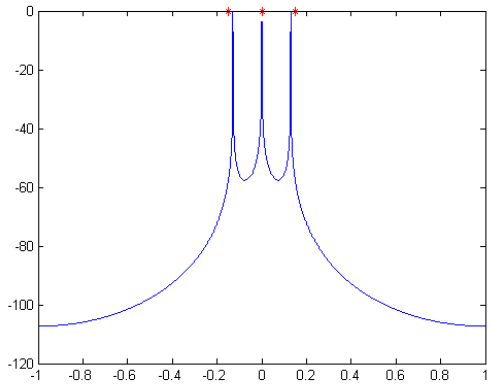

Figure 2.21: Three-element Uniform Linear Array - $\text{SNR}(\omega_0) = 20dB, \text{SNR}(\omega_1) = 10dB$

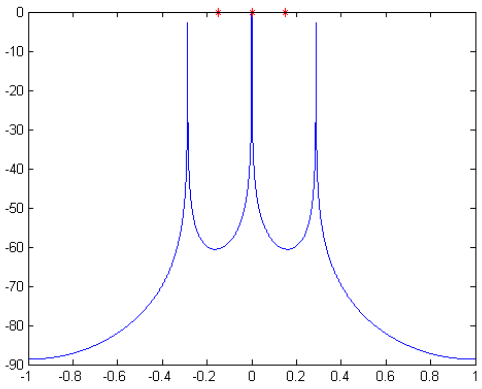

Figure 2.22: Three-element Uniform Linear Array - $\text{SNR}(\omega_0) = 0dB, \text{SNR}(\omega_1) = 10dB$

$\alpha_l = \frac{M-1+l}{M-1}$. When the frequency $\omega_l = \alpha_l \omega_0$ is used, the coarray points $\pm(M-1)\frac{\lambda_0}{2}$ (at the reference frequency) are dilated to the points $\pm\alpha_l(M-1)\frac{\lambda_0}{2} = \pm(M-1+l)\frac{\lambda_0}{2}$.

Examining the expression for α_1, as M increases, less bandwidth is needed to include the next extra coarray point in a uniform linear coarray.

$$\begin{aligned} \text{Bandwidth for extra coarray point } &= |\omega_1 - \omega_0| = |\alpha_1 - 1|\omega_0 \\ &= \left| \frac{M}{M-1} - 1 \right| \omega_0 \to 0 \text{ as } M \text{ increases} \end{aligned} \tag{2.96}$$

This means for larger arrays, it is less expensive in terms of bandwidth to resolve an extra point source.

2.7.2 Example: Five-Element Non-Uniform Linear Array

Much attention has been given to "fully-augmentable arrays" - those arrays which produce a uniformly spaced coarray [15, 21, 41]. When arrays are only partially-augmentable (not fully-augmentable), [22] develops a convex optimization technique to fill in the missing coarray points.

With our technique, for sources with proportional spectra, partially-augmentable arrays can be filled in by using multiple frequencies. Also, as in the previous examples, the multiples frequencies can be used to extend the length of the coarray.

Borrowing portions of an example from [22] to show how our techniques extends array capabilities, consider a five element non-uniformly spaced linear array with elements at

$$\{x_{Rn}\} = \{0, 1, 4, 9, 11\}\frac{\lambda_0}{2}. \tag{2.97}$$

The sources are wideband incoherent sources and they can be assumed to have proportional spectra in the band [1,1.2] GHz. They may be emitting in a wider band than this, but we are assuming this is the band our array elements can receive. With this array using conventional high-resolution imaging techniques, four sources can be resolved.

The narrowband coarray at the reference frequency is given by

$$\begin{aligned}\{y_l\} = \{&-11, -10, -9, -8, -7, -5, -4, -3, -2, -1, ... \\ &0, 1, 2, 3, 4, 5, 7, 8, 9, 10, 11\}\frac{\lambda_0}{2}.\end{aligned} \tag{2.98}$$

The coarray points $\pm 6\frac{\lambda_0}{2}$ are missing, which means that it does not produce a uniform linear coarray and cannot be arranged in such a way that it appears to have come from a uniform linear array [15, 21]. In [22], Toeplitz matrix completion is used to fill-in the missing coarray points, yielding a matrix which is almost coarray equivalent to a 12 element uniformly spaced linear array, and thus up to 11 sources can be resolved. In our method with sources of proportional spectra, we use extra frequencies to obtain these coarray points. Without using any extra bandwidth beyond what was used to fill in the missing coarray points, a few extra coarray points to extend the coarray length can be obtained as well. Then by creating a virtual correlation matrix, it is

possible to resolve up to 13 sources.

If data from the frequencies

$$f_q = \{1, \frac{13}{11}, 1.2\}\omega_0 \tag{2.99}$$

are used then the multi-frequency coarray becomes

$$\begin{aligned} &\bigcup_{q=0}^{2} \alpha_q \{0, \pm 1, \pm 2, \pm 3, \pm 4, \pm 5, ... \\ &\qquad ..., \pm 7, \pm 8, \pm 9, \pm 10, \pm 11\} \frac{\lambda_0}{2} \\ &\supset \{0, \pm 1, \pm 2, \pm 3, \pm 4, \pm 5, \pm 6, \pm 7, ... \\ &\qquad ..., \pm 8, \pm 9, \pm 10, \pm 11, \pm 12, \pm 13\} \frac{\lambda_0}{2} \\ &= \{\tilde{y}_l\} \end{aligned} \tag{2.100}$$

where $\alpha_q = \frac{f_q}{f_0} \in \{1, \frac{13}{11}, 1.2\}$. The subset $\{\tilde{y}_l\}$ of the multi-frequency coarray appears to have come from a virtual array

$$\{\tilde{x}_{Rn}\} = \{0, 1, 2, 3, 4, 5, 6, 7, 8, 9, 10, 11, 12, 13\} \frac{\lambda_0}{2}. \tag{2.101}$$

Thus the narrowband correlation matrices can be arranged into a 14×14 virtual correlation matrix. Since the sources are assumed to have proportional spectra, this virtual correlation matrix appears to have come exactly from the virtual array and up to 13 sources can be resolved.

Figures 2.23-2.25 show the simulation results from this example. This simulation behaves much like the previous example. The 13 sources can be resolved when they are not too close together and the SNR is not too low, though these simulations

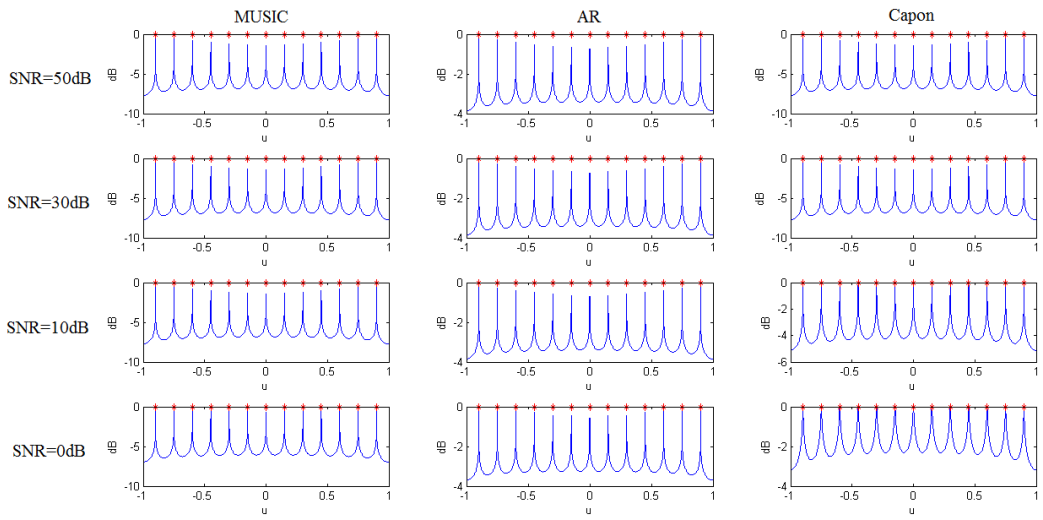

Figure 2.23: Five-element Non-uniform Linear Array - Spacing between elements: .15

are slightly more sensitive than the three source example because there are many more sources. From a 5 element array, up to 13 sources can be resolved within the limitations of the high-resolution technique used.

It is interesting to note that linear beamforming is almost at it's resolution threshold when the spacing is at about .15 between sources. High-resolution techniques with virtual arrays allow us to resolve sources that are more closely spaced together without additional array elements.

2.8 Conclusion

It was shown in this chapter that the effect of a larger array can be synthesized by using multiple frequencies, and existing direction-of-arrival estimation techniques can be applied without modification. Synthesizing a larger array allows for more sources to be resolved in DOA estimation than can be resolved with a narrowband correlation matrix alone. However, to locate the sources correctly, the sources must have

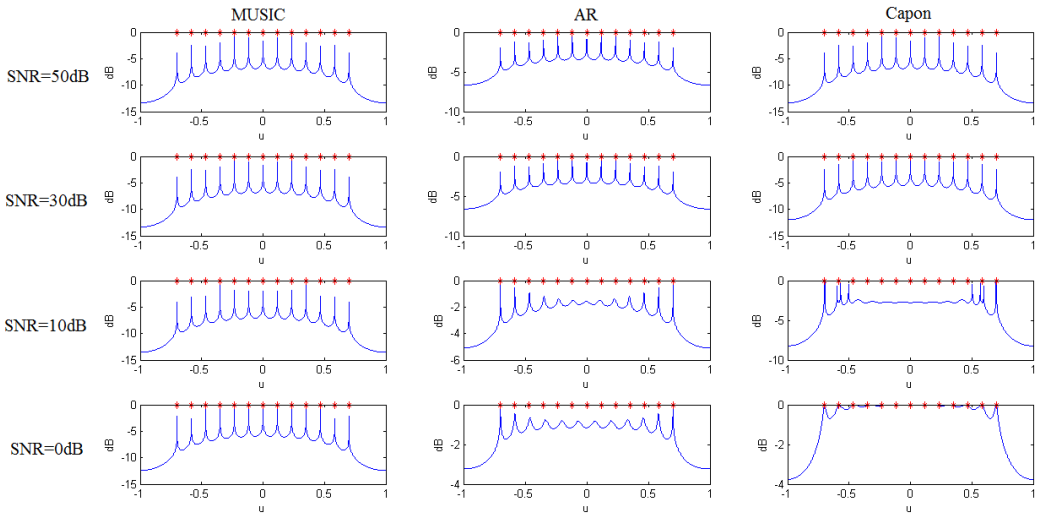

Figure 2.24: Five-element Non-uniform Linear Array - Spacing between elements: .1

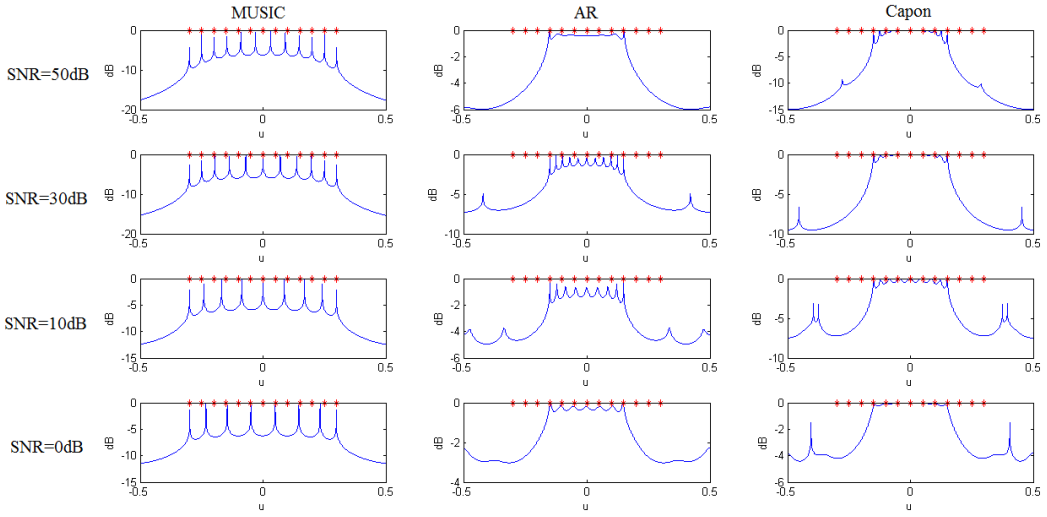

Figure 2.25: Five-element Non-uniform Linear Array - Spacing between elements: .05

proportional spectra. While this is a somewhat restrictive requirement, many situations exist where closely spaced targets are identical or similar in nature, including wideband noise-like sources and intentionally designed sources for tagging.

When the virtual correlation matrix is used in an existing high-resolution estimator, there is no performance degradation in the presence of noise compared to using a narrowband correlation matrix of the same size provided that care is taken to select the correlation data corresponding to the zero-coarray points in the virtual correlation.

If the spectra of the sources are not proportional, the virtual correlation matrix can be modified to attempt to equalize the source spectra. In this chapter, there were three methods shown to correct errors in the source location estimates for an example with two array elements and two frequencies, forming a 3×3 virtual correlation matrix. The method using array interpolation is the most promising to extend to examples with larger arrays and more sources, but more research will need to be done.

When the spectra of the sources are proportional, the number of sources which can be resolved is limited only by the bandwidth available. Even with only two array elements, with enough bandwidth, as many sources can be resolved as is necessary. Sparse non-uniform linear arrays (that do not necessarily have a full uniform linear coarray) are particularly useful with this technique, as a virtual correlation matrix with dimension much larger than the number of array elements can be constructed, where missing coarray lags are filled in with multiple frequencies. To fill in coarray points, a continuous band is not needed - only a sparse sampling of frequencies, which may make this technique appealing for multi-band applications.

2.9 Appendix

In this appendix, we show that having a group of K sources with each source having the same normalized power at each frequency is equivalent to sources having proportional power spectra. This is helpful because when considering the statistical characteristics of the sources, it is natural to look at each source spectrum varying over frequency; however, when forming the narrowband correlation matrices, it is natural to normalize each of the source powers by the total power received from all sources at that frequency. This is a frequency specific normalization across all K sources.

The k^{th} source has sampled spectrum

$$[P_k(\omega_0), P_k(\omega_1), ...P_k(\omega_{Q-1})]. \tag{2.102}$$

When comparing sources to each other, it is also generally useful to normalize the spectrum of each source. For example, sources may be at different distances (though still in the farfield) and normalization will compensate for this difference. The normalized spectrum for the k^{th} source is obtained by dividing the spectrum by the sum of the powers at each frequency,

$$\left[\frac{P_k(\omega_0)}{\sum_{q=0}^{Q-1} P_k(\omega_q)}, \frac{P_k(\omega_1)}{\sum_{q=0}^{Q-1} P_k(\omega_q)}, ...\frac{P_k(\omega_{Q-1})}{\sum_{q=0}^{Q-1} P_k(\omega_q)}\right]. \tag{2.103}$$

We call this the frequency-normalized spectrum since we are summing over frequencies. This is a source-specific normalization across all frequencies.

When we are forming narrowband correlation matrices, each matrix is normalized by the sum of the powers of each source at that frequency, i.e. frequency-specific normalization. This is a useful normalization because then at each frequency, all of

the zero-coarray points are normalized to 1. The vector of source powers at frequency ω_q is given by

$$[P_1(\omega_q), P_2(\omega_q), ..., P_K(\omega_q)], \tag{2.104}$$

and the frequency-specific normalized source power vector is

$$\begin{aligned}&[\bar{P}_1(\omega_q),\bar{P}_2(\omega_q), ..., \bar{P}_K(\omega_q)] \\ &\quad = \left[\frac{P_1(\omega_q)}{\sum_{k=1}^{K} P_k(\omega_q)}, \frac{P_2(\omega_q)}{\sum_{k=1}^{K} P_k(\omega_q)}, ..., \frac{P_K(\omega_q)}{\sum_{k=1}^{K} P_k(\omega_q)}\right].\end{aligned} \tag{2.105}$$

We will show that if the set of K sources has identical normalized source power vectors for different frequencies defined by Equation 2.105, all sources equivalently have identical normalized spectra defined by Equation 2.103, i.e.,

$$\frac{P_k(\omega_q)}{\sum_{l=1}^{K} P_l(\omega_q)} = A_k \text{ for all } q, k \Leftrightarrow \frac{P_k(\omega_q)}{\sum_{r=0}^{Q-1} P_k(\omega_r)} = B_q \text{ for all } q, k \tag{2.106}$$

First we will prove the left to right implication. If

$$\frac{P_k(\omega_q)}{\sum_{l=1}^{K} P_l(\omega_q)} = A_k \text{ for all } q, k, \tag{2.107}$$

then

$$\begin{aligned}\frac{P_k(\omega_q)}{\sum_{l=1}^{K} P_l(\omega_q)} &= \frac{P_k(\omega_p)}{\sum_{l=1}^{K} P_l(\omega_p)} \\ &\Rightarrow P_k(\omega_q) = C_{q,p} P_k(\omega_p).\end{aligned} \tag{2.108}$$

It follows that

$$\frac{P_k(\omega_q)}{\sum_{r=0}^{Q-1} P_k(\omega_r)} = \frac{C_{q,p} P_k(\omega_p)}{\sum_{r=0}^{Q-1} C_{r,p} P_k(\omega_p)} = \frac{C_{q,p} P_k(\omega_p)}{\sum_{r=0}^{Q-1} C_{r,p} P_k(\omega_p)} = \frac{C_{q,p}}{\sum_{r=0}^{Q-1} C_{r,p}}. \tag{2.109}$$

Since this is independent of k, we also have:

$$\frac{P_m(\omega_q)}{\sum_{r=0}^{Q-1} P_m(\omega_r)} = \frac{C_{q,p}}{\sum_{r=0}^{Q-1} C_{r,p}}. \tag{2.110}$$

Therefore

$$\frac{P_k(\omega_q)}{\sum_{r=0}^{Q-1} P_k(\omega_r)} \tag{2.111}$$

is independent of k and only depends on q:

$$\frac{P_k(\omega_q)}{\sum_{r=0}^{Q-1} P_k(\omega_r)} = B_q \text{ for all } q, k. \tag{2.112}$$

We prove the right to left implication similarly. We start with

$$\begin{aligned} \frac{P_k(\omega_q)}{\sum_{r=0}^{Q-1} P_k(\omega_r)} &= \frac{P_m(\omega_q)}{\sum_{r=0}^{Q-1} P_m(\omega_r)} \\ \Rightarrow P_k(\omega_q) &= \frac{\sum_{r=0}^{Q-1} P_k(\omega_r)}{\sum_{r=0}^{Q-1} P_m(\omega_r)} P_m(\omega_q) = D_{k,m} P_m(\omega_q) \end{aligned} \tag{2.113}$$

then,

$$\frac{P_k(\omega_q)}{\sum_{l=1}^{K} P_l(\omega_q)} = \frac{D_{k,m} P_m(\omega_q)}{\sum_{l=1}^{K} D_{l,m} P_m(\omega_q)} = \frac{D_{k,m}}{\sum_{l=1}^{K} D_{l,m}} \tag{2.114}$$

Since this is independent of q, we also have:

$$\frac{P_k(\omega_p)}{\sum_{l=1}^{K} P_l(\omega_p)} = \frac{D_{k,m}}{\sum_{l=1}^{K} D_{l,m}}. \tag{2.115}$$

Therefore,

$$\frac{P_k(\omega_q)}{\sum_{l=1}^{K} P_l(\omega_q)} \tag{2.116}$$

is independent of q and depends on k

$$\frac{P_k(\omega_q)}{\sum_{l=1}^{K} P_l(\omega_q)} = A_k. \tag{2.117}$$

QED.

Chapter 3

High-Resolution Active Imaging using Multiple Frequencies

3.1 Introduction

MUltiple SIgnal Classification (MUSIC) is a well-known high-resolution direction-of-arrival technique. In its original form for passive receive-only imaging, only incoherent sources can be resolved and the number of sources must be less than the number of receiving elements. For the narrowband passive imaging case, methods to increase the dimensions of the array correlation matrix, and thus the number of targets that can be resolved, have been proposed in [15, 21]. MUSIC was extended to active transmit/receive imaging in [13] to resolve both incoherent and coherent narrowband reflectors. The number of reflectors that can be resolved using MUSIC in active imaging is limited by the size of the array correlation matrix obtained directly from the array elements. However, it was shown that if the ability to resolve coherent reflectors is sacrificed, more incoherent reflectors can be resolved by using *virtual arrays*.

In this work, we seek to increase the number of coherent reflectors that can be resolved using MUSIC with active imaging. Essentially, *virtual correlation matrices* will be constructed so that they maximize the total number of reflectors that can be resolved as in [13]. By using array interpolation [19], we combine virtual correlation matrices at different frequencies in a way such that the resulting matrix can be used to resolve coherent reflectors.

Averaging over frequency is similar in spirit to spatial smoothing [9, 31] or pattern diversity [10] because they all allow for coherent targets to be resolved using imaging techniques intended for incoherent targets. With spatial smoothing, there is a reduction in the dimension of the spatial correlation matrix, meaning fewer targets can be resolved. For small arrays, but many targets, this reduction in dimensionality can be a problem. The frequency averaging technique proposed here does not cause a reduction in the dimension of the correlation matrix. Pattern diversity does not necessarily cause a reduction in the dimension of the spatial correlation matrix, but to preserve the dimension of the spatial correlation matrix, each array element must be capable of producing independent patterns. For frequency averaging, all that is necessary is that the array elements must be capable of transmitting and receiving multiple frequencies. The ability to resolve coherent targets by frequency averaging does not come for free. The trade-off is that only a fraction of the scene can be imaged. Because of this restriction, we consider imaging scenarios where the targets are clustered together. However, this may not be too restrictive an assumption since we are considering high-resolution techniques.

3.2 Active Imaging

Active imaging is used to estimate the locations of targets which do not emit their own radiation. Radiation sent by an array of emitting elements is reflected by a distribution of targets. The reflections are received by an array of sensing elements. The received signals are processed to yield an estimate of the target locations. There are many ways to process the received signals. In this chapter, we focus on high-resolution techniques, specifically Multiple Signal Classification (MUSIC). Classical beamforming will also be discussed briefly, as it is used later in the chapter to assist with target location.

In this chapter, we restrict our discussion to line arrays. To understand the array geometry, it is helpful to consider the array elements and targets to lie in the x-z plane, see Figure 3.1. The transmit and receive array elements lie on the x-axis. The transmit array elements are located at $\{x_{Tn}, n = 1, 2, ..., N\}$ and the receive array elements at $\{x_{Rm}, m = 1, 2, ..., M\}$ with respect to an arbitrary origin. The two arrays may or may not share elements. We define the array diameter, D_A, as the furthest distance between any two transmit or receive array elements. The z-axis, which is normal to the x-axis, is referred to as broadside of the array and serves as a reference for direction. We assume K reflectors in the scene are located at (R_k, u_k), where R_k is the distance from the origin to the k^{th} reflector, $u_k = \sin\theta_k$ and θ_k is the direction to the k^{th} reflector from broadside.

Both of the arrays are assumed to be capable of wideband operation. A waveform, $s(t)$, is sent from the transmit array elements. We construct $s(t)$ from multiple frequencies, $\omega_q, q = 0, 1, ..., Q-1$, i.e., $s(t) = \sum_{q=0}^{Q-1} e^{j(\omega_q t + \xi_q)}$ with Fourier Transform $S(\omega) = \sum_{q=0}^{Q-1} e^{j\xi_q}\delta(\omega - \omega_q)$. The phase $\xi_q \in [-\pi, \pi]$ is the random, but fixed, phase associated with the frequency ω_q. In practice, we cannot realistically construct such a

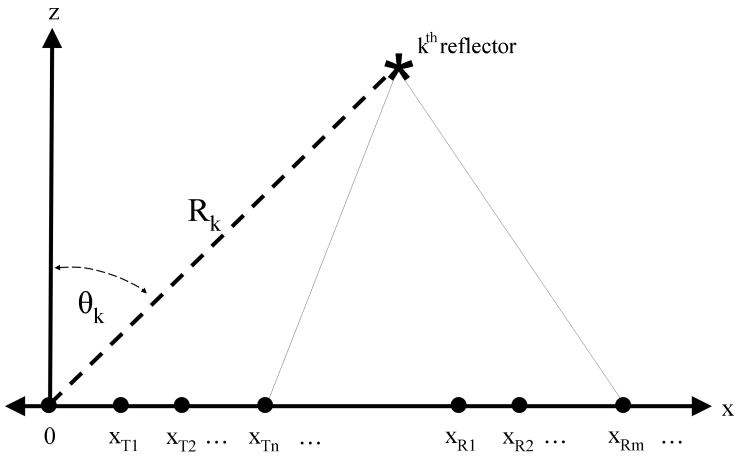

Figure 3.1: Array Geometry

pulse, as it would be infinite in time. The true signal would consist of a summation of narrowband pulses about the Q frequencies. Approximating the narrowband pulses as ideal, single frequencies is often done in the literature for narrowband imaging, and we make use of the same approximation for simplicity.

The frequency ω_0 is called the *reference frequency* because the array spacing is based on wavelength λ_0 corresponding to ω_0. In this chapter, we assume the transmit and receive arrays are uniformly spaced arrays with each array having spacing between the elements of $\frac{\lambda_0}{2}$. This is the Nyquist spatial sampling rate. Frequencies other than the reference frequency can be represented as a multiple of the reference frequency, $\omega_q = \alpha_q \omega_0$.

It is assumed that the targets lie in the far-field of the array. Thus, the targets are far enough away from the array that the wavefronts arriving at the targets from the transmit array and the reflections arriving at the receive array can be approximated as plane waves. An accepted condition is that [40]

$$\min_k R_k >> \frac{D_A^2}{\min_q \lambda_q}. \tag{3.1}$$

This condition ensures that the far-field condition is satisfied for all target ranges and frequencies.

When radiation of frequency ω_q is incident on k^{th} reflector, it reflects with complex amplitude $\tilde{a}_k(\omega_q)$. This amplitude takes into account the power of reflection and the reflection phase. Two reflectors are said to be *coherent* if the phase difference received at the array origin from reflections by each one, at any frequency, is the same at every snapshot. This may occur when the reflectors and array are fixed in space with respect to each other. Groups of reflectors may be mutually coherent, each pair having a fixed phase relationship. On the other hand, reflectors are *incoherent* when they do not reflect with the same phase between snapshots. This may occur if the targets move independently of each other between snapshots. This phase relationship is important because not all imaging techniques can resolve targets which have a coherent phase relationship. Coherent targets are generally more difficult to image and will be the focus of this chapter. Recall that K denotes the total number of targets and we let K_c denote the number of them that are mutually coherent. For simplicity of discussion, we assume that there is only a single group of mutually coherent targets. It is explained in [41] that considering this case is mathematically sufficient and can easily be generalized to multiple groups of mutually coherent targets.

3.2.1 Data Collection

Since we may possibly be imaging coherent targets, it is necessary that we collect the data so that the data from each transmit/receive pair can be accessed individually. To do this, the waveform $s(t)$ is transmitted individually from each transmitting element and received by all receiving elements.

Assuming $s(t)$ is transmitted from x_{Tn}, the wavefront arrives at the k^{th} target

with delay $\tau_{k,Tn}$, where

$$\tau_{k,Tn} = \frac{\sqrt{(R_k u_k - x_{Tn})^2 + R_k^2(1-u_k^2)}}{c}, \tag{3.2}$$

and c is the speed of light. Similarly, the reflected signal from the k^{th} target arrives at receiving element x_{Rm} with delay $\tau_{k,Rm}$:

$$\tau_{k,Rm} = \frac{\sqrt{(R_k u_k - x_{Rm})^2 + R_k^2(1-u_k^2)}}{c}. \tag{3.3}$$

Assuming additive, zero-mean, temporally and spatially white, circular Gaussian observation noise processes, the total received signal at x_{Rm} from x_{Tn} is the sum of all reflections from the targets:

$$[\sum_{q=0}^{Q-1}\sum_{k=1}^{K}\tilde{a}_k(\omega_q)e^{j\omega_q(t-\tau_{k,Tn}-\tau_{k,Rm})}e^{j\xi_q}] + w_{m,n}(t) \tag{3.4}$$

where $w_{m,n}(t)$ is the observation noise process from the n^{th} transmission at the m^{th} receiver. Since the targets are assumed to be in the farfield, we can make a simplification in Equation 3.4. Expanding $c\tau_{k,Tn}$ and $c\tau_{k,Rm}$ in $\frac{1}{R_k}$ we get

$$\begin{aligned} c\tau_{k,Tn} &= R_k - u_k x_{Tn} + \frac{1}{2R_k}[x_{Tn}^2 - u_k^2 x_{Tn}^2] + \frac{1}{2R_k^2}[u_k x_{Tn}^3 - u_k^3 x_{Tn}^3] + ... \\ c\tau_{k,Rm} &= R_k - u_k x_{Rm} + \frac{1}{2R_k}[x_{Rm}^2 - u_k^2 x_{Rm}^2] + \frac{1}{2R_k^2}[u_k x_{Rm}^3 - u_k^3 x_{Rm}^3] + ..., \end{aligned} \tag{3.5}$$

and in the far-field they can be approximated as

$$\begin{aligned} c\tau_{k,Tn} &\approx R_k - u_k x_{Tn} \\ c\tau_{k,Rm} &\approx R_k - u_k x_{Rm}. \end{aligned} \tag{3.6}$$

By matched filtering at each frequency at the receivers, the complex amplitude we

receive at x_{Rm} from x_{Tn} at frequency ω_q is

$$\begin{aligned}\mathbf{X}_{m,n}(\omega_q) &= \sum_{k=1}^{K} \tilde{a}_k(\omega_q) e^{-jk_q 2R_k} e^{j\xi_q} e^{jk_q u_k(x_{Rm}+x_{Tn})} + w_{m,n}(\omega_q) \\ &= \sum_{k=1}^{K} a_k(\omega_q) e^{jk_q u_k(x_{Rm}+x_{Tn})} + w_{m,n}(\omega_q),\end{aligned} \tag{3.7}$$

where

$$a_k(\omega_q) = \tilde{a}_k(\omega_q) e^{-jk_q 2R_k} e^{j\xi_q} \tag{3.8}$$

and $w_{m,n}(\omega_q)$ is independent, complex, circular, Gaussian noise with variance σ^2. The complex amplitude $a_k(\omega_q)$ now depends on not only the characteristics of the target, but the phase depends on the distance from the target to the array and the phase associated with each frequency at transmission, which vary over frequency. Because of this, even for otherwise identical targets, generally

$$a_k(\omega_q) \neq a_l(\omega_p) \text{ for all } k \neq l, q \neq p \tag{3.9}$$

except under very strict conditions on the target ranges and chosen frequencies. The received phase from each reflection changes over frequency in two ways: at the reflection and from the propagation.

The complex amplitudes received from all transmitters and receivers at each frequency can be arranged into data matrices, $\{\mathbf{X}(\omega_q)\}$, where the data resulting from the transmission from x_{Tn} received at x_{Rm} at frequency ω_q is the $(m,n)^{th}$ element of $\mathbf{X}(\omega_q)$. This is what is given in Equation 3.7.

For each frequency, the data matrix can be factored as follows:

$$\mathbf{X}(\omega_q) = \mathbf{A_R}(\omega_q)\mathbf{S}(\omega_q)\mathbf{A_T}(\omega_q)^T + \mathbf{W}(\omega_q), \tag{3.10}$$

where $\mathbf{A_R}(\omega_q)$ is the receive array manifold matrix,

$$\mathbf{A_R}(\omega_q) = \begin{bmatrix} e^{jk_q u_1 x_{R1}} & e^{jk_q u_2 x_{R1}} & ... & e^{jk_q u_K x_{R1}} \\ e^{jk_q u_1 x_{R2}} & e^{jk_q u_2 x_{R2}} & ... & e^{jk_q u_K x_{R2}} \\ \vdots & \vdots & \vdots & \vdots \\ e^{jk_q u_1 x_{RM}} & e^{jk_q u_2 x_{RM}} & ... & e^{jk_q u_K x_{RM}} \end{bmatrix}, \tag{3.11}$$

the transmit array manifold matrix, $\mathbf{A_T}(\omega_q)$, is

$$\mathbf{A_T}(\omega_q) = \begin{bmatrix} e^{jk_q u_1 x_{T1}} & e^{jk_q u_2 x_{T1}} & ... & e^{jk_q u_K x_{T1}} \\ e^{jk_q u_1 x_{T2}} & e^{jk_q u_2 x_{T2}} & ... & e^{jk_q u_K x_{T2}} \\ \vdots & \vdots & \vdots & \vdots \\ e^{jk_q u_1 x_{TN}} & e^{jk_q u_2 x_{TN}} & ... & e^{jk_q u_K x_{TN}} \end{bmatrix}, \tag{3.12}$$

$\mathbf{S}(\omega_q) = \text{diag}[a_1(\omega_q), a_2(\omega_q), ...a_K(\omega_q)]$ is the diagonal matrix of reflectivities and $\mathbf{W}(\omega_q)$ is the matrix of observation noise at frequency ω_q.

3.2.2 Coarray

In active imaging, the sum coarray is defined as the set of all possible pairwise sums between a transmit array element position and a receive array element position:

$$\{y_l\} = \{y_l | y_l = x_{Rm} + x_{Tn}, m = 1, 2, ..., M, n = 1, 2, ..., M\}. \tag{3.13}$$

The coarray is an important concept in imaging. For beamforming, the coarray determines the resolution and other image characteristics obtainable by the array. For high-resolution imaging, we will see that the coarray helps us understand the structure of the data matrices. At the reference frequency ω_0, the $(m, n)^{th}$ element of

the noiseless data matrix is

$$\mathbf{X}_{m,n}(\omega_0) = \sum_{k=1}^{K} a_k(\omega_0) e^{jk_0 u_k (x_{Rm} + x_{Tn})} \tag{3.14}$$

It is supported on the coarray point $x_{Rm} + x_{Tn}$. Notice this is a sum coarray point. We use the known coarray support structure of the data matrix to better help us understand high-resolution imaging.

For frequencies other than the reference frequency, $\omega_q = \alpha_q \omega_0$, the $(m,n)^{th}$ data matrix at the frequency ω_q is

$$\mathbf{X}_{m,n}(\omega_q) = \sum_{k=1}^{K} a_k(\omega_q) e^{jk_q u_k (x_{Rm} + x_{Tn})} = \sum_{k=1}^{K} a_k(\omega_q) e^{jk_0 u_k \alpha_q (x_{Rm} + x_{Tn})}. \tag{3.15}$$

This has the same structure as Equation 3.14, except for the factor α_q in the argument of the exponential. The α_q factor arises because when a frequency other than the reference frequency is used, the coarray dilates by the factor α_q [17]. Even though all frequencies are transmitted and received by the same arrays, they have different coarray support. Thus, by using multiple frequencies, we generate additional coarray points compared to using a single frequency.

The complex amplitude associated with each coarray point can be thought of as a unique piece of information about the target locations and reflectivities. The more coarray points we have, the more information we have about the targets, so using multiple frequencies provides more information about the targets compared to using a single frequency.

3.2.3 Active Imaging Techniques

The focus of this chapter is on high-resolution techniques. Here we derive the high-resolution technique Multiple Signal Classification. The derivation reveals important conditions that must be considered later in the chapter. Linear beamforming is also briefly described since it will be used in conjunction with the high-resolution techniques.

Beamforming

In linear beamforming, the transmitted radiation and received radiation is focused by applying appropriate delays to the transmit and receive elements. First, the transmitted radiation is focused in the direction desired, u, by applying phase delay weights on the transmit array elements so that the wavefronts add constructively in the direction u. If there is a reflector at u, the focused radiation reflects strongly and the reflection is received at the receive array elements. The received signals are given a phase weighting profile so that they add constructively from the direction u. The image is a sum of all focused received signals as a function of u. Disregarding noise, the image expression is easily seen to be obtained as follows:

$$\begin{aligned} I(u) &= \sum_{m=1}^{M}\sum_{n=1}^{M} \mathbf{X}(\omega_0)_{m,n} e^{-jk_0 u x_{Rm}} e^{-jk_0 u x_{Tn}} \\ &= \sum_{m=1}^{M}\sum_{n=1}^{M}\sum_{k=1}^{K} a_k(\omega_0) e^{-jk_0(u-u_k)(x_{Rm}+x_{Tn})} \end{aligned} \tag{3.16}$$

The image magnitude has peaks when $u = u_k$. However, there is a limit on how closely the targets can be spaced. This limit depends on the length of the coarray [14]. For small arrays, closely spaced targets cannot be resolved. They appears as a single peak in the image. High-resolution techniques can be used when the beamforming

resolution of the array is not sufficient.

Multiple Signal Classification (MUSIC)

In [13], it was shown that high-resolution techniques, which in their conventional form are used to passively image incoherent sources, can also be used in active imaging to resolve coherent targets. MUltiple SIgnal Classification (MUSIC) is a well-known high-resolution imaging technique and is the technique we will use for simulations. The basis of MUSIC is the eigendecomposition of the narrowband correlation matrix $\mathbf{R}(\omega_0)$, [42]. Since conventional high-resolution techniques are narrowband, we assume operation at the reference frequency throughout this section.

Temporarily ignoring observation noise, the array correlation matrix for active imaging is defined as

$$\mathbf{R}(\omega_0) = \mathbb{E}[\mathbf{X}(\omega_0)\mathbf{X}(\omega_0)^H], \tag{3.17}$$

where the expectation is taken over multiple snapsnots. The array correlation matrix has the following structure in terms of the array manifold matrices:

$$\mathbf{R}(\omega_0) = \mathbf{A_R}(\omega_0)\mathbb{E}[\mathbf{S}(\omega_0)\mathbf{A_T}(\omega_0)^T\mathbf{A_T}(\omega_0)^*\mathbf{S}(\omega_0)^H]\mathbf{A_R}(\omega_0)^H \tag{3.18}$$

We define

$$\mathbf{S_T}(\omega_0) = \mathbb{E}[\mathbf{S}(\omega_0)\mathbf{A_T}(\omega_0)^T\mathbf{A_T}(\omega_0)^*\mathbf{S}(\omega_0)^H] \tag{3.19}$$

as the source correlation matrix at frequency ω_0. Note that it depends on the target reflectivities as well as the transmit array positions. For incoherent targets, over multiple snapshots, the target reflectivities are uncorrelated and

$$\mathbf{S_T}(\omega_0) = N\text{diag}[|a_1|^2, |a_2|^2, ..., |a_K|^2]. \tag{3.20}$$

When the targets are incoherent, the correlation matrix has the same structure as a correlation matrix obtained from a passive imaging system observing incoherent sources, and no additional consideration is necessary to use high-resolution techniques with active imaging. However, for coherent targets, the target reflectivities do not become uncorrelated over multiple snapshots. They are completely correlated. When the expectation is taken, the source correlation matrix has the following form:

$$\begin{aligned} \mathbf{S_T}(\omega_0) &= \mathbb{E}[\mathbf{S}(\omega_0)\mathbf{A_T}(\omega_0)^T\mathbf{A_T}(\omega_0)^*\mathbf{S}(\omega_0)^H] \\ &= \mathbf{S}(\omega_0)\mathbf{A_T}(\omega_0)^T\mathbf{A_T}(\omega_0)^*\mathbf{S}(\omega_0)^H. \end{aligned} \tag{3.21}$$

Even though we take the expectation, since there is no randomness in the reflectivities and we are assuming no noise, the source correlation matrix is a deterministic quantity for coherent sources. Recall that $\mathbf{A_R}(\omega_0)$ has dimension $M \times K$ and $\mathbf{A_T}(\omega_0)$ has dimension $N \times K$. It is reasonable to assume that the columns of the array manifold matrices are linearly independent for $\{u_k\} \in [-1, 1]$, thus $\mathbf{A_R}(\omega_0)$ has rank $\min(M, K)$ and $\mathbf{A_T}(\omega_0)$ has rank $\min(N, K)$. The matrix $\mathbf{S}(\omega_0)$ is a full-rank diagonal matrix with dimension $K \times K$.

Since $\mathbf{A_R}(\omega_0)$, $\mathbf{A_T}(\omega_0)$ and $\mathbf{S}(\omega_0)$ are all full rank, rank of $\mathbf{S}_T(\omega_0)$ is $\min(N, K)$ and it is full rank if $N \geq K$. Having a full-rank source correlation matrix $\mathbf{S_T}(\omega_0)$ is necessary to use MUSIC. Provided that the source correlation matrix $\mathbf{S_T}(\omega_0)$ has full rank K, $\mathbf{R}(\omega_0)$ has rank $\min(M, K)$. If $M > K$, $\mathbf{R}(\omega_0)$ is rank deficient. These rank conditions are important to understand because MUSIC exploits the rank deficiency of the array correlation matrix.

When imaging both incoherent and coherent targets, it was shown in [13] that the rank conditions derived above hold as long as $N \geq K_c$ and $M > K$.

In summary, the conditions needed to use high-resolution imaging techniques depend on the rank of the source correlation matrix and the rank of the array correlation

matrix. The rank conditions are satisfied for all types of targets as long as

$$\begin{aligned} N &\geq K_c \\ M &> K. \end{aligned} \tag{3.22}$$

Given that the conditions in Equation 3.22 are satisfied, existing high-resolution techniques can be applied to the correlation matrix $\mathbf{R}(\omega_0)$ for active imaging of coherent targets.

If $K < M$ and $K_c \leq N$, there exist $M - K$ zero eigenvalues of $\mathbf{R}(\omega_0)$ with corresponding eigenvectors $\mathbf{v^0}_i(\omega_0), i = 1, 2, ...M - K$, and the $\{\mathbf{v^0}_i(\omega_0)\}$ are orthogonal to the columns of the array manifold matrix, $\mathbf{A_R}(\omega_0)$ [42]:

$$\begin{aligned} &\mathbf{v^0}_i(\omega_0)^H \mathbf{R}(\omega_0)\mathbf{v^0}_i(\omega_0) = 0 \\ &\Leftrightarrow \mathbf{v^0}_i(\omega_0)^H \mathbf{A_R}(\omega_0)\mathbf{S_T}(\omega_0)^{\frac{1}{2}} = \mathbf{0} \\ &\Leftrightarrow \mathbf{v^0}_i(\omega_0)^H \mathbf{A_R}(\omega_0) = \mathbf{0} \\ &\Leftrightarrow \mathbf{v^0}_i(\omega_0)^H \mathbf{a_R}(u, \omega_0) = 0 \quad \text{for} \quad u = u_k \end{aligned} \tag{3.23}$$

where

$$\mathbf{a_R}(u, \omega_0) = [e^{jk_0 u x_{R1}} \quad e^{jk_0 u x_{R2}} \quad ... \quad e^{jk_0 u x_{RM}}]^T \tag{3.24}$$

is the array steering vector. Note that $\mathbf{a_R}(u, \omega_0)$ is equal to the k^{th} column of $\mathbf{A_R}(\omega_0)$ when $u = u_k$. Exploiting this orthogonality, the MUSIC pseudo-spectrum is defined as [42]

$$P_{\text{MUSIC}}(u) = \frac{1}{\sum_{i=1}^{M-K} |\mathbf{a_R}^H(u, \omega_0)\mathbf{v^0}_i(\omega_0)|^2}. \tag{3.25}$$

The peaks of $P_{\text{MUSIC}}(u)$ correspond to the directions-of-arrival, $\{u_k\}$ of the reflectors.

We see from the second and third lines in Equation 3.23 that derivation of MUSIC depends on $\mathbf{S_T}(\omega_0)$ being full rank. If $N < K_c$, $\mathbf{S_T}(\omega_0)$ is not full rank and MUSIC

will fail to correctly locate the coherent targets.

Note that when additive spatially-white Gaussian observation noise of variance σ^2 is present, this adds a scaled identity matrix to the correlation matrix:

$$\mathbb{E}[\mathbf{X}(\omega_0)\mathbf{X}(\omega_0)^H] = \mathbf{A_R}(\omega_0)\mathbf{S_T}(\omega_0)\mathbf{A_R}(\omega_0)^H + \sigma^2\mathbf{I}. \tag{3.26}$$

The addition of a scaled identity does not change the eigenvectors. The only change in the above analysis is that the "zero-eigenvectors" are chosen to be those with the $M - K$ smallest eigenvalues.

3.3 Constructing the Virtual Data and Correlation Matrices

The idea behind creating virtual data and correlation matrices is that, presumably, the virtual correlation matrix will have a dimension larger than the correlation matrix obtained directly from the array. From Equation 3.22, a correlation matrix with larger dimension should allow for more total targets to be resolved. However, we will see that these targets cannot necessarily all be mutually coherent. There is a trade off between the number of coherent targets which can be resolved and the increase in the dimension of the virtual correlation matrix.

3.3.1 Virtual Arrays

In active imaging, there are two arrays, the transmit and receive arrays. We assume that both of these arrays are uniformly spaced with N and M elements respectively. The coarray generated by these arrays is a uniformly spaced coarray with $N + M - 1$ elements. This same uniformly spaced coarray could also be generated by transmit

and receive arrays of lengths $\tilde{M}$ and $\tilde{N}$ provided that $\tilde{N}+\tilde{M} = N+M$. Such arrays of virtual transmit and receive elements are called *virtual arrays*; their effect is obtained by viewing the actual data matrix in a different way. To avoid confusion, we will call the physical array the natural array. In terms of the coarray, we must choose a virtual array that is *coarray equivalent* to the natural array, meaning that they have the same coarray.

The virtual array element locations are denoted by $\{\tilde{x}_{Rm}\}, m = 1, 2, ..., \tilde{M}$ and $\{\tilde{x}_{Tn}\}, n = 1, 2, ..., \tilde{N}$, and their array manifold matrices are

$$\tilde{\mathbf{A}}_{\mathbf{R}}(\omega_q) = \begin{bmatrix} e^{jk_q u_1 \tilde{x}_{R1}} & e^{jk_q u_2 \tilde{x}_{R1}} & ... & e^{jk_q u_K \tilde{x}_{R1}} \\ e^{jk_q u_1 \tilde{x}_{R2}} & e^{jk_q u_2 \tilde{x}_{R2}} & ... & e^{jk_q u_K \tilde{x}_{R2}} \\ \vdots & \vdots & \vdots & \vdots \\ e^{jk_q u_1 \tilde{x}_{R\tilde{M}}} & e^{jk_q u_2 \tilde{x}_{R\tilde{M}}} & ... & e^{jk_q u_K \tilde{x}_{R\tilde{M}}} \end{bmatrix} \tag{3.27}$$

and

$$\tilde{\mathbf{A}}_{\mathbf{T}}(\omega_q) = \begin{bmatrix} e^{jk_q u_1 \tilde{x}_{T1}} & e^{jk_q u_2 \tilde{x}_{T1}} & ... & e^{jk_q u_K \tilde{x}_{T1}} \\ e^{jk_q u_1 \tilde{x}_{T2}} & e^{jk_q u_2 \tilde{x}_{T2}} & ... & e^{jk_q u_K \tilde{x}_{T2}} \\ \vdots & \vdots & \vdots & \vdots \\ e^{jk_q u_1 \tilde{x}_{T\tilde{N}}} & e^{jk_q u_2 \tilde{x}_{T\tilde{N}}} & ... & e^{jk_q u_K \tilde{x}_{T\tilde{N}}} \end{bmatrix}. \tag{3.28}$$

Since the virtual and natural arrays are coarray equivalent, we can use the coarray concept to help us understand how to construct the virtual data matrix, $\tilde{\mathbf{X}}(\omega_q)$.

$\tilde{\mathbf{X}}(\omega_q)$ is an $\tilde{M} \times \tilde{N}$ matrix and we will only consider virtual arrays where $\tilde{M} > M$ because we are interested in increasing the number of targets that can be resolved. As we increase the number of virtual receivers, $\tilde{M}$, the number of virtual transmitters, $\tilde{N}$, decreases.

The virtual data matrix, $\tilde{\mathbf{X}}(\omega_q) = \tilde{\mathbf{A}}_{\mathbf{R}}(\omega_q)\mathbf{S}(\omega_q)\tilde{\mathbf{A}}_{\mathbf{T}}(\omega_q)^T$, can be constructed from the natural data matrix, $\mathbf{X}(\omega_q)$, in such a way that it appears to have come from the

virtual arrays.

3.3.2 Coarray Support Matrix

Since we are dealing with data matrices, it is useful to consider the coarray in matrix form. The *coarray support matrix* is the coarray in matrix form. It is defined as a matrix that is the same dimension as $\mathbf{X}(\omega_0)$. The $(m,n)^{th}$ element of the $M \times N$ natural coarray support matrix for frequency ω_0 is

$$\mathbf{C}_{m,n}(\omega_0) = x_{Rm} + x_{Tn}. \tag{3.29}$$

From Equation 3.7, the coarray support matrix is simply the coarray support of the narrowband data matrix.

Likewise, the $(m,n)^{th}$ element of the $\tilde{M} \times \tilde{N}$ virtual coarray support matrix is

$$\tilde{\mathbf{C}}_{m,n}(\omega_0) = \tilde{x}_{Rm} + \tilde{x}_{Tn}. \tag{3.30}$$

This is a useful way of viewing the coarray for high-resolution imaging because we primarily deal with matrices. The $(m,n)^{th}$ element of the sum coarray support matrix at frequency ω_0 gives us the coarray support point for the $(m,n)^{th}$ element of the data matrix at frequency ω_0.

3.3.3 Virtual Data and Virtual Correlation Matrices

The objective is to create a virtual data matrix, $\tilde{\mathbf{X}}(\omega_0)$, that appears to have come from virtual arrays with transmit and receive elements at $\{\tilde{x}_{Tn}\}$ and $\{\tilde{x}_{Rm}\}$, respectively, with enough elements to resolve the total number of reflectors desired. Since we know the natural and virtual arrays are coarray equivalent, we can find a map that

matches the elements of the natural coarray support matrix, $\mathbf{C}(\omega_0)$, to the elements of the desired virtual coarray support matrix, $\tilde{\mathbf{C}}(\omega_0)$,

$$\mathbf{C}(\omega_0) \xrightarrow{f} \tilde{\mathbf{C}}(\omega_0). \tag{3.31}$$

Then we can construct the virtual data matrix, $\tilde{\mathbf{X}}(\omega_0)$, from the natural data matrix, $\mathbf{X}(\omega_0)$, using the same map:

$$\mathbf{X}(\omega_0) \xrightarrow{f} \tilde{\mathbf{X}}(\omega_0). \tag{3.32}$$

The autocorrelation of the virtual data matrix yields an $\tilde{M} \times \tilde{M}$ *virtual correlation matrix*:

$$\begin{aligned} \tilde{\mathbf{R}}(\omega_q) &= \mathbb{E}[\tilde{\mathbf{X}}(\omega_q)\tilde{\mathbf{X}}(\omega_q)^H] \\ &= \tilde{\mathbf{A}}_{\mathbf{R}}(\omega_q)\tilde{\mathbf{S}}_{\mathbf{T}}(\omega_q)\tilde{\mathbf{A}}_{\mathbf{R}}(\omega_q)^H. \end{aligned} \tag{3.33}$$

Comparing the virtual correlation matrix to the natural correlation matrix in Equation 3.18, we see that they have the same structure except that the virtual source correlation matrix,

$$\tilde{\mathbf{S}}_{\mathbf{T}}(\omega_q) = \mathbb{E}[\mathbf{S}(\omega_q)\tilde{\mathbf{A}}_{\mathbf{T}}(\omega_q)^T\tilde{\mathbf{A}}_{\mathbf{T}}(\omega_q)^*\mathbf{S}(\omega_q)^H], \tag{3.34}$$

now depends on the virtual transmit array and no longer the natural transmit array. This changes the rank characteristics. The virtual transmit array manifold, $\tilde{\mathbf{A}}_{\mathbf{T}}(\omega_q)$, has dimension $\tilde{N} \times K$ and rank $\min(\tilde{N}, K)$, and the virtual source correlation matrix, $\tilde{\mathbf{S}}_{\mathbf{T}}(\omega_q)$, also has rank $\min(\tilde{N}, K)$. We are only considering cases where $\tilde{M} > M$, thus $\tilde{N} < N$, and as was shown in [13], there is a decrease in the number of coherent targets that can be resolved.

By maximizing $\tilde{M}$, i.e. $\tilde{M} = M + N - 1$ and $\tilde{N} = 1$, this maximizes the total

number of reflectors which can be resolved. The problem is that none of them can be coherent. It is desirable to increase the number of coherent reflectors that can be resolved and in the next section, we will address how we can allow for additional coherent targets to be resolved using virtual data matrices.

For frequencies other than the reference frequency, using the same map, f, additional virtual data and correlation matrices can be constructed at frequencies $\{\omega_q\}$,

$$\begin{aligned} \mathbf{X}(\omega_q) &\xrightarrow{f} \tilde{\mathbf{X}}(\omega_q) \\ \tilde{\mathbf{R}}(\omega_q) &= \mathbb{E}[\tilde{\mathbf{X}}(\omega_q)\tilde{\mathbf{X}}(\omega_q)^H] \\ &= \tilde{\mathbf{A}}_{\mathbf{R}}(\omega_q)\tilde{\mathbf{S}}_{\mathbf{T}}(\omega_q)\tilde{\mathbf{A}}_{\mathbf{R}}(\omega_q)^H. \end{aligned} \tag{3.35}$$

For all ω_q, $\tilde{\mathbf{R}}(\omega_q)$ and $\tilde{\mathbf{S_T}}(\omega_q)$ share the same rank characteristics as $\tilde{\mathbf{R}}(\omega_0)$ and $\tilde{\mathbf{S_T}}(\omega_0)$.

3.3.4 Averaged Virtual Correlation Matrix

In this section, we consider using virtual arrays to resolve all the way up to $\tilde{M} - 1$ coherent targets. This is done by averaging the virtual correlation matrix over frequencies. This frequency averaging produces a similar effect to spatial smoothing [9, 31] and pattern diversity [10], but without a reduction in the dimensionality of the correlation matrix. However, the averaged virtual correlation matrix is only valid in a sector of the scene.

Array Interpolation

Array interpolation matrices allow us to add correlation matrices at different frequencies while retaining to structure given in Equation 3.18.

We want to find an array interpolation matrix $\mathbf{B}_0(\omega_q)$ such that [19]

$$\tilde{\mathbf{A}}_{\mathbf{R}}(\omega_0) \approx \mathbf{B}_0(\omega_q)\tilde{\mathbf{A}}_{\mathbf{R}}(\omega_q). \tag{3.36}$$

Since the $\{\tilde{\mathbf{A}}_{\mathbf{R}}(\omega_q)\}$ are functions of the unknown $\{u_k\}$, we cannot directly solve for the $\{\mathbf{B}_0(\omega_q)\}$. However, we assume it is known that $u_k \in [u_s, u_f]$, thus we can find $\mathbf{B}_0(\omega_q)$ by a least squares fit over the sector $[u_s, u_f]$. The optimal $\mathbf{B}_0(\omega_q)$ in the least squares sense minimizes

$$\int_{u_s}^{u_f} ||\tilde{\mathbf{a}}_{\mathbf{R}}(u, \omega_0) - \mathbf{B}_0(\omega_q)\tilde{\mathbf{a}}_{\mathbf{R}}(u, \omega_q)||^2 du \tag{3.37}$$

with respect to $\mathbf{B}_0(\omega_q)$, where $\tilde{\mathbf{a}}_{\mathbf{R}}(u, \omega_q)$ is the virtual receive array steering vector at frequency ω_q:

$$\tilde{\mathbf{a}}_{\mathbf{R}}(u, \omega_q) = [e^{jk_q u\tilde{x}_{R1}}, e^{jk_q u\tilde{x}_{R2}}, ..., e^{jk_q u\tilde{x}_{R\tilde{M}}}]^T. \tag{3.38}$$

To find $\mathbf{B}_0(\omega_q)$, we approximate the integral in Equation 3.37 by a summation taken over points in the sector. The sector is sampled $P \geq M$ times and the matrices $\tilde{\mathbf{A}}_q$ are constructed as follows:

$$\tilde{\mathbf{A}}_q = \begin{bmatrix} \tilde{\mathbf{a}}_{\mathbf{R}}(u^1, \omega_q)^H \\ \tilde{\mathbf{a}}_{\mathbf{R}}(u^2, \omega_q)^H \\ \vdots \\ \tilde{\mathbf{a}}_{\mathbf{R}}(u^i, \omega_q)^H \\ \vdots \\ \tilde{\mathbf{a}}_{\mathbf{R}}(u^P, \omega_q)^H \end{bmatrix} \tag{3.39}$$

Here u^i is the i^{th} sample of the sector. Assuming that $P \geq M$ and that the matrices

$\tilde{\mathbf{A}}_q$ each have full column rank, the least squares solution is given by [44]:

$$\mathbf{B}_0(\omega_p) = \tilde{\mathbf{A}}_0^H \tilde{\mathbf{A}}_p [\tilde{\mathbf{A}}_p^H \tilde{\mathbf{A}}_p]^{-1}. \tag{3.40}$$

When we pre- and post-multiply the spatial correlation matrix at frequency ω_q by the appropriate array interpolation matrix, the correlation matrix at frequency ω_q appears to have come from frequency ω_0 in the sector,

$$\begin{aligned} \mathbf{B}_0(\omega_q)\tilde{\mathbf{R}}(\omega_q)\mathbf{B}_0(\omega_q)^H &= \mathbf{B}_0(\omega_q)\tilde{\mathbf{A}}_{\mathbf{R}}(\omega_q)\tilde{\mathbf{S}}_{\mathbf{T}}(\omega_q)\tilde{\mathbf{A}}_{\mathbf{R}}(\omega_q)^H\mathbf{B}_0(\omega_q)^H \\ &\approx \tilde{\mathbf{A}}_{\mathbf{R}}(\omega_0)\tilde{\mathbf{S}}_{\mathbf{T}}(\omega_q)\tilde{\mathbf{A}}_{\mathbf{R}}(\omega_0)^H, \end{aligned} \tag{3.41}$$

but with a different source correlation matrix at each frequency.

Averaged Correlation Matrix

Recall that if the source correlation matrix $\mathbf{S}_{\mathbf{T}}(\omega_0)$ is not full rank (i.e. $K_c > \tilde{N}$), MUSIC will be unable to resolve the coherent targets. We show that averaging the virtual correlation matrices over multiple frequencies can increase the rank of the source correlation matrix and allow coherent targets to be resolved. This effectively decorrelates the targets.

The correlation matrices cannot be directly averaged over frequency since they each have different coarray support, so we use array interpolation to force each spatial narrowband correlation matrix to appear to have come from frequency ω_0 as in Equation 3.41. This forces each correlation matrix to have approximately the same coarray support.

The averaged virtual correlation matrix is defined as:

$$\begin{aligned}
\bar{\mathbf{R}}(\omega_0) &= \frac{1}{Q}[\tilde{\mathbf{R}}(\omega_0) + \sum_{q=1}^{Q-1} \mathbf{B}_0(\omega_q)\tilde{\mathbf{R}}(\omega_q)\mathbf{B}_0(\omega_q)^H] \\
&= \frac{1}{Q}[\tilde{\mathbf{A}}_{\mathbf{R}}(\omega_0)\tilde{\mathbf{S}}_{\mathbf{T}}(\omega_0)\tilde{\mathbf{A}}_{\mathbf{R}}(\omega_0)^H + \sum_{q=1}^{Q-1} \mathbf{B}_0(\omega_q)\tilde{\mathbf{A}}_{\mathbf{R}}(\omega_q)\tilde{\mathbf{S}}_{\mathbf{T}}(\omega_q)\tilde{\mathbf{A}}_{\mathbf{R}}(\omega_q)^H\mathbf{B}_0(\omega_q)^H] \\
&\approx \frac{1}{Q}\sum_{q=0}^{Q-1} \tilde{\mathbf{A}}_{\mathbf{R}}(\omega_0)\tilde{\mathbf{S}}_{\mathbf{T}}(\omega_q)\tilde{\mathbf{A}}_{\mathbf{R}}(\omega_0)^H \\
&= \tilde{\mathbf{A}}_{\mathbf{R}}(\omega_0)[\frac{1}{Q}\sum_{q=0}^{Q-1} \tilde{\mathbf{S}}_{\mathbf{T}}(\omega_q)]\tilde{\mathbf{A}}_{\mathbf{R}}(\omega_0)^H \\
&= \tilde{\mathbf{A}}_{\mathbf{R}}(\omega_0)\bar{\mathbf{S}}_{\mathbf{T}}\tilde{\mathbf{A}}_{\mathbf{R}}(\omega_0)^H
\end{aligned} \tag{3.42}$$

The averaged correlation matrix has the same structure as a correlation matrix observing the scene at a frequency ω_0, but since we averaged over frequencies, we have a new averaged source correlation matrix,

$$\bar{\mathbf{S}}_{\mathbf{T}} = \frac{1}{Q}\sum_{q=0}^{Q-1} \tilde{\mathbf{S}}_{\mathbf{T}}(\omega_q). \tag{3.43}$$

Recall that for $\bar{\mathbf{R}}(\omega_0)$ to be useful in high-resolution techniques, $\bar{\mathbf{S}}_T(\omega_0)$ must be full-rank. We show that $\bar{\mathbf{S}}_T(\omega_0)$ has full rank when the number of frequencies is greater than or equal to the number of coherent targets,

$$Q \geq K_c. \tag{3.44}$$

To show this, we assume the worst case where all of the reflectors are coherent,

$K = K_c$, and the virtual transmit array only has one element at $\{0\}$. Then

$$\mathbf{S_T}(\omega_q) = \mathbf{S}(\omega_q) \begin{bmatrix} 1 \\ 1 \\ \vdots \\ 1 \end{bmatrix} \begin{bmatrix} 1 & 1 & ... & 1 \end{bmatrix} \mathbf{S}(\omega_q)^H = \mathbf{s}(\omega_q)\mathbf{s}(\omega_q)^H, \tag{3.45}$$

has rank 1, where

$$\mathbf{s}(\omega_q) = [a_1(\omega_q), a_2(\omega_q), ..., a_K(\omega_q)]^T. \tag{3.46}$$

It is reasonable to assume that the vectors $\{\mathbf{s}(\omega_q)\}$ are linearly independent,

$$\mathbf{s}(\omega_q) \neq \sum_{p \neq q} \eta_p \mathbf{s}(\omega_p) \text{ for all } q \tag{3.47}$$

because the phases of the complex amplitudes $\{a_k(\omega_q)\}$ depend on frequency in two ways: the phase at the reflection boundary and the phase resulting from the propagation delay, see Equations 3.8 and 3.9.

The averaged correlation matrix can be written as a sum of Q dyadic products:

$$Q\bar{\mathbf{S}}_\mathbf{T} = \sum_{q=0}^{Q-1} \mathbf{s}(\omega_q)\mathbf{s}(\omega_q)^H. \tag{3.48}$$

From the linear independence assumption in Equation 3.47, Equation 3.48 shows that $\bar{\mathbf{S}}_\mathbf{T}$ has a basis of Q linearly independent vectors. Since $\bar{\mathbf{S}}_\mathbf{T}$ is a $K \times K$ matrix, it has rank $\min(K, Q)$. Thus if $Q \geq K$, it has full rank.

More generally, when imaging both coherent and incoherent target, the number of frequencies used should be greater than the number of coherent targets, $Q \geq K_c$. If this condition is satisfied, $\bar{\mathbf{S}}_\mathbf{T}$ has full rank and thus $\bar{\mathbf{R}}(\omega_0)$ is useful in MUSIC.

3.4 Illustration of the Construction and Use of the Averaged Virtual Correlation Matrix

In this example, we illustrate the construction and use of the averaged virtual correlation matrix. First we consider a noiseless example, then we study the effect of noise.

3.4.1 Noiseless

Consider a small array with two transmit/receive elements at

$$\{x_{Rm}\} = \{\frac{-\lambda_0}{4}, \frac{\lambda_0}{4}\}, M = 2$$
$$\{x_{Tn}\} = \{\frac{-\lambda_0}{4}, \frac{\lambda_0}{4}\}, N = 2.$$

From Equation 3.29, the natural coarray support matrix at the reference frequency is

$$\mathbf{C}(\omega_0) = \begin{bmatrix} -\frac{\lambda_0}{2} & 0 \\ 0 & \frac{\lambda_0}{2} \end{bmatrix}. \tag{3.49}$$

To maximize the total number of targets that can be resolved, we choose the virtual arrays with the maximum number of receivers and a single transmitter:

$$\{\tilde{x}_{Rm}\} = \{\frac{-\lambda_0}{2} \quad 0 \quad \frac{\lambda_0}{2}\}, \tilde{M} = 3$$
$$\{\tilde{x}_{Tn}\} = \{0\}, \tilde{N} = 1.$$

This virtual array yields the virtual coarray support matrix

$$\tilde{\mathbf{C}}(\omega_0) = \begin{bmatrix} -\frac{\lambda_0}{2} \\ 0 \\ \frac{\lambda_0}{2} \end{bmatrix}. \tag{3.50}$$

To construct the virtual data matrix $\tilde{\mathbf{X}}(\omega_0)$ from $\mathbf{X}(\omega_0)$, we first must find a map from $\mathbf{C}(\omega_0)$ to $\tilde{\mathbf{C}}(\omega_0)$. There are three possible maps:

$$\bar{\mathbf{C}}(\omega_0) = \begin{bmatrix} \mathbf{C}(\omega_0)_{1,1} \\ \mathbf{C}(\omega_0)_{2,1} \\ \mathbf{C}(\omega_0)_{2,2} \end{bmatrix}, \begin{bmatrix} \mathbf{C}(\omega_0)_{1,1} \\ \mathbf{C}(\omega_0)_{1,2} \\ \mathbf{C}(\omega_0)_{2,2} \end{bmatrix}, \begin{bmatrix} \mathbf{C}(\omega_0)_{1,1} \\ \frac{1}{2}(\mathbf{C}(\omega_0)_{1,2} + \mathbf{C}(\omega_0)_{2,1}) \\ \mathbf{C}(\omega_0)_{2,2} \end{bmatrix}. \tag{3.51}$$

The latter is the preferred map. It may yield better statistical results as is suggested in [13] since it averages over redundant coarray points. The resulting virtual data matrix $\tilde{\mathbf{X}}(\omega_0)$ is formed by using a map that matches the elements of $\mathbf{C}(\omega_0)$ to $\tilde{\mathbf{C}}(\omega_0)$ and applying it to $\mathbf{X}(\omega_0)$:

$$\tilde{\mathbf{X}}(\omega_0) = \begin{bmatrix} \mathbf{X}(\omega_0)_{1,1} \\ \frac{1}{2}(\mathbf{X}(\omega_0)_{1,2} + \mathbf{X}(\omega_0)_{2,1}) \\ \mathbf{X}(\omega_0)_{2,2} \end{bmatrix} \tag{3.52}$$

The virtual data matrix is used to construct the virtual correlation matrix given in Equation 3.33:

$$\tilde{\mathbf{R}}(\omega_0) = \mathbb{E}[\tilde{\mathbf{X}}(\omega_0)\tilde{\mathbf{X}}(\omega_0)^H]. \tag{3.53}$$

The resulting virtual correlation matrix is a rank 1, 3×3 matrix. As was discussed in Section 3.3.3, using this correlation matrix, up to two targets can be resolved, but they cannot be coherent.

Similarly, by transmitting and receiving a different frequency ω_1, different virtual data and correlation matrices can be formed:

$$\tilde{\mathbf{X}}(\omega_1) = \begin{bmatrix} \mathbf{X}(\omega_1)_{1,1} \\ \frac{1}{2}(\mathbf{X}(\omega_1)_{1,2} + \mathbf{X}(\omega_1)_{2,1}) \\ \mathbf{X}(\omega_1)_{2,2} \end{bmatrix}, \tag{3.54}$$

$$\tilde{\mathbf{R}}(\omega_1) = \mathbb{E}[\tilde{\mathbf{X}}(\omega_1)\tilde{\mathbf{X}}(\omega_1)^H]. \tag{3.55}$$

Averaging the virtual correlation matrix over frequency can allow for coherent targets to be resolved. From Equation 3.44, two frequencies should be sufficient to resolve two coherent targets. The averaged virtual correlation matrix is formed as follows:

$$\begin{aligned} \bar{\mathbf{R}} &= \frac{1}{2}[\tilde{\mathbf{R}}(\omega_0) + \mathbf{B}_0(\omega_1)\tilde{\mathbf{R}}(\omega_1)\mathbf{B}_0(\omega_1)^H] \\ &\approx \tilde{\mathbf{A}}_{\mathbf{R}}(\omega_0)\frac{1}{2}[\tilde{\mathbf{S}}_{\mathbf{T}}(\omega_0) + \tilde{\mathbf{S}}_{\mathbf{T}}(\omega_1)]\tilde{\mathbf{A}}_{\mathbf{R}}(\omega_0)^H \\ &= \tilde{\mathbf{A}}_{\mathbf{R}}(\omega_0)\bar{\mathbf{S}}_{\mathbf{T}}\tilde{\mathbf{A}}_{\mathbf{R}}(\omega_0)^H \end{aligned} \tag{3.56}$$

If we assume that we have two coherent reflectors with complex amplitudes

$$a_1(\omega_0), a_2(\omega_0), a_1(\omega_1), a_2(\omega_1), \tag{3.57}$$

we can examine the source correlation matrix $\tilde{\mathbf{S}}_{\mathbf{T}}(\omega_0)$ and averaged source correlation matrix $\bar{\mathbf{S}}_{\mathbf{T}}$ more closely.

The source correlation matrix written out is

$$\tilde{\mathbf{S}}_{\mathbf{T}}(\omega_0) = \begin{bmatrix} a_1(\omega_0)^2 & a_1(\omega_0)a_2(\omega_0) \\ a_2(\omega_0)a_1(\omega_0) & a_2(\omega_0)^2 \end{bmatrix}. \tag{3.58}$$

It is easy to see that the columns of $\tilde{\mathbf{S}}_{\mathbf{T}}(\omega_0)$ are linearly dependent for any reflectivities. Thus $\tilde{\mathbf{S}}_{\mathbf{T}}(\omega_0)$ is not full rank. This is why $\tilde{\mathbf{R}}(\boldsymbol{\omega_0})$ alone will not work in MUSIC for coherent targets. The same analysis applies to $\tilde{\mathbf{S}}_{\mathbf{T}}(\omega_1)$.

However, the averaged source correlation matrix from Equation 3.56 is

$$\bar{\mathbf{S}}_{\mathbf{T}} = \frac{1}{2}\begin{bmatrix} \sum_{q=0}^{1} a_1(\omega_q)^2 & \sum_{q=0}^{1} a_1(\omega_q)a_2(\omega_q) \\ \sum_{q=0}^{1} a_2(\omega_q)a_1(\omega_q) & \sum_{q=0}^{1} a_2(\omega_q)^2 \end{bmatrix}. \tag{3.59}$$

This matrix is full rank unless

$$\begin{aligned} \det \bar{\mathbf{S}}_{\mathbf{T}} = 0 &\Leftrightarrow a_1(\omega_1)a_2(\omega_0) = a_2(\omega_1)a_1(\omega_0) \\ &\Leftrightarrow \tilde{a}_1(\omega_1)e^{-jk_1 2R_1}\tilde{a}_2(\omega_0)e^{-jk_0 2R_2} = \tilde{a}_2(\omega_1)e^{-jk_1 2R_2}\tilde{a}_1(\omega_0)e^{-jk_0 2R_1}. \end{aligned} \tag{3.60}$$

Recall that $\tilde{a}_k(\omega_q)$ encompasses the strength of reflection and the phase change at the reflection boundary for the k^{th} target at frequency ω_q, but not the phase change due to propagation. The exponentials are the phase change due to propagation delay and depend on the target range, R_k, and the frequency. Equation 3.60 is not true in general, and thus $\bar{\mathbf{S}}_{\mathbf{T}}$ is full rank in general. However, to explore where problems may arise with the rank conditions, assume that the target reflectivities are identical, i.e.,

$$\begin{aligned} \tilde{a}_1(\omega_0) &= \tilde{a}_2(\omega_0) \\ \tilde{a}_1(\omega_1) &= \tilde{a}_2(\omega_1). \end{aligned} \tag{3.61}$$

Then, Equation 3.60 is satisfied if

$$\begin{aligned} e^{-jk_1 2R_1}e^{-jk_0 2R_2} = e^{-jk_1 2R_2}e^{-jk_0 2R_1} &\Leftrightarrow e^{-jk_0 2(\alpha_1 R_1 - R_2)} = e^{-jk_0 2(\alpha_1 R_2 - R_1)} \\ &\Leftrightarrow R_1 = R_2 + \frac{n\lambda_0}{2(1+\alpha_1)} \text{ for integer } n. \end{aligned} \tag{3.62}$$

This condition implies that for some target ranges, at certain frequencies (governed

by α_1), there may be rank problems with the averaged source correlation matrix $\bar{\mathbf{S}}_{\mathbf{T}}$. However, recall that we assume the targets are identical. For different targets, Equation 3.62 will not cause rank deficiency in $\bar{\mathbf{S}}_{\mathbf{T}}$. If it is a worry that the targets may be identical, a few different frequencies could be used to ensure that Equation 3.62 is not satisfied for some frequency.

Thus, it is generally reasonable to assume that the columns of $\bar{\mathbf{S}}_{\mathbf{T}}$ are linearly independent. Assuming this, $\bar{\mathbf{S}}_{\mathbf{T}}$ has full rank and $\bar{\mathbf{R}}(\omega_0)$ can be used in MUSIC to resolve up to two coherent targets. This is an improvement over using the natural correlation matrix, which could resolve only one target, and also over the non-averaged virtual correlation matrix, which could resolve two non-coherent targets.

Simulation

For our simulation, there are two coherent reflectors located at $(R_1, u_1) = (3.1, 0)$ and $(R_2, u_2) = (3.7, .15)$, which meet the far-field conditions. We will use frequencies 1 GHz and 1.1 GHz to average the virtual correlation matrices. The sector we use to calculate the array interpolation matrix $\mathbf{B}_0(\omega_1)$ is $[-.1, .2]$ and it is calculated using 100 uniformly spaced samples of the sector.

The averaged virtual correlation matrix is used in MUSIC. Note that in the MUSIC estimator from Equation 3.25, we are now using the virtual array steering vector,

$$\tilde{\mathbf{a}}_R(u, \omega_0) = [e^{-jk_0 u \frac{\lambda_0}{4}}, 1, e^{jk_0 u \frac{\lambda_0}{4}}]^T, \tag{3.63}$$

in place of the natural array steering vector given in Equation 3.25 because we are using virtual arrays.

The result using the averaged virtual correlation matrix $\bar{\mathbf{R}}(\omega_0)$ in MUSIC is shown in Figure 3.2. We see that the coherent reflectors are successfully located. The stars

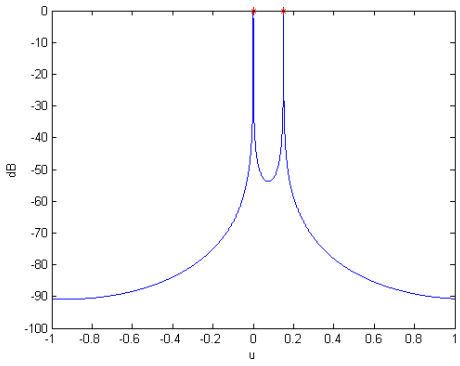

Figure 3.2: Averaged Virtual Correlation Matrix used in MUSIC, noiseless

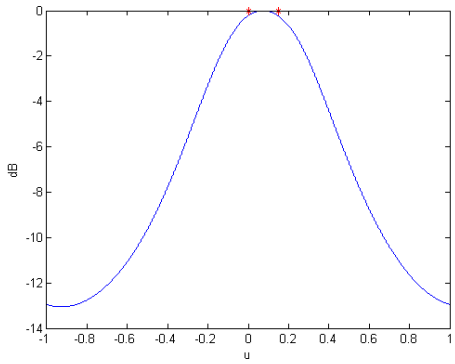

Figure 3.3: Non-averaged Virtual Correlation Matrix used in MUSIC, noiseless

denote actual reflector locations.

For comparison, Figure 3.3 shows the result when only the virtual correlation matrix $\tilde{\mathbf{R}}(\omega_0)$ is used in MUSIC. It is unable to resolve the coherent reflectors because the source correlation matrix is not full rank.

Using the averaged virtual correlation matrix, we were able to resolve two coherent reflectors with just two transmit/receive array elements, where with active MUSIC using virtual arrays in [13], the targets could not be resolved because they are coherent.

3.4.2 Examining the Effect of Noise on the Averaged Virtual Correlation Matrix

When additive, zero-mean, circular, spatially white Gaussian observation noise of variance σ^2 is present, the virtual correlation matrices have a scaled identity added to them:

$$\begin{aligned} &\tilde{\mathbf{R}}(\omega_0) + \sigma^2\mathbf{I} \\ &\tilde{\mathbf{R}}(\omega_1) + \sigma^2\mathbf{I} \end{aligned} \tag{3.64}$$

Generally, MUSIC does well in such a noise environment because the addition of a scaled identity matrix preserves the eigenvectors. However, when the correlation matrices are averaged over frequency, the averaged virtual correlation matrix in noise becomes

$$\begin{aligned} \bar{\mathbf{R}} &= \frac{1}{2}[\tilde{\mathbf{R}}(\omega_0) + \sigma^2\mathbf{I} + \mathbf{B}_0(\omega_1)[\tilde{\mathbf{R}}(\omega_1) + \sigma^2\mathbf{I}]\mathbf{B}_0(\omega_1)^H] \\ &\approx \tilde{\mathbf{A}}_{\mathbf{R}}(\omega_0)\bar{\mathbf{S}}_{\mathbf{T}}\tilde{\mathbf{A}}_{\mathbf{R}}(\omega_0)^H + \frac{\sigma^2}{2}[\mathbf{I} + \mathbf{B}_0(\omega_1)\mathbf{B}_0(\omega_1)^H]. \end{aligned} \tag{3.65}$$

Since $\mathbf{B}_0(\omega_1)$ is not necessarily an orthogonal matrix, the effective additive noise may no longer be a scaled identity. This may lead to problems when used in MUSIC because it changes the eigenvectors and thus the estimated target locations.

We define the reflectivity power to noise power ratio, or signal-to-noise ratio (SNR), as the ratio of maximum reflectivity power over noise power:

$$SNR = \frac{\max_{q,k} |a_k(\omega_q)|^2}{\sigma^2}. \tag{3.66}$$

For this example, assuming an SNR of 20 dB, and using 1000 snapshots to estimate each of the virtual correlation matrices, the result using the averaged virtual

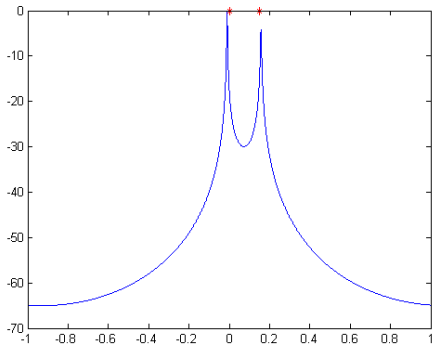

Figure 3.4: Averaged Virtual Correlation Matrix used in MUSIC, SNR = 20 dB

correlation matrix is shown in Figure 3.4. The reflector location estimates are quite close to the actual reflector locations. They are estimated to be at $u_1 = -0.0106$ and $u_2 = 0.1574$.

The fact that $\mathbf{B}_0(\omega_1)$ is not an orthogonal matrix does not appear to affect the reflector location estimates drastically in this example. This is consistent with the results in [46]. The effect of noise will be further examined in Section 3.5.

3.5 Averaging the Virtual Correlation Matrices in the Presence of Noise

As was considered at the end of the previous section, when using array interpolation in the presence of observation noise, the effective noise correlation matrix may no longer be a scaled identity and could potentially cause problems with estimation. We further examine this problem.

In general, the averaged virtual correlation matrix takes the form

$$\bar{\mathbf{R}}(\omega_0) + \frac{\sigma^2}{Q} \sum_{q=0}^{Q-1} \mathbf{B}_0(\omega_q) \mathbf{B}_0(\omega_q)^H. \tag{3.67}$$

If the addition of the effective noise matrix, $\frac{\sigma^2}{Q}\sum_{q=0}^{Q-1}\mathbf{B}_0(\omega_q)\mathbf{B}_0(\omega_q)^H$, drastically changes the eigenvectors of the sum from those of $\bar{\mathbf{R}}(\omega_0)$, there may be problems with estimating the target locations since MUSIC is based on the eigenvectors. For high SNR, σ^2 is small compared to the reflection powers, and will not change the eigenvectors by much. However, for lower SNR, σ^2 is large compared to the reflection powers, and if the effective noise matrix is highly non-orthogonal, the effect on target location can be problematic.

Consider an example with transmit and receive array elements in positions

$$\begin{aligned}\{x_{Rm}\} &= \{\frac{-\lambda_0}{2}, 0, \frac{\lambda_0}{2}\} \\ \{x_{Tn}\} &= \{\frac{-\lambda_0}{2}, 0, \frac{\lambda_0}{2}\}.\end{aligned} \tag{3.68}$$

We want to create a virtual correlation matrix based on the virtual array

$$\begin{aligned}\{\tilde{x}_{Rm}\} &= \{-\lambda_0, \frac{-\lambda_0}{2}, 0, \frac{\lambda_0}{2}, \lambda_0\} \\ \{\tilde{x}_{Tn}\} &= \{0\}.\end{aligned} \tag{3.69}$$

To resolve up to four coherent targets, we must use at least four frequencies for averaging the virtual correlation matrices. First, we choose the frequencies $1.0, 1.1, 1.2$ and $1.3GHz$. The simulation for four coherent targets at locations

$$\{(R_k, u_k)\} = \{(5.1, 0), (4.98, .09), (5.24, .21), (4.72, .3)\}, \tag{3.70}$$

assuming an SNR of 20 dB, is shown in Figure 3.5. The targets are not properly resolved. However, if we increase the bandwidth used so that we average over four frequencies $1.0, 1.25, 1.5$ and $2.0GHz$, we see in Figure 3.6 that the targets are successfully resolved.

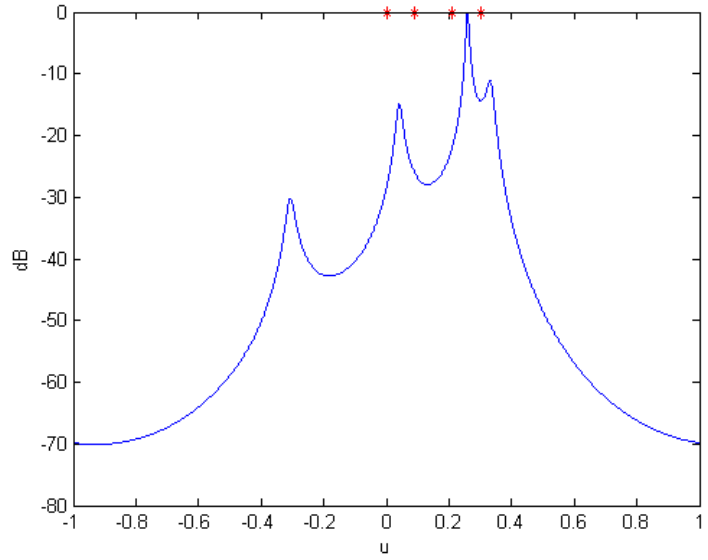

Figure 3.5: Averaged Virtual Correlation Matrix used in MUSIC, SNR = 20 dB, Four frequencies 1-1.3 GHz

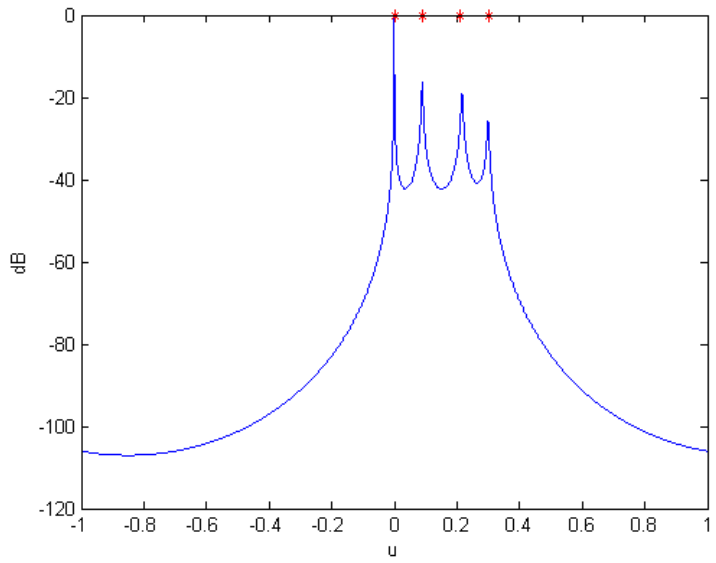

Figure 3.6: Averaged Virtual Correlation Matrix used in MUSIC, SNR = 20 dB, Four frequencies 1-2 GHz

Using a wider band may help combat the problems associated with array interpolation in the presence of observation noise.

For the array interpolation matrices calculated in the band $1.0 - 1.3GHz$, the average of the array interpolation matrices over frequency is

$$\frac{1}{5}\sum_{q=0}^{4}\mathbf{B}_0(\omega_q)\mathbf{B}_0(\omega_q)^H = \begin{bmatrix} 1.1331 & .3496-.1781j & -.1973+.2716j & +.0002j & -.1126-.3465j \\ .3496+.1781j & .8555 & .1599-.0815j & -.0283+.0389j & +.0002j \\ -.1973-.2716j & .1599+.0815j & 1.0000 & .1599-.0815j & -.1973+.2716j \\ -.0002j & -.0283-.0389j & .1599+.0815j & .8555 & .3496-.1781j \\ -.1126+.3465j & -.0002j & -.1973-.2716j & .3496+.1781j & 1.1331 \end{bmatrix}. \tag{3.71}$$

The matrix elements $(5,1)$ and $(1,5)$ cause the matrix to be highly non-orthogonal. Comparing this to the average of the array interpolation matrices in the band $1.0 - 2.0GHz$,

$$\frac{1}{5}\sum_{q=0}^{4}\mathbf{B}_0(\omega_q)\mathbf{B}_0(\omega_q)^H = \begin{bmatrix} 1.1708 & .3537-.1802j & -.1089+.1500j & -.0212+.1340j & -.0714-.2198j \\ .3537+.1802j & .8101 & .3601-.1835j & .0539-.0742j & -.0212+.1340j \\ -.1089-.1500j & .3601+.1835j & 1.0000 & .3601-.1835j & -.1089+.1500j \\ -.0212-.1340j & .0539+.0742j & .3601+.1835j & .8101 & .3537-.1802j \\ -.0714+.2198j & -.0212-.1340j & -.1089-.1500j & .3537+.1802j & 1.1708 \end{bmatrix}, \tag{3.72}$$

the off diagonal-elements are considerably smaller and the matrix is more like an orthogonal matrix.

Since we are able to choose the frequencies used, we could choose the frequencies to ensure that their sum does not yield a highly non-orthogonal matrix. A measure that could be used is one of the form

$$\text{Degree of Non-orthogonality} = ||W \odot (\frac{1}{Q}\sum_{q=0}^{Q-1}\mathbf{B}_0(\omega_q)\mathbf{B}_0(\omega_q)^H - \mathbf{I})||_F \tag{3.73}$$

where W is a weighting matrix that weights difference more heavily for non-diagonal elements.

In this example, the matrix in Equation 3.71 for a narrower band of frequencies has a non-orthogonality measure of 0.8490, where the weighting matrix W was taken to be zero for the main and secondary diagonals and 1 for remaining diagonals. The matrix in Equation 3.72 for the wider band of frequencies, the non-orthogonality measure is 0.5786. The array interpolation matrices which yield correct results have a lower non-orthogonality measure.

3.6 Out-of-Sector Targets

Until this point, we have only considered cases where all of the targets were clustered within a sector. In this section, we will examine what happens when there are targets that do not fit in a sector of sufficiently small size. For targets that cover a wide angular sector, the fit of the array interpolation matrix may be poor.

Using the same example in the previous section with array

$$\begin{aligned} \{x_{Rm}\} &= \{\frac{-\lambda_0}{2}, 0, \frac{\lambda_0}{2}\} \\ \{x_{Tn}\} &= \{\frac{-\lambda_0}{2}, 0, \frac{\lambda_0}{2}\}, \end{aligned} \tag{3.74}$$

and virtual array

$$\begin{aligned} \{\tilde{x}_{Rm}\} &= \{-\lambda_0, \frac{-\lambda_0}{2}, 0, \frac{\lambda_0}{2}, \lambda_0\} \\ \{\tilde{x}_{Tn}\} &= \{0\}, \end{aligned} \tag{3.75}$$

we simulate a noiseless scene with four coherent targets located at $\{-.5, .4, .47, .59\}$. To get a rough idea of where the targets are located, we process the received signals using beamforming first. The beamformed image is shown in Figure 3.7. We clearly see that there are two sectors corresponding to the peaks of the beamformed image

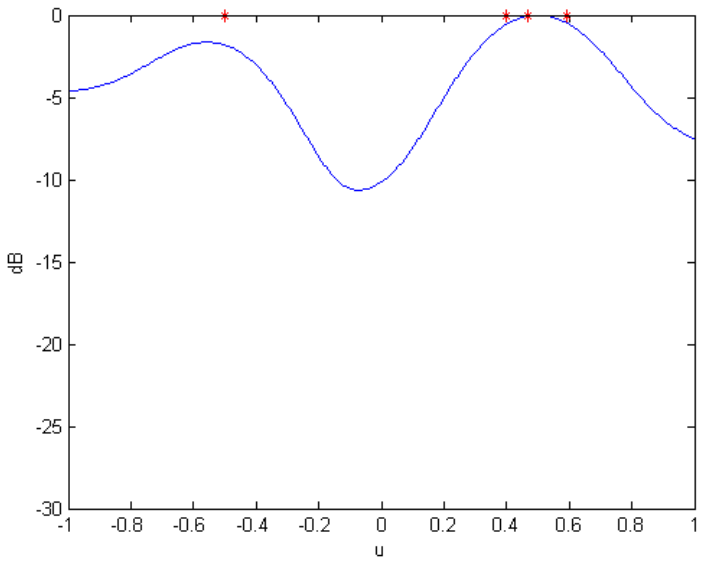

Figure 3.7: Beamformed Image for defining sectors

containing the targets. The stars denote the actual target locations. Having targets in two separate sectors is a problem since the methods we have derived for averaging the virtual correlation matrices assume only one sector.

Using a large enough sector to cover both peaks causes the problems with target location estimation. This is demonstrated in Figure 3.8. Here the array interpolation matrices are calculated using the sector $[-.6, .65]$ and the frequencies $1.0, 1.25, 1.5$ and $2GHz$ are used to average the virtual correlation matrices.

Another approach is to take two different sectors and average the virtual correlation matrices over frequency for each sector. Figure 3.9, shows the simulations for two different sectors, $[-.6, -.4]$ and $[.35, .65]$, for four frequencies in 1-2 GHz. This, unfortunately, also does not give good results.

There exist MUSIC techniques that allow power within desired sector and null power outside of the sector [47]. Beamspace MUSIC is a technique where the data matrix $\tilde{\mathbf{X}}(\omega_0)$ is pre-multiplied by some beamforming matrix, $\mathbf{F}(\omega_0)$. For beamspace

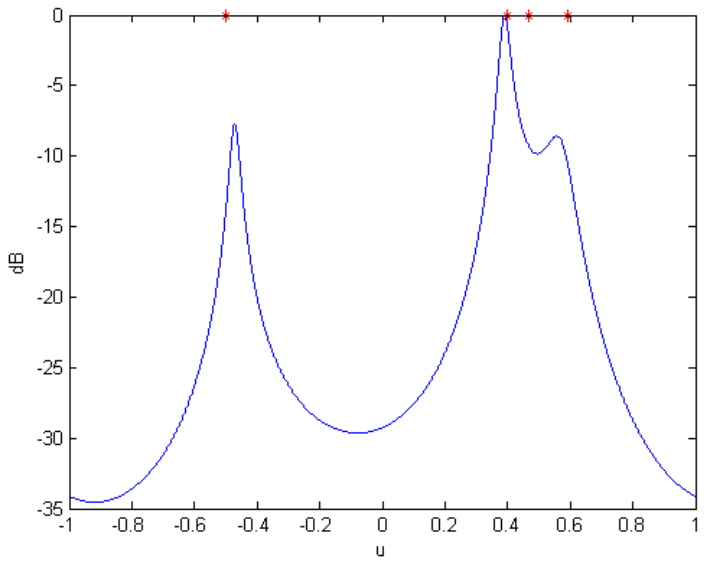

Figure 3.8: Averaged Virtual Correlation Matrix used in MUSIC, Four frequencies 1-2 GHz, Sector $[-.6, .65]$

techniques, the virtual correlation matrix becomes

$$\begin{aligned}\tilde{\mathbf{R}}(\omega_0) &= \mathbf{F}(\omega_0)\mathbb{E}[\tilde{\mathbf{X}}(\omega_0)\tilde{\mathbf{X}}(\omega_0)^H]\mathbf{F}(\omega_0)^H \\ &= \mathbf{F}(\omega_0)\tilde{\mathbf{A}}_{\mathbf{R}}(\omega_0)\tilde{\mathbf{S}}_{\mathbf{T}}(\omega_0)\tilde{\mathbf{A}}_{\mathbf{R}}(\omega_0)^H\mathbf{F}(\omega_0)^H.\end{aligned} \tag{3.76}$$

Then in MUSIC, instead of using the virtual array steering vector given in Equation 3.38, the modified vector $\mathbf{F}(\omega_0)\tilde{\mathbf{a}}_{\mathbf{R}}(u,\omega_0)$ is used and the estimator for beamspace MUSIC is

$$P_{\text{BS-MUSIC}}(u) = \frac{1}{\sum_{i=1}^{M-K} |\tilde{\mathbf{a}}_{\mathbf{R}}(u,\omega_0)^H\mathbf{F}(\omega_0)^H\mathbf{v}^{\mathbf{0}}{}_i(\omega_0)|^2}. \tag{3.77}$$

The array interpolation we use is a type of beamspace technique, but it is not robust against out-of-sector targets.

We suggest, but do not investigate further, a technique to find matrices $\{\mathbf{F}(\omega_q)\}$ such that they compensate for both the array interpolation and selecting the appro-

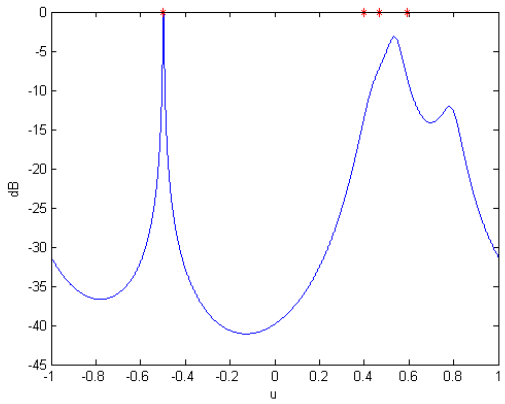

(a) Sector taken as (.35,.65)

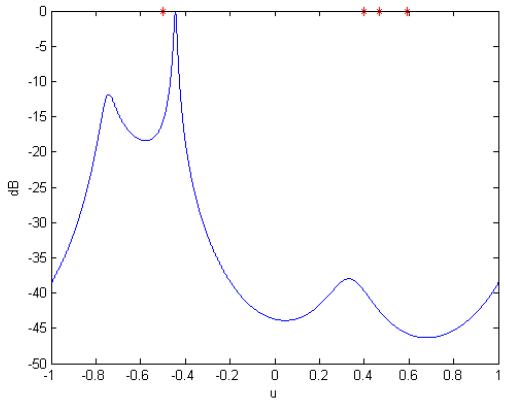

(b) Sector taken as (-.6,-.4)

Figure 3.9: Finding the Averaging Virtual Correlation Matrix in Two Different Sectors

priate sector. This can be done by minimizing

$$\int_{u_s}^{u_f} ||\mathbf{F}(\omega_0)\tilde{\mathbf{a}}_{\mathbf{R}}(u,\omega_0) - \mathbf{F}(\omega_q)\tilde{\mathbf{a}}_{\mathbf{R}}(u,\omega_q)||^2 du \tag{3.78}$$

with respect to $\mathbf{F}(\omega_q)$. In this expression, $\mathbf{F}(\omega_0)$ is known. It is the beamspace matrix that selects the desired sector and nulls the undesired sector. The matrices $\{\mathbf{F}(\omega_q)\}$ are found and the virtual correlation matrix is

$$\begin{aligned}
\bar{\mathbf{R}}(\omega_0) &= \frac{1}{Q}\sum_{q=0}^{Q-1} \mathbf{F}(\omega_q)\tilde{\mathbf{R}}(\omega_q)\mathbf{F}(\omega_q)^H \\
&= \frac{1}{Q}\sum_{q=0}^{Q-1} \mathbf{F}(\omega_q)\tilde{\mathbf{A}}_{\mathbf{R}}(\omega_q)\tilde{\mathbf{S}}_{\mathbf{T}}(\omega_q)\tilde{\mathbf{A}}_{\mathbf{R}}(\omega_q)^H\mathbf{F}(\omega_q)^H \\
&\approx \frac{1}{Q}\sum_{q=0}^{Q-1} \mathbf{F}(\omega_0)\tilde{\mathbf{A}}_{\mathbf{R}}(\omega_0)\tilde{\mathbf{S}}_{\mathbf{T}}(\omega_q)\tilde{\mathbf{A}}_{\mathbf{R}}(\omega_0)^H\mathbf{F}(\omega_0)^H \\
&= \mathbf{F}(\omega_0)\tilde{\mathbf{A}}_{\mathbf{R}}(\omega_0)\bar{\mathbf{S}}_{\mathbf{T}}\tilde{\mathbf{A}}_{\mathbf{R}}(\omega_0)^H\mathbf{F}(\omega_0)^H
\end{aligned} \tag{3.79}$$

Since there is a beamspace matrix, beamspace MUSIC given in Equation 3.77 should be used to estimate the target locations.

3.7 Conclusion

The existing idea of using virtual data and correlation matrices in direction-of-arrival estimation was combined with array interpolation to allow for additional coherent targets to located above the conventional limit. For transmit and receive arrays of N and M elements, respectively, it was shown that up to $N + M - 2$ coherent targets can be resolved when the virtual correlation matrices are averaged over multiple frequencies. The conventional limit is $\min(N, M-1)$. However, the ability to resolve coherent targets is only obtained by restricting the area to be imaged to a sector.

The targets must lie within a reasonably small sector, but this is not an unreasonable assumption since high-resolution techniques are used.

For this technique, a low SNR environment may cause estimation problems, but using a larger bandwidth may help alleviate some of these problems. Also, it was shown that if a target lies outside of the sector in consideration, there may be problems with estimating the target locations. A method based on beamspace MUSIC was suggested to mitigate this problem, but additional research and simulation needs to be carried out. Both of these issues may be able to be solved by more carefully choosing the array interpolation matrix, i.e., adding constraints to the least squares fit, and finding a way in which frequencies can be chosen optimally.

Chapter 4

High-resolution Imaging with Multiple Frequencies using Planar Arrays

4.1 Introduction

In Chapters 2 and 3, we used the concept of virtual arrays to increase the number of point sources/targets that can be resolved in passive and active imaging with line arrays. In this chapter, we suggest ways these ideas from the previous chapters can be extended to planar arrays. This is a desirable extension because with planar arrays, both elevation and azimuthal angle can be resolved, where with a line array, only elevation angle can be [23].

For passive imaging, we will see that extending the idea formulated in Chapter 2 to planar arrays is not always possible in the general case, but we will describe a class of arrays for which the extension works. For active imaging, the extension of the virtual array method in Chapter 3 is relatively straightforward for rectangular lattice

arrays.

The background and problem development from the previous chapters are briefly reviewed with the necessary modifications for planar arrays. However, it is assumed that the reader has read the previous two chapters and is familiar with the high-resolution techniques and the motivation behind using virtual arrays.

4.2 Imaging with a Planar Array

4.2.1 Array Geometry

In Chapters 2 and 3, we restricted the array elements to be in a line. In this chapter we allow them to be distributed in a plane. This is advantageous because with a planar array, both elevation and azimuthal angle can be reseolved.

Consider the transmit and receive array elements to be located in the x-y plane at positions $\{\mathbf{x_{Tn}}, n = 1, 2, ..., N\}$ and $\{\mathbf{x_{Rm}}, m = 1, 2, ..., M\}$, respectively. In the following discussions, we will use multiple representations of the array element positions. We represent the positions in three ways:

- As a vector in Cartesian coordinates:

$$\begin{aligned} \mathbf{x_{Tn}} &= [x_{Tn}, y_{Tn}] \text{ is the } n^{th} \text{ transmitting element position} \\ \mathbf{x_{Rm}} &= [x_{Rm}, y_{Rm}] \text{ is the } m^{th} \text{ receiving element position.} \end{aligned} \tag{4.1}$$

- In polar coordinates:

$$\begin{aligned} &(r_{Tn}, \varphi_{Tn}) \text{ is the } n^{th} \text{ transmitting element position} \\ &(r_{Rm}, \varphi_{Rm}) \text{ is the } m^{th} \text{ receiving element position,} \end{aligned} \tag{4.2}$$

where r_{Rm} and r_{Tn} are the radii from the origin and φ_{Rm} and φ_{Tn} are the angles measured from the x-axis.

- As a complex scalar:

$$\begin{aligned} &x_{Tn} + jy_{Tn} \text{ is the } n^{th} \text{ transmitting element position} \\ &x_{Rm} + jy_{Rm} \text{ is the } m^{th} \text{ receiving element position.} \end{aligned} \tag{4.3}$$

It should be obvious which notation is being used, and we will switch between them often, as each one has its advantages for understanding the array geometry.

We consider arrays that are fixed to a lattice with spacing $\frac{\lambda_0}{2}$. The wavelength λ_0 is the wavelength corresponding to frequency ω_0. We call this the reference frequency because it is the frequency on which the array spacing is based.

4.2.2 Target and Source Distributions

The array elements are located in the x-y plane. We define the z-axis (broadside) as normal to the x-y plane, see Figure 4.1. We assume that there are K targets/sources in the scene. Their positions are represented in spherical coordinates, where the k^{th} target location is (R_k, ϕ_k, θ_k). R_k is the distance of the target from the origin. The elevation angle θ_k is measured from the z-axis and ϕ_k is the azimuthal angle measured with respect to the x-axis in the array plane. We restrict $\theta_k \in [0, \frac{\pi}{2}]$ $(z > 0)$ so that there is no ambiguity, and take $\phi_k \in [-\pi, \pi]$.

We restrict the targets/sources considered to be in the farfield of the array. That is, the wavefronts arriving from the targets/sources at the array can be approximated as plane waves. Thus, we only consider the direction of the targets/sources and denote

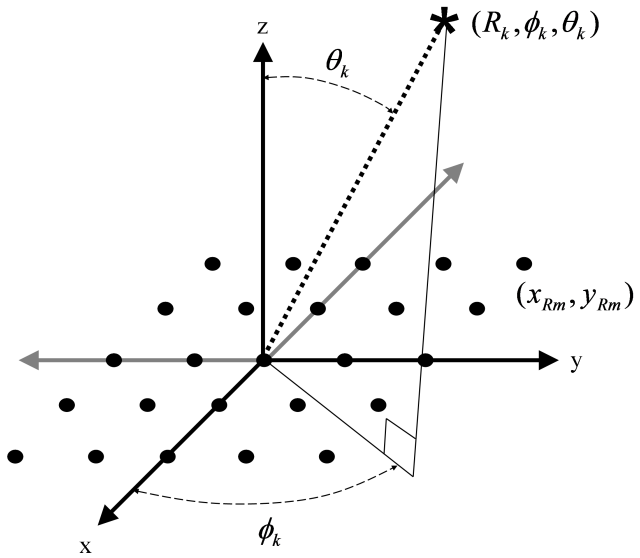

Figure 4.1: Array Geometry for Planar Arrays

the direction of k^{th} target/source by the vector

$$\mathbf{u_k} = [\sin\theta_k \cos\phi_k, \sin\theta_k \sin\phi_k]. \tag{4.4}$$

Even though the array geometry may be basically the same for passive or active imaging, the nature of the targets/sources is different for each and we recall their properties from Chapters 2 and 3.

Passive imaging

In passive imaging, sources emitting wideband radiation are observed by the array. The frequencies $\{\omega_q, q = 0, 1, ..., Q-1\}$ are assumed to be in the band and the array performs narrowband filtering to extract the signal at each frequency considered.

Recall that the frequency ω_0 is the reference frequency - the frequency on which the array spacing is based.

We assume that these sources are emitting independently of each other, that is, over multiple observations, the radiation emitted from different sources is uncorrelated. Mathematically, the complex amplitudes, $\{S_k(\omega_q)\}$, received at the origin of the array, have the following relationship between sources over multiple snapshots at each frequency:

$$\mathbb{E}[S_k(\omega_q)S_n^*(\omega_q)] = \begin{cases} P_k(\omega_q) & \text{for } k = n \\ 0 & \text{for } k \neq n. \end{cases} \tag{4.5}$$

Here $P_k(\omega_q)$ is the power of the k^{th} source at frequency ω_q.

Active Imaging

In active imaging, the targets are not emitting their own radiation, but they are reflecting transmitted radiation. Radiation consisting of frequencies $\{\omega_q, q = 0, 1, ..., Q-1\}$ is transmitted from the transmit array and when radiation of frequency ω_q is incident on the k^{th} target, the target reflects with reflectivity $\tilde{a}_k(\omega_q)$. This reflectivity embodies the strength of the reflection as well as the reflection phase. The reflectivities between a pair of targets may be incoherent or coherent. We assume that they are coherent, as this is the more difficult and interesting case. Over multiple snapshots, the coherent relationship means that each pair of targets always reflects with the same phase difference between them. We further assume that the reflections are deterministic, that is

$$\mathbb{E}[\tilde{a}_k(\omega_q)\tilde{a}_n^*(\omega_q)] = \tilde{a}_k(\omega_q)\tilde{a}_n^*(\omega_q) \text{ for all } k, n. \tag{4.6}$$

4.2.3 Data Collection

The data collection for passive imaging differs from active imaging since with active imaging, we must consider transmitting the signals. Since the effect of noise was studied in Chapters 2 and 3, we ignore it here for simplicity of discussion.

For the mathematical represention of the data collected, we make use of the farfield approximation. The propagation delays from a target/source at (R_k, ϕ_k, θ_k) to a receive array element position $\mathbf{x_{Rm}}$ is

$$c\tau_{k,Rm} \approx R_k - \mathbf{u_k}^T \mathbf{x_{Rm}}, \tag{4.7}$$

where c is the speed of light. Likewise, the propagation delay from a transmit array element at $\mathbf{x_{Tn}}$ to the same target is

$$c\tau_{k,Tn} \approx R_k - \mathbf{u_k}^T \mathbf{x_{Tn}}. \tag{4.8}$$

Passive Imaging

Suppose an array of M co-planar elements with positions $\{\mathbf{x_{Rm}}, m = 1, 2, ..., M\}$ is receiving narrowband radiation at frequency ω_q from K farfield sources. The complex amplitudes received at frequency ω_q at the set of array elements is stored in the data

vector $\mathbf{x}(\omega_q)$, given by

$$\begin{aligned}\mathbf{x}(\omega_q) = \mathbf{A_R}(\omega_q)\mathbf{s}(\omega_q) &= \begin{bmatrix} \sum_k S_k(\omega_q) e^{jk_q \mathbf{u_k}^T \mathbf{x_{R1}}} \\ \sum_k S_k(\omega_q) e^{jk_q \mathbf{u_k}^T \mathbf{x_{R2}}} \\ \vdots \\ \sum_k S_k(\omega_q) e^{jk_q \mathbf{u_k}^T \mathbf{x_{RM}}} \end{bmatrix} \\ &= \begin{bmatrix} \sum_k S_k(\omega_q) e^{jk_0 \mathbf{u_k}^T \alpha_q \mathbf{x_{R1}}} \\ \sum_k S_k(\omega_q) e^{jk_0 \mathbf{u_k}^T \alpha_q \mathbf{x_{R2}}} \\ \vdots \\ \sum_k S_k(\omega_q) e^{jk_0 \mathbf{u_k}^T \alpha_q \mathbf{x_{RM}}} \end{bmatrix}.\end{aligned} \tag{4.9}$$

Here $k_0 = \frac{2\pi}{\lambda_0}$ is the wavenumber associated with the reference frequency. We define α_q so that the frequency ω_q is represented as a multiple of the reference frequency, $\omega_q = \alpha_q \omega_0$. The receive array manifold matrix at frequency ω_q, $\mathbf{A_R}(\omega_q)$, is given by

$$\mathbf{A_R}(\omega_q) = \begin{bmatrix} e^{jk_q \mathbf{u_1}^T \mathbf{x_{R1}}} & e^{jk_q \mathbf{u_2}^T \mathbf{x_{R1}}} & ... & e^{jk_q \mathbf{u_K}^T \mathbf{x_{R1}}} \\ e^{jk_q \mathbf{u_1}^T \mathbf{x_{R2}}} & e^{jk_q \mathbf{u_2}^T \mathbf{x_{R2}}} & ... & e^{jk_q \mathbf{u_K}^T \mathbf{x_{R2}}} \\ \vdots & \vdots & \vdots & \vdots \\ e^{jk_q \mathbf{u_1}^T \mathbf{x_{RM}}} & e^{jk_q \mathbf{u_2}^T \mathbf{x_{RM}}} & ... & e^{jk_q \mathbf{u_K}^T \mathbf{x_{RM}}} \end{bmatrix}, \tag{4.10}$$

and $\mathbf{s}(\omega_q) = [S_1(\omega_q), S_2(\omega_q), ..., S_K(\omega_q)]^T$ is the vector of the complex amplitudes of each source. Note that because the source radiation is incoherent and we assume farfield sources, we do not need to account for the exact path lengths from the sources to the elements. The path length differences are sufficient and are captured in the $\{\mathbf{u_k}^T \mathbf{x_{Rm}}\}$ products in the argument of the exponentials in the array manifold matrix.

Active Imaging

Since we may possibly be imaging coherent targets, it is necessary that we collect the data so that the data from each transmit/receive pair can be accessed individually. To do this, the waveform $s(t)$ is constructed from multiple frequencies, transmitted individually from each transmitting element and received by all receiving elements.

The total received signal at $\mathbf{x_{Rm}}$ from $\mathbf{x_{Tn}}$ is the sum of all reflections from the targets:

$$\sum_{q=0}^{Q-1}\sum_{k=1}^{K}\tilde{a}_k(\omega_q)e^{j(\omega_q(t-\tau_{k,Tn}-\tau_{k,Rm})+\xi_q)}, \tag{4.11}$$

where $\xi_q \in [-\pi, \pi]$ is a random but fixed phase associated with frequency ω_q Since the targets are assumed to be in the farfield, we can make a simplification in Equation 4.11. Using the farfield approximation given in Equations 4.7 and 4.8, and matched filtering at the receivers about frequency ω_q, the complex amplitude we receive at $\mathbf{x_{Rm}}$ from $\mathbf{x_{Tn}}$ at frequency ω_q is

$$\begin{aligned}\mathbf{X}_{m,n}(\omega_q) &= \sum_{k=1}^{K}\tilde{a}_k(\omega_q)e^{-jk_q 2R_k}e^{j\xi_q}e^{jk_q \mathbf{u_k}^T(\mathbf{x_{Rm}}+\mathbf{x_{Tn}})} \\ &= \sum_{k=1}^{K}a_k(\omega_q)e^{jk_q \mathbf{u_k}^H(\mathbf{x_{Rm}}+\mathbf{x_{Tn}})},\end{aligned} \tag{4.12}$$

where

$$a_k(\omega_q) = \tilde{a}_k(\omega_q)e^{-jk_q 2R_k}e^{j\xi_q}. \tag{4.13}$$

The complex amplitude $a_k(\omega_q)$ now depends on not only the characteristics of the target, but the phase depends on the distance from the target to the array and the transmit phase, which vary over frequency. As for linear arrays, because of this, even

for otherwise identical targets, generally

$$a_k(\omega_q) \neq a_l(\omega_p) \text{ for all } k \neq l, q \neq p, \tag{4.14}$$

except under strict conditions on the target ranges and chosen frequencies.

After matched filtering about the Q frequencies, the complex amplitudes received from all transmitters and receivers at each frequency can be arranged into data matrices, $\{\mathbf{X}(\omega_q)\}$, where Equation 4.12, the data resulting from the transmission from $\mathbf{x_{Tn}}$ received at $\mathbf{x_{Rm}}$ at frequency ω_q, is the $(m,n)^{th}$ element of $\mathbf{X}(\omega_q)$.

For each frequency, the data matrix can be factored as follows:

$$\mathbf{X}(\omega_q) = \mathbf{A_R}(\omega_q)\mathbf{S}(\omega_q)\mathbf{A_T}(\omega_q)^T, \tag{4.15}$$

where $\mathbf{A_R}(\omega_q)$ is the receive array manifold matrix given in Equation 4.10, the transmit array manifold matrix, $\mathbf{A_T}(\omega_q)$, is

$$\mathbf{A_T}(\omega_q) = \begin{bmatrix} e^{jk_q\mathbf{u_1}^T\mathbf{x_{T1}}} & e^{jk_q\mathbf{u_2}^T\mathbf{x_{T1}}} & \dots & e^{jk_q\mathbf{u_K}^T\mathbf{x_{T1}}} \\ e^{jk_q\mathbf{u_1}^T\mathbf{x_{T2}}} & e^{jk_q\mathbf{u_2}^T\mathbf{x_{T2}}} & \dots & e^{jk_q\mathbf{u_K}^T\mathbf{x_{T2}}} \\ \vdots & \vdots & \vdots & \vdots \\ e^{jk_q\mathbf{u_1}^T\mathbf{x_{TN}}} & e^{jk_q\mathbf{u_2}^T\mathbf{x_{TN}}} & \dots & e^{jk_q\mathbf{u_K}^T\mathbf{x_{TN}}} \end{bmatrix}, \tag{4.16}$$

and $\mathbf{S}(\omega_q) = \text{diag}[a_1(\omega_q), a_2(\omega_q), ...a_K(\omega_q)]$ is the diagonal matrix of reflectivities.

4.2.4 Correlation

For high-resolution techniques, in both passive and active imaging, the spatial correlation matrix is used. This is the autocorrelation of the data vector or data matrix with itself.

For passive imaging, the spatial correltation matrix at frequency ω_q is given as

$$\mathbf{R}(\omega_q) = \mathbb{E}[\mathbf{x}(\omega_q)\mathbf{x}(\omega_q)^H], \tag{4.17}$$

where $\mathbf{x}(\omega_q)$ is the data vector arising from observing radiating sources. The expectation is estimated by averaging over multiple snapshots. The spatial correlation matrix for passive imaging can be factored as

$$\mathbf{R}(\omega_q) = \mathbf{A_R}(\omega_q)\mathbf{P}(\omega_q)\mathbf{A_R}(\omega_q)^H, \tag{4.18}$$

where $\mathbf{P}(\omega_q)$ is the diagonal matrix of source powers,

$$\mathbf{P}(\omega_q) = \text{diag}[P_1(\omega_q), P_2(\omega_q), ..., P_K(\omega_q)], \tag{4.19}$$

and $\mathbf{A_R}(\omega_q)$ is the receive array manifold matrix in Equation 4.10. The $(m,n)^{th}$ element of the spatial correlation matrix for passive imaging at frequency ω_q is

$$\begin{aligned} \mathbf{R}(\omega_q)_{m,n} &= \sum_{k=1}^{K}\sum_{l=1}^{K} \mathbb{E}[S_k(\omega_q)S_l(\omega_q)^*] e^{jk_q \mathbf{u_k}^T \mathbf{x_{Rm}}} e^{-jk_q \mathbf{u_l}^T \mathbf{x_{Rn}}} \\ &= \sum_{k=1}^{K} P_k(\omega_q) e^{jk_0 \mathbf{u_k}^T \alpha_q (\mathbf{x_{Rm}} - \mathbf{x_{Rn}})}. \end{aligned} \tag{4.20}$$

This represents the correlation between what is received at the m^{th} and n^{th} receive array elements.

For active imaging, the correlation matrix at frequency ω_q is

$$\mathbf{R}(\omega_q) = \mathbb{E}[\mathbf{X}(\omega_q)\mathbf{X}(\omega_q)^H], \tag{4.21}$$

where $\mathbf{X}(\omega_q)$ is the data matrix. In practice, the expectation is estimated by averaging

over multiple snapshots. However, since we are assuming coherent targets and no noise, there is no randomness in the signal, and $\mathbf{R}(\omega_q)$ is treated as a deterministic quantity. The spatial correlation matrix can be factored in the following way:

$$\begin{aligned}\mathbf{R}(\omega_q) &= \mathbf{A_R}(\omega_q)\mathbf{S}(\omega_q)\mathbf{A_T}(\omega_q)^T\mathbf{A_T}(\omega_q)^*\mathbf{S}(\omega_q)^H\mathbf{A_R}(\omega_q)^H \\ &= \mathbf{A_R}(\omega_q)\mathbf{S_T}(\omega_q)\mathbf{A_R}(\omega_q)^H,\end{aligned} \tag{4.22}$$

where $\mathbf{S}(\omega_q)$ is the diagonal matrix of target reflectivities,

$$\mathbf{S}(\omega_q) = \text{diag}[a_1(\omega_q), a_2(\omega_q), ..., a_K(\omega_q)], \tag{4.23}$$

$\mathbf{A_R}(\omega_q)$ is the receive array manifold matrix given in Equation 4.10, and $\mathbf{A_T}(\omega_q)$ is the transmit array manifold matrix in Equation 4.16. We define the *source correlation matrix* $\mathbf{S_T}(\omega_q)$ as

$$\mathbf{S_T}(\omega_q) = \mathbf{S}(\omega_q)\mathbf{A_T}(\omega_q)^T\mathbf{A_T}(\omega_q)^*\mathbf{S}(\omega_q)^H. \tag{4.24}$$

Comparing Equations 4.18 and 4.22, we see that the correlation matrices for both passive and active imaging have the same basic structure. This means that we can applying the same high-resolution techniques to either passive or active imaging. We consider the well-known two-dimensional high-resolution technique MUSIC.

4.2.5 MUSIC for Planar Arrays

MUSIC has already been derived in Chapters 2 and 3 for both passive and active imaging. Here, we state the changes we need in order to use it for two-dimensional imaging [23]. MUSIC for two-dimensional imaging is similar to that of one-dimensional imaging. The main difference is that instead of varying just the elevation angle, we now

vary both the elevation angle and the azimuthal angle. Since this is a narrowband technique, we assume operation at the reference frequency.

We define the array steering vector as

$$\mathbf{a_R}(\mathbf{u},\omega_0) = \mathbf{a_R}(\theta,\phi,\omega_0) = [e^{jk_0\mathbf{u}^T\mathbf{x_{R1}}}, e^{jk_0\mathbf{u}^T\mathbf{x_{R2}}}, ..., e^{jk_0\mathbf{u}^T\mathbf{x_{RM}}}]^T. \tag{4.25}$$

.

The two-dimensional MUSIC estimator is defined as

$$P_{\text{MUSIC}}(\theta,\phi) = \frac{1}{\sum_{i=1}^{M-K} |\mathbf{a_R}(\theta,\phi,\omega_0)^H \mathbf{v}_{0i}(\omega_0)|^2} \tag{4.26}$$

where as in one-dimensional MUSIC, the $\{\mathbf{v}_{0i}(\omega_0)\}$ are the zero-eigenvectors of the correlation matrix $\mathbf{R}(\omega_0)$.

This estimator is derived assuming $\mathbf{P}(\omega_0)$ or $\mathbf{S_T}(\omega_0)$ of the correlation matrix $\mathbf{R}(\omega_0)$ is full-rank, which is always true in passive imaging of incoherent targets and in active imaging when $N \geq K$. Assuming this, in passive imaging, up to $M-1$ incoherent sources can be resolved using MUSIC and in active imaging, up to $M-1$ total targets can be resolved of which N can be coherent. This is the same result as for one-dimensional MUSIC except the azimuthal location of the targets/sources can also be resolved.

4.2.6 Coarray

The difference and sum coarrays for planar arrays are no different than for line arrays except that now the vector sum or difference is taken between array element positions

[14]. The difference coarray for passive imaging at the reference frequency is

$$\{\mathbf{y^D}_l\} = \{\mathbf{y^D}_l | \mathbf{y^D}_l = \mathbf{x_{Rm}} - \mathbf{x_{Rn}}, m = 1, 2, .., M, n = 1, 2, ..., M\}. \tag{4.27}$$

We see that this is the support for the correlation matrix at the reference frequency ω_0 for incoherent targets, Equation 4.20.

Likewise, the sum coarray for active imaging at the reference frequency is

$$\{\mathbf{y^S}_l\} = \{\mathbf{y^S}_l | \mathbf{y^S}_l = \mathbf{x_{Tn}} + \mathbf{x_{Rm}}, m = 1, 2, .., M, n = 1, 2, ..., N\}. \tag{4.28}$$

This is the support in the data matrix for frequency ω_0.

Any sum or difference coarray point, $\mathbf{y_l}$, can be represented in Cartesian, polar or complex coordinates, just as for array element positions. The notations, respectively, are $\mathbf{y_l} = [x_l, y_l]$, (r_l, φ_l) and $x_l + jy_l$.

For a sum or difference coarray $\{\mathbf{y}_l\}$ at the reference frequency, the coarray at frequency ω_q is dilated version of the coarray, $\alpha_q\{\mathbf{y}_l\}$ [17]. In polar coordinates, this dilated coarray is $\{(\alpha_q r_l, \varphi_l)\}$. Thus, when a frequency other than the reference frequency is used, the coarray dilates radially from the origin, but does not change the coarray angle at all. We will see that this has consequences for when we attempt to use virtual arrays for passive imaging because we need to be able to generate arbitrary coarray points by using multiple frequencies.

Note that for line arrays, $\mathbf{y_l} = [x_l, 0]$ for every coarray point. In polar coordinates, the representation is $(x_l, 0)$. All of the coarray points for a line array lie along the same radial direction, thus, by using some frequency, we can generate any arbitrary coarray point along the line.

4.3 Using a Virtual Array for Passive Imaging

4.3.1 Generating Difference Coarray Points Using Multiple Frequencies

Recall from Chapter 2 that the effect of a larger, virtual array can be synthesized by the physical array using multiple frequencies, provided that the multi-frequency difference coarray covers the virtual difference coarray. This condition can be expressed in terms of the coarray support matrices defined in Chapter 2. For a planar array, to define the difference coarray support matrices, we use the complex representation of the array element positions. The $(m,n)^{th}$ element of the difference coarray support matrix at frequency ω_q is

$$\mathbf{C}(\omega_q)_{m,n} = \alpha_q((x_{Rm} - x_{Rn}) + j(y_{Rm} - y_{Rn})), \text{ for all } q. \tag{4.29}$$

Likewise, the $(m,n)^{th}$ element of the virtual difference coarray support matrix is

$$\tilde{\mathbf{C}}(\omega_0)_{m,n} = (\tilde{x}_{Rm} - \tilde{x}_{Rn}) + j(\tilde{y}_{Rm} - \tilde{y}_{Rn}), \tag{4.30}$$

where $\{\tilde{\mathbf{x}}_{\mathbf{Rm}}, m = 1, 2, ..., \tilde{M}\}$ are the virtual array element positions.

We can construct the virtual correlation matrix corresponding to the virtual array from the narrowband correlation matrices provided that

$$\tilde{\mathbf{C}}(\omega_0)_{m,n} = \mathbf{C}(\omega_q)_{i,j} \text{ for some } q, i, j, \text{ for all } m, n. \tag{4.31}$$

In Chapter 2, for line arrays, this equation could be satisfied for any array and virtual array if we had access to a wide enough band of frequencies. We will see that for planar arrays, this is not always the case.

As an example, consider an array with elements at positions

$$\{\mathbf{x_{Rm}}\} = \{[0,0],[1,0],[0,1]\}\frac{\lambda_0}{2}. \tag{4.32}$$

The complex representation is shown in Figure 4.2. The difference coarray support matrix at the reference frequency is

$$\mathbf{C}(\omega_0) = \begin{bmatrix} 0 & j\frac{\lambda_0}{2} & -\frac{\lambda_0}{2} + j\frac{\lambda_0}{2} \\ -j\frac{\lambda_0}{2} & 0 & -\frac{\lambda_0}{2} \\ \frac{\lambda_0}{2} - j\frac{\lambda_0}{2} & \frac{\lambda_0}{2} & 0 \end{bmatrix}, \tag{4.33}$$

and the difference coarray is illustrated in Figure 4.3. If we use a frequency that is a multiple of the reference frequency, $\omega_q = \alpha_q\omega_0$, the dilated difference coarray support matrix at frequency ω_q becomes

$$\mathbf{C}(\omega_q) = \begin{bmatrix} 0 & j\alpha_q\frac{\lambda_0}{2} & \alpha_q(-\frac{\lambda_0}{2} + j\frac{\lambda_0}{2}) \\ -j\alpha_q\frac{\lambda_0}{2} & 0 & -\alpha_q\frac{\lambda_0}{2} \\ \alpha_q(\frac{\lambda_0}{2} - j\frac{\lambda_0}{2}) & \alpha_q\frac{\lambda_0}{2} & 0 \end{bmatrix}. \tag{4.34}$$

The union of the difference coarray at the reference freqeuncy and the dilated difference coarray is shown in Figure 4.4. From Figure 4.4, geometrically we see that for no α_q could we ever generate the coarray point $\frac{\lambda_0}{2} + j\frac{\lambda_0}{2}$. Thus, Equation 4.31 could not be satisfied for an arbitary virtual array.

Another way to think about this is by examining the coarray angles generated by the array. For this array, the available coarray angles are

$$\{0, \frac{\pi}{2}, \frac{3\pi}{4}, \pi, -\frac{\pi}{2}, \frac{-\pi}{4}\}. \tag{4.35}$$

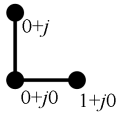

Figure 4.2: Array for Passive Three-element Example - Normalized by $\frac{\lambda_0}{2}$

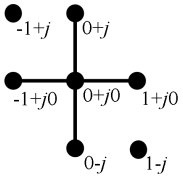

Figure 4.3: Difference Coarray for Passive Three-element Example - Normalized by $\frac{\lambda_0}{2}$

The coarray angle of the point we wish to generate, $\frac{\lambda_0}{2} + j\frac{\lambda_0}{2}$, is $\frac{\pi}{4}$ and is not available, thus we cannot generate this difference coarray point using multiple frequencies. However, we could, for example, generate the difference coarray point $\frac{3\lambda_0}{4} + 0j$ by using the frequency $1.5\omega_0$, because the coarray angle associated with this difference coarray point is 0 and is indeed covered by the obtainable coarray angles.

Relating this idea of coarray angles to Chapter 2, for imaging with linear arrays, the only possible configuration for arrays and coarrays is a line, so for line arrays, we do not have to worry about coarray angles since all coarray points lie on the same coarray angle. Because of this, when dilating a linear coarray by using multiple frequencies to synthesize the effect of a linear virtual array, any desired coarray point can be synthesized with a large enough bandwidth. However, for planar arrays, this is not the case. We cannot generate a coarray point that does not lie in a radial direction of an existing coarray point. Thus, in general, it is much more difficult to find an array and a corresponding virtual array for planar arrays than it is for linear arrays.

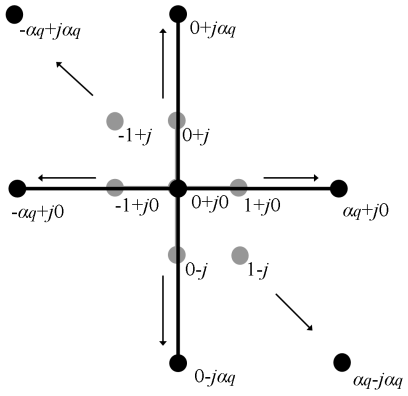

Figure 4.4: Multi-frequency Difference Coarray for Passive Three-element Example - Normalized by $\frac{\lambda_0}{2}$

A necessary condition for the condition in Equation 4.31 is that the set of coarray angles produced by the physical array covers the set of virtual coarray angles:

$$\{\varphi_l\} \supseteq \{\tilde{\varphi}_l\}. \tag{4.36}$$

If this condition is not satisfied, we cannot use multiple frequencies to augment the difference coarray and synthesize the effect of a larger virtual array, regardless of the band of frequencies we have available. In the following section, we suggest a class of arrays and virtual arrays for multi-frequency high-resolution imaging that satisfy Equation 4.36 and examine their effectiveness compared to existing narrowband virtual array techniques.

4.3.2 A Class of Arrays and Virtual Arrays for High-resolution Techniques with Multiple Frequencies

As discussed in the previous section, the problem with finding a virtual array for planar arrays in passive imaging is that we cannot generate arbitrary difference coarray

points. Any difference coarray points we need to generate by using multiple frequencies must lie in the same coarray direction as an existing difference coarray point. However, if we restrict ourselves to virtual arrays yielding virtual coarrays whose coarray angles are covered by the difference coarray at the reference frequency, then we will always be able to generate the points that we need.

Suppose we have the arrow-shaped array shown in Figure 4.5. It is capable of resolving up to six point sources using the correlation matrix directly obtainable from the array. Its difference coarray, a filled square coarray, is illustrated in Figure 4.6. Existing narrowband virtual array techniques can be used to resolve additional sources. Notice that this difference coarray could also have been generated by the virtual array in Figure 4.7. With this virtual array, it is possible to resolve to up eight point sources if the correlation matrix is rearranged as is described in [13]. This virtual array can be obtained by using only the reference frequency. Multiple frequencies do not need to be used to synthesize the effect of this array.

However, we can use multiple frequencies to synthesize the effect of a different virtual array shown in Figure 4.8. Its coarray is shown in Figure 4.9. Notice that the virtual difference coarray consists of the 5×5 square we know we can generate with the arrow array, plus extra difference coarray points that lie on existing coarray directions. Since these extra coarray points lie in covered coarray directions, we can use multiple frequencies to generate them. By using two extra frequencies, $1.5\omega_0$ and $2\omega_0$, we obtain the multi-frequency difference coarray in Figure 4.10. This multi-frequency coarray covers the virtual coarray points we needed to generate. Thus, we can construct our virtual correlation matrix from the narrowband correlation matrices as explained in Chapter 2.

For this example, the coarray points we needed to generate with multiple frequencies lay in the coarray directions $[0, \frac{\pi}{2}, \pi, -\frac{\pi}{2}]$. These coarray angles were covered by

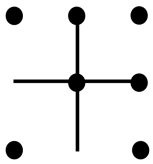

Figure 4.5: Physical 3×3 Arrow-shaped Array

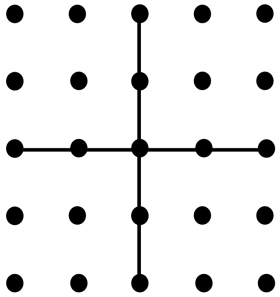

Figure 4.6: 5×5 Square Difference Coarray

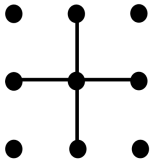

Figure 4.7: Virtual 3×3 Filled Square Array

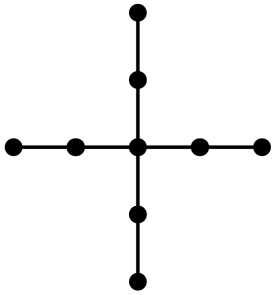

Figure 4.8: 5×5 Virtual Cross Array

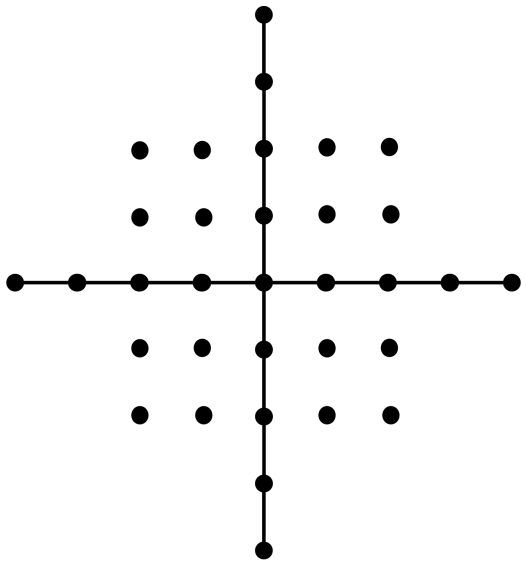

Figure 4.9: Virtual Difference Coarray for 5×5 Cross Array

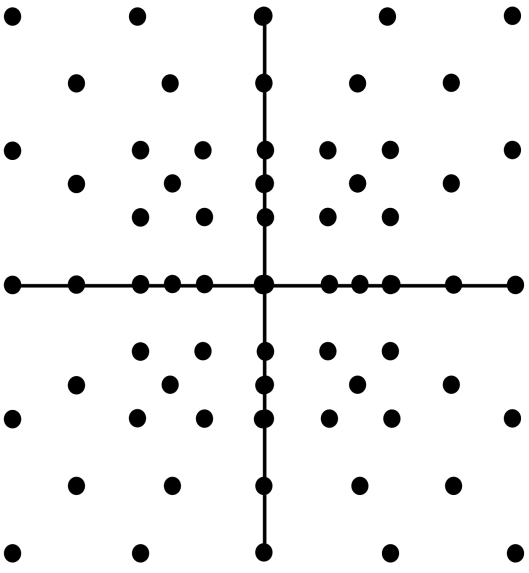

Figure 4.10: Multi-frequency 5×5 Square Difference Coarray

the coarray and we could generate these points using multiple frequencies. In fact, for any array that produces a square difference coarray, the angles $[0, \frac{\pi}{2}, \pi, -\frac{\pi}{2}]$ will be covered. Also, for a cross shaped virtual array, it always produces a difference coarray with a filled square, plus additional coarray points along the coarray directions $[0, \frac{\pi}{2}, \pi, -\frac{\pi}{2}]$. Since the coarray points' angles we need to generate are covered, with the arrow array, we can synthesize the effect of the cross array using multiple frequencies. We suggest this as an example of a class of arrays for which multiple frequencies can be used to synthesize the effect of a larger, planar array.

The class of arrays to generate the square difference coarray we propose is the $M \times M$ arrow array shown in Figure 4.11. This array was chosen because the arrow array is a sparse array generating the square coarray. With this array, there are $3M - 2$ physical array elements and thus $3(M - 1)$ point sources can be resolved. This array generates a $(2M - 1) \times (2M - 1)$ filled square coarray. By using multiple frequencies, we can synthesize the effect of the $(2M-1)\times(2M-1)$ cross array shown in Figure 4.12, which has $4M - 3$ virtual elements and can resolve up to $4(M - 1)$ point sources. That is an improvement of $M - 1$ point sources. The coarray for this virtual array is shown in Figure 4.13, which consists of an $(2M - 1) \times (2M - 1)$ filled square difference coarray plus additional coarray points in the directions $[0, \frac{\pi}{2}, \pi, -\frac{\pi}{2}]$, which we know we can generate using multiple frequencies.

However, recall in the example at the beginning of this section that without using multiple frequencies, the effect of a filled square array can be synthesized by the arrow array since these arrays are coarray equivalent. Without using multiple frequencies, using the $M \times M$ arrow array, we can synthesize the effect of a filled square array with M^2 elements shown in Figure 4.14 and resolve up to $M^2 - 1$ point sources. Whereas using multiple frequencies and assuming a cross virtual array, we can only resolve up to $4(M-1)$ point sources. Thus, the virtual array without using multiple frequencies

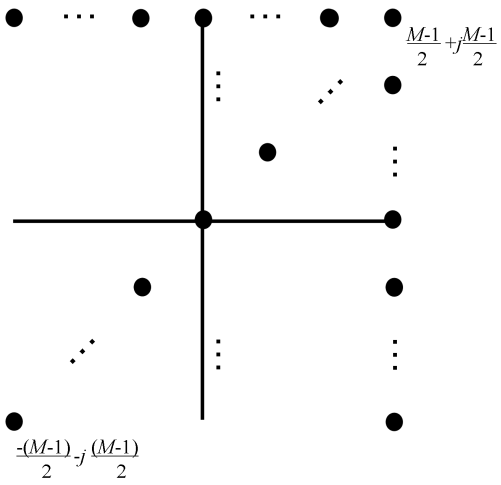

Figure 4.11: $M \times M$ Arrow-shaped Array - Normalized by $\frac{\lambda_0}{2}$

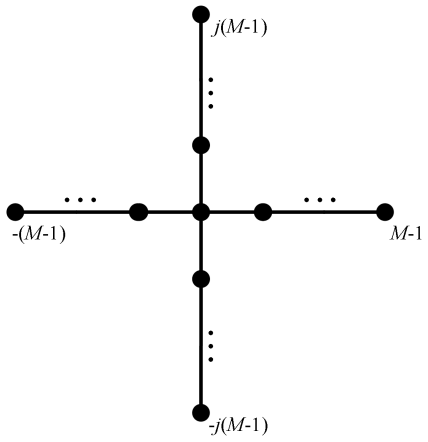

Figure 4.12: $(2M-1)\times(2M-1)$ Cross-shaped Virtual Array Geometry - Normalized by $\frac{\lambda_0}{2}$

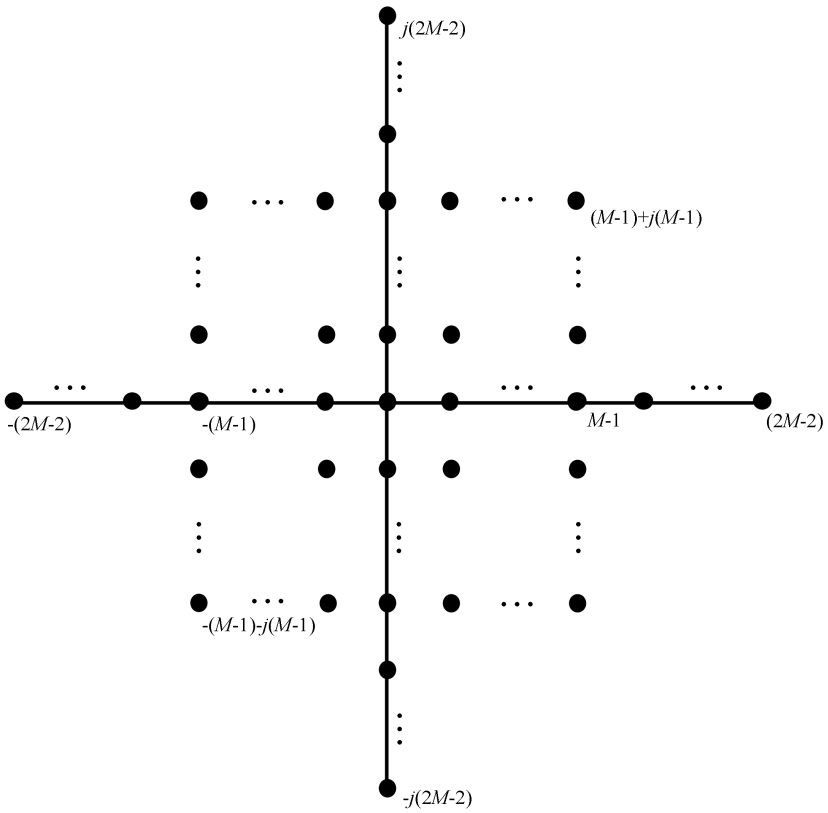

Figure 4.13: Difference Coarray for the $(2M-1) \times (2M-1)$ Cross-shaped Virtual Array - Normalized by $\frac{\lambda_0}{2}$

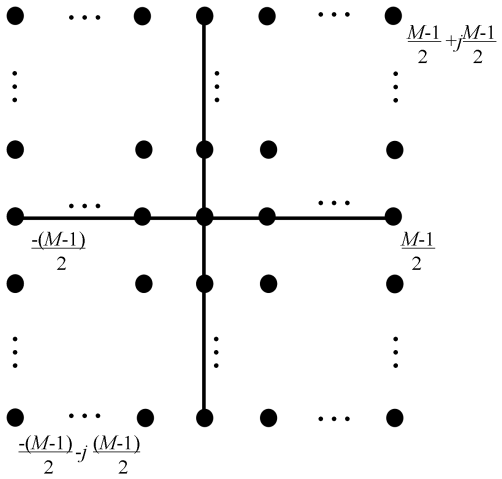

Figure 4.14: $M \times M$ Filled Square Virtual Array - Normalized by $\frac{\lambda_0}{2}$

provides better performance in terms of number of point sources that can be resolved for $M > 3$.

Using multiple frequencies with passive imaging is not straightforward. For the class of arrays we have found that works, the increase in the number of sources that can be resolved is small compared to using existing techniques for single frequency virtual arrays. However, there may exist other classes of arrays and virtual arrays that yield better results using multiple frequencies and additional research will need to be carried out.

4.4 Virtual Array for Active Imaging

As we did for passive imaging, we can extend the virtual array for active imaging to planar arrays. The difference is that instead of constructing a virtual correlation matrix from multiple frequencies, we construct multiple virtual data matrices, each at a single frequency, then average them over frequency using array interpolation.

For active imaging, we restrict ourseves to rectangular arrays. As in passive imaging, we form the coarray support matrix by using the complex representation, except that in active imaging, we use the sum coarray. The complex representation that is the $(m,n)^{th}$ of the coarray support matrix is

$$\mathbf{C}(\omega_0)_{m,n} = (x_{Rm} + x_{Tm}) + j(y_{Rm} + y_{Tm}). \tag{4.37}$$

Likewise, the $(m,n)^{th}$ element of the virtual coarray support matrix is

$$\tilde{\mathbf{C}}(\omega_0)_{m,n} = (\tilde{x}_{Rm} + \tilde{x}_{Tm}) + j(\tilde{y}_{Rm} + \tilde{y}_{Tm}), \tag{4.38}$$

where $\{\tilde{\mathbf{x}}_{\mathbf{Rm}}, m = 1, 2, ..., \tilde{M}\}$ and $\{\tilde{\mathbf{x}}_{\mathbf{Tn}}, n = 1, 2, ..., \tilde{N}\}$ are the virtual receive and

transmit element positions, respectively.

To construct a virtual data matrix, $\tilde{\mathbf{X}}(\omega_0)$, a map that takes the elements of $\mathbf{C}(\omega_0)$ to $\tilde{\mathbf{C}}(\omega_0)$ is found and applied to $\mathbf{X}(\omega_0)$ to form $\tilde{\mathbf{X}}(\omega_0)$. Additional virtual data matrices can be constructed by applying the same map to $\mathbf{X}(\omega_q)$ to form $\tilde{\mathbf{X}}(\omega_q)$.

The virtual correlation matrices are formed by taking the autocorrelation of the virtual data matrices:

$$\begin{aligned}\tilde{\mathbf{R}}(\omega_q) &= \mathbb{E}[\tilde{\mathbf{X}}(\omega_q)\tilde{\mathbf{X}}(\omega_q)^H] \\ &= \tilde{\mathbf{A}}_{\mathbf{R}}(\omega_q)\mathbf{S}(\omega_q)\tilde{\mathbf{A}}_{\mathbf{T}}(\omega_q)^T\tilde{\mathbf{A}}_{\mathbf{T}}(\omega_q)^*\mathbf{S}(\omega_q)^H\tilde{\mathbf{A}}_{\mathbf{R}}(\omega_q)^H \\ &= \tilde{\mathbf{A}}_{\mathbf{R}}(\omega_q)\tilde{\mathbf{S}}_{\mathbf{T}}(\omega_q)\tilde{\mathbf{A}}_{\mathbf{R}}(\omega_q)^H,\end{aligned} \tag{4.39}$$

where $\tilde{\mathbf{A}}_{\mathbf{R}}(\omega_q)$ is the virtual receive array manifold matrix,

$$\tilde{\mathbf{A}}_{\mathbf{R}}(\omega_q) = \begin{bmatrix} e^{jk_q\mathbf{u_1}^T\tilde{\mathbf{x}}_{\mathbf{R1}}} & e^{jk_q\mathbf{u_2}^T\tilde{\mathbf{x}}_{\mathbf{R1}}} & \dots & e^{jk_q\mathbf{u_K}^T\tilde{\mathbf{x}}_{\mathbf{R1}}} \\ e^{jk_q\mathbf{u_1}^T\tilde{\mathbf{x}}_{\mathbf{R2}}} & e^{jk_q\mathbf{u_2}^T\tilde{\mathbf{x}}_{\mathbf{R2}}} & \dots & e^{jk_q\mathbf{u_K}^T\tilde{\mathbf{x}}_{\mathbf{R2}}} \\ \vdots & \vdots & \vdots & \vdots \\ e^{jk_q\mathbf{u_1}^T\tilde{\mathbf{x}}_{\mathbf{R}\tilde{\mathbf{M}}}} & e^{jk_q\mathbf{u_2}^T\tilde{\mathbf{x}}_{\mathbf{R}\tilde{\mathbf{M}}}} & \dots & e^{jk_q\mathbf{u_K}^T\tilde{\mathbf{x}}_{\mathbf{R}\tilde{\mathbf{M}}}} \end{bmatrix} \tag{4.40}$$

$\tilde{\mathbf{A}}_{\mathbf{T}}(\omega_q)$ is the virtual transmit array manifold matrix,

$$\tilde{\mathbf{A}}_{\mathbf{T}}(\omega_q) = \begin{bmatrix} e^{jk_q\mathbf{u_1}^T\tilde{\mathbf{x}}_{\mathbf{T1}}} & e^{jk_q\mathbf{u_2}^T\tilde{\mathbf{x}}_{\mathbf{T1}}} & \dots & e^{jk_q\mathbf{u_K}^T\tilde{\mathbf{x}}_{\mathbf{T1}}} \\ e^{jk_q\mathbf{u_1}^T\tilde{\mathbf{x}}_{\mathbf{T2}}} & e^{jk_q\mathbf{u_2}^T\tilde{\mathbf{x}}_{\mathbf{T2}}} & \dots & e^{jk_q\mathbf{u_K}^T\tilde{\mathbf{x}}_{\mathbf{T2}}} \\ \vdots & \vdots & \vdots & \vdots \\ e^{jk_q\mathbf{u_1}^T\tilde{\mathbf{x}}_{\mathbf{T}\tilde{\mathbf{N}}}} & e^{jk_q\mathbf{u_2}^T\tilde{\mathbf{x}}_{\mathbf{T}\tilde{\mathbf{N}}}} & \dots & e^{jk_q\mathbf{u_K}^T\tilde{\mathbf{x}}_{\mathbf{T}\tilde{\mathbf{N}}}} \end{bmatrix}. \tag{4.41}$$

and $\tilde{\mathbf{S}}_{\mathbf{T}}(\omega_q)$ is the virtual source correlation matrix,

$$\tilde{\mathbf{S}}_{\mathbf{T}} = \mathbf{S}(\omega_q)\tilde{\mathbf{A}}_{\mathbf{T}}(\omega_q)^T\tilde{\mathbf{A}}_{\mathbf{T}}(\omega_q)^*\mathbf{S}(\omega_q)^H. \tag{4.42}$$

The individual correlation matrices formed from the narrowband data matrices allow for up to $\tilde{M}-1$ total targets to be resolved, and only $\tilde{N}$ may be coherent. We use array interpolation to combine the matrices at different frequencies to allow for coherent targets to be resolved as we did in Chapter 3. Array interpolation for planar arrays is described in the following section.

4.4.1 Array Interpolation Matrices for Planar Arrays

Array interpolation matrices allow us to add correlation matrices at different frequencies while retaining the structure necessary to use MUSIC.

We want to find an array interpolation matrix $\mathbf{B}_0(\omega_q)$ such that [19]

$$\tilde{\mathbf{A}}_{\mathbf{R}}(\omega_0) \approx \mathbf{B}_0(\omega_q)\tilde{\mathbf{A}}_{\mathbf{R}}(\omega_q). \tag{4.43}$$

Since the $\{\tilde{\mathbf{A}}_{\mathbf{R}}(\omega_q)\}$ are functions of the unknown $\{\mathbf{u_k}\}$, we cannot directly solve for the $\{\mathbf{B}_0(\omega_q)\}$. However, we assume it is known that $\mathbf{u_k}$ is in some spherical sector, $\phi \in [\phi_s, \phi_f]$ and $\theta \in [\theta_s, \theta_f]$, thus we can find $\mathbf{B}_0(\omega_q)$ by a least squares fit over the spherical sector. The optimal $\mathbf{B}_0(\omega_q)$ in the least squares sense minimizes

$$\int_{\phi_s}^{\phi_f}\int_{\theta_s}^{\theta_f} ||\tilde{\mathbf{a}}_{\mathbf{R}}(\mathbf{u},\omega_0) - \mathbf{B}_0(\omega_q)\tilde{\mathbf{a}}_{\mathbf{R}}(\mathbf{u},\omega_q)||^2 d\phi d\theta \tag{4.44}$$

with respect to $\mathbf{B}_0(\omega_q)$, where $\tilde{\mathbf{a}}_{\mathbf{R}}(\mathbf{u},\omega_q)$ is the virtual receive array steering vector at frequency ω_q:

$$\tilde{\mathbf{a}}_{\mathbf{R}}(\mathbf{u},\omega_q) = \tilde{\mathbf{a}}_{\mathbf{R}}(\theta,\phi,\omega_q) = [e^{jk_q\mathbf{u}^T\tilde{\mathbf{x}}_{\mathbf{R1}}}, e^{jk_q\mathbf{u}^T\tilde{\mathbf{x}}_{\mathbf{R2}}}, ..., e^{jk_q\mathbf{u}^T\tilde{\mathbf{x}}_{\mathbf{R}\tilde{\mathbf{M}}}}]^T. \tag{4.45}$$

To find $\mathbf{B}_0(\omega_q)$, we approximate the integral in Equation 4.44 by a summation taken over points in the sector. The sector is sampled $P \geq M$ times and the matrices

$\tilde{\mathbf{A}}_q$ are constructed as follows:

$$\tilde{\mathbf{A}}_q = \begin{bmatrix} \tilde{\mathbf{a}}_{\mathbf{R}}(\mathbf{u^1}, \omega_q)^H \\ \tilde{\mathbf{a}}_{\mathbf{R}}(\mathbf{u^2}, \omega_q)^H \\ \vdots \\ \tilde{\mathbf{a}}_{\mathbf{R}}(\mathbf{u^i}, \omega_q)^H \\ \vdots \\ \tilde{\mathbf{a}}_{\mathbf{R}}(\mathbf{u^P}, \omega_q)^H \end{bmatrix} \tag{4.46}$$

Here $\mathbf{u^i}$ is the i^{th} sample of the sector. Assuming that $P \geq M$ and that the matrices $\tilde{\mathbf{A}}_q$ each have full column rank, the least squares solution is given by [44]:

$$\mathbf{B}_0(\omega_p) = \tilde{\mathbf{A}}_0^H \tilde{\mathbf{A}}_p [\tilde{\mathbf{A}}_p^H \tilde{\mathbf{A}}_p]^{-1}. \tag{4.47}$$

When we pre- and post-multiply the spatial correlation matrix at frequency ω_q by the appropriate array interpolation matrix, the correlation matrix at frequency ω_q appears to have come from frequency ω_0 in the sector,

$$\begin{aligned} \mathbf{B}_0(\omega_q)\tilde{\mathbf{R}}(\omega_q)\mathbf{B}_0(\omega_q)^H &= \mathbf{B}_0(\omega_q)\tilde{\mathbf{A}}_{\mathbf{R}}(\omega_q)\tilde{\mathbf{S}}_{\mathbf{T}}(\omega_q)\tilde{\mathbf{A}}_{\mathbf{R}}(\omega_q)^H\mathbf{B}_0(\omega_q)^H \\ &\approx \tilde{\mathbf{A}}_{\mathbf{R}}(\omega_0)\tilde{\mathbf{S}}_{\mathbf{T}}(\omega_q)\tilde{\mathbf{A}}_{\mathbf{R}}(\omega_0)^H, \end{aligned} \tag{4.48}$$

but with a different source correlation matrix at each frequency.

Averaged Correlation Matrix

Recall that if the virtual source correlation matrix $\tilde{\mathbf{S}}_{\mathbf{T}}(\omega_0)$ is not full rank (i.e. $K > \tilde{N}$), MUSIC will be unable to resolve the coherent targets. Averaging the virtual correlation matrices over multiple frequencies can increase the rank of the source correlation matrix and allow coherent targets to be resolved.

As in Chapter 3, the averaged virtual correlation matrix is defined as:

$$\begin{aligned}
\bar{\mathbf{R}}(\omega_0) &= \frac{1}{Q}[\tilde{\mathbf{R}}(\omega_0) + \sum_{q=1}^{Q-1} \mathbf{B}_0(\omega_q)\tilde{\mathbf{R}}(\omega_q)\mathbf{B}_0(\omega_q)^H] \\
&= \frac{1}{Q}[\tilde{\mathbf{A}}_{\mathbf{R}}(\omega_0)\tilde{\mathbf{S}}_{\mathbf{T}}(\omega_0)\tilde{\mathbf{A}}_{\mathbf{R}}(\omega_0)^H + \sum_{q=1}^{Q-1} \mathbf{B}_0(\omega_q)\tilde{\mathbf{A}}_{\mathbf{R}}(\omega_q)\tilde{\mathbf{S}}_{\mathbf{T}}(\omega_q)\tilde{\mathbf{A}}_{\mathbf{R}}(\omega_q)^H\mathbf{B}_0(\omega_q)^H] \\
&\approx \frac{1}{Q}\sum_{q=0}^{Q-1} \tilde{\mathbf{A}}_{\mathbf{R}}(\omega_0)\tilde{\mathbf{S}}_{\mathbf{T}}(\omega_q)\tilde{\mathbf{A}}_{\mathbf{R}}(\omega_0)^H \\
&= \tilde{\mathbf{A}}_{\mathbf{R}}(\omega_0)[\frac{1}{Q}\sum_{q=0}^{Q-1} \tilde{\mathbf{S}}_{\mathbf{T}}(\omega_q)]\tilde{\mathbf{A}}_{\mathbf{R}}(\omega_0)^H \\
&= \tilde{\mathbf{A}}_{\mathbf{R}}(\omega_0)\bar{\mathbf{S}}_{\mathbf{T}}\tilde{\mathbf{A}}_{\mathbf{R}}(\omega_0)^H
\end{aligned} \tag{4.49}$$

The averaged correlation matrix has the same structure as a correlation matrix observing the scene at a frequency ω_0, but since we averaged over frequencies, we have a new averaged source correlation matrix,

$$\bar{\mathbf{S}}_{\mathbf{T}} = \frac{1}{Q}\sum_{q=0}^{Q-1} \tilde{\mathbf{S}}_{\mathbf{T}}(\omega_q). \tag{4.50}$$

Recall that for $\bar{\mathbf{R}}(\omega_0)$ to be useful in high-resolution techniques, $\bar{\mathbf{S}}_T$ must be full-rank. In Chapter 3, the averaged source correlation matrix, $\bar{\mathbf{S}}_T$, was shown to have full rank when the number of frequencies is greater than or equal to the number of coherent targets,

$$Q \geq K. \tag{4.51}$$

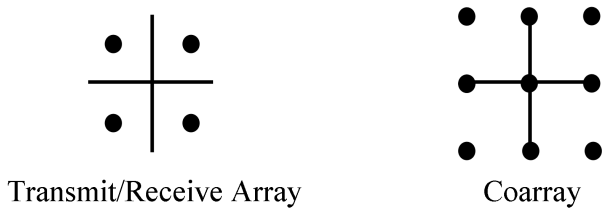

Figure 4.15: Rectangular Array Example

4.4.2 Example

As an example, consider a four element transmit/receive array with elements in locations

$$\{\frac{\lambda_0}{4}+j\frac{\lambda_0}{4},-\frac{\lambda_0}{4}+j\frac{\lambda_0}{4},\frac{\lambda_0}{4}-j\frac{\lambda_0}{4},-\frac{\lambda_0}{4}-j\frac{\lambda_0}{4}\}. \tag{4.52}$$

This array has the 9 element sum coarray

$$\{0,\frac{\lambda_0}{2}+j\frac{\lambda_0}{2},-\frac{\lambda_0}{2}-j\frac{\lambda_0}{2},-\frac{\lambda_0}{2}+j\frac{\lambda_0}{2},\frac{\lambda_0}{2}-j\frac{\lambda_0}{2},j\frac{\lambda_0}{2},\frac{\lambda_0}{2},0,-\frac{\lambda_0}{2},-j\frac{\lambda_0}{2}\}. \tag{4.53}$$

This is illustrated in Figure 4.15. Some virtual arrays that are coarray equivalent to this array are shown in Figure 4.16. From the virtual arrays, we choose the one with nine receivers and a single transmitter in order to resolve the maximum number of targets, but they must all be incoherent.

In general, for an $M \times N$ rectangular transmit/receive array, to resolve the maximum number of total targets, we can consider the virtual receive array to be a $2M-1 \times 2N-1$ rectangular array and have only a single virtual transmitter. With this, up to $(2M-1)(2N-1)-1$ coherent targets can be resolved if at least $(2M-1)(2N-1)-1$ frequencies are used to average the virtual correlation matrices. There of course is a limit to this. Even though this is a high-resolution technique, the number of targets that can be resolve is limited because the sector must be sufficiently

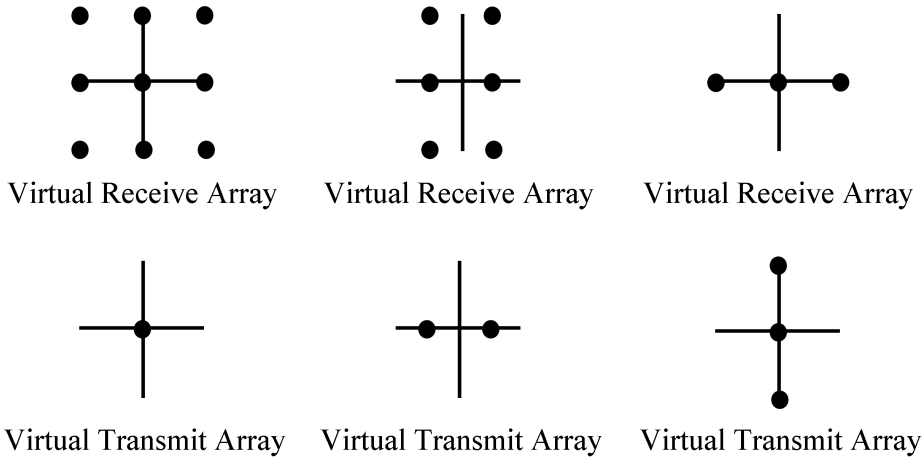

Figure 4.16: Possible Virtual Arrays

small. Too many targets in a small sector will lead to location estimation errors.

4.5 Conclusion

The results in Chapter 2 and 3 can be extended to two dimensions. For passive imaging, we have seen that it is extendable to a class of arrays and virtual arrays, but not necessarily any arbitrary array and virtual array. For active imaging, the extension is straight-forward for rectangular arrays and should work for a sufficiently small spherical sector of the scene.

One obstacle that must be considered before pursuing further research is that two-dimensional MUSIC is computationally intensive. A search must be performed over two angular variables. For large spherical sectors, this is a problem. The trend in the literature for direction of arrival estimation with planar arrays seems to be to use "search-free" techniques such as root-MUSIC [24, 32, 25, 33]. However, since root-MUSIC is not designed for planar arrays in its conventional form, approximate numerical techniques are used to compensate for this. This may cause complications

with search-free techniques since we are already under strict conditions on the sources' spectra in passive imaging and using array interpolation in active imaging.

Chapter 5

Active Imaging using Retransmission

5.1 Introduction

In active imaging with phased linear arrays, radiation is sent from an array of transmitting elements into a scene and the reflections from the scene are received by a line array a receiving elements. The quality of the image depends on the width of the *coarray* [14]. Generally, the wider the coarray, the higher the resolution of the image. Increasing the length of the coarray can be done be adding additional array elements to either the transmit or the receive array, or by using multiple frequencies [17].

Another possible way in which the length of the coarray can be increased is retransmission, which was proposed in [26], but has not been studied in depth. Retransmission is an imaging scheme where radiation is sent out by the transmit array, reflected by the scene and received by an intermediate array - called the retransmit array - then this received signal is sent back out into the scene and finally received at the receive array. As will be shown, this retransmission step lengthens the coarray

in the point spread function. Theoretically, lengthening the coarray should provide higher resolution, but as was shown in [26], extraneous estimated target locations called *crossterms* arise. In this chapter, we will investigate the crossterms in depth for two coherent point targets and examine various techniques to reduce or eliminate crossterms. Retransmission with multiple targets and/or multiple retransmissions will also briefly be studied.

5.2 Review of Active Imaging and the Coarray

Active imaging is used to obtain an image of a scene of reflectors that do not emit their own radiation. Radiation is sent out from a transmit array, reflected by the reflectors and the returns are collected by a receive array. From these received returns, an estimate of the angular reflected power density is made.

Suppose the transmit array has transmitting elements in a line at positions $\{x_{Tn}|n = 1, 2, ..., N\}$ and the receive array has receiving elements in a line at positions $\{x_{Rm}|m = 1, 2, ..., M\}$. The array may or may not share some or all of their elements, and the positions are measured from an arbitrary origin which also may or may not be an array element. We say the arrays are operating at the reference frequency ω_0 if the array element spacings are based on the wavelength λ_0 corresponding to frequency ω_0. For example, a common spacing is the Nyquist spacing of $\frac{\lambda_0}{2}$. It is possible transmit and receive frequencies, $\omega_q = \alpha_q\omega_0$, other than the reference frequency.

The scene being imaged consists of K point targets (reflectors). The reflectors are assumed to be small enough and far enough away from the arrays that they can be viewed as far-field point targets. Then for both the transmitted radiation arriving at the targets and the reflections arriving at receive array, the wavefronts can be approximated as plane waves. The targets are located at angles $\{\theta_k, k = 1, 2, ..., K\}$

measured from broadside and the notation $u_k = \sin\theta_k$ is used. Each source is assumed to have complex reflectivity $S_k(\omega_q)$ for frequency ω_q. This reflectivity embodies the power of the reflection, the phase shift due to reflection and the phase due propagation delay received at the origin. The parenthetical argument will be dropped unless we are dealing with frequencies other than the reference frequency. The relationship between reflection phase shifts for different targets is important. If the phase shifts due to reflection between targets is indepedent, we say that the targets are incoherent. If there is a fixed relationship between the phase shifts, the targets are called coherent. We will assume that the targets are phase coherent with each other, unless stated otherwise, as this is the more difficult, interesting case for imaging.

5.2.1 Beamforming

Beamforming is used to "steer" the transmitted radiation in a desired direction, u, and is used to phase align the returns at the receive array so that if there were a target at u, the returns would add constructively. For a single frequency (assume the reference frequency), this is done by applying appropriate phase shifts at the transmit and receive elements. To transmit narrowband radiation in direction u using linear beamforming, the element in the transmit array at x_{Tn} must be phase-delayed by $e^{-jk_0ux_{Tn}}$. Here $k_0 = \frac{2\pi}{\lambda_0}$ is the wavenumber associated with frequency ω_0. Likewise, to receive in direction u, the receive element at x_{Rm} is phase-delayed by $e^{-jk_0ux_{Rm}}$. We assume that the radiation is sent from each transmit element individually and received by all receive elements. This way, we have access to each transmit/receive pair individually and this allows for off-line processing. The complex signal amplitude

received at x_{Rm} from x_{Tn} is

$$I_{m,n} = \sum_{k=1}^{K} S_k e^{jk_0 u_k (x_{Tn} + x_{Rm})}. \tag{5.1}$$

Adding the beamforming phase-delays to look in direction u, and additional weights w_{Tn} and w_{Rm} to the transmit and receive elements respectively for mainbeam width and sidelobe control of the beampattern, yields

$$I_{m,n}(u) = \sum_{k=1}^{K} S_k w_{Tn} w_{Rm} e^{-jk_0 (u-u_k)(x_{Tn} + x_{Rm})}. \tag{5.2}$$

The image as a function of u is given by summing over the transmit and receive element pairs:

$$I(u) = \sum_{m=1}^{M} \sum_{n=1}^{N} \sum_{k=1}^{K} S_k w_{Tn} w_{Rm} e^{-jk_0 (u-u_k)(x_{Tn} + x_{Rm})} \tag{5.3}$$

Notice that the image function is "supported" on the set of points

$$\{x_{Tn} + x_{Rm} | m = 1, 2, ..., M, n = 1, 2, ..., N\}. \tag{5.4}$$

The sum $x_{Tn} + x_{Rm}$ is called a coarray point and is an important concept in linear beamforming [14]. In Equation 5.3, there may be multiple element pairs with the same value for $x_{Tn} + x_{Rm}$, and the sum of the corresponding $w_{Tn} w_{Rm}$ weight products is the coarray weight for the coarray point at $x_{Tn} + x_{Rm}$. We can label the coarray points with indices l and call the l^{th} coarray point y_l and its corresponding weighting γ_l. The coarray points and weights together are collectively referred to as the *sum*

coarray. Equation 5.3 can be rewritten as

$$I(u) = \sum_{l=1}^{L} \sum_{k=1}^{K} S_k \gamma_l e^{-jk_0(u-u_k)y_l}. \tag{5.5}$$

5.2.2 Point Spread Function

The response of the imaging system to a unit-reflectivity point target at broadside ($u_1 = 0$) is called the point spread function. Note this is analagous to the impulse response of a linear time-invariant system. Equation 5.3 becomes

$$PSF(u) = \sum_{l=1}^{L} \gamma_l e^{-jk_0 u y_l}, \tag{5.6}$$

where $\{y_l\}$ are the coarray points and $\{\gamma_l\}$ are the corresponding weights. We see that the point spread function is the Fourier transform of the coarray, where u is the variable in the Fourier domain. Ideally, $PSF(u)$ would be a delta function at 0 since there is just a single point target, but this is not possible with finite L. As L becomes large, $PSF(u)$ can effectively approch $\delta(u)$. Thus, the more coarray points we have, the better the image resolution. For a more detailed explanation of the coarray concept, see [14].

The relationship among coarray, array and image quality can be better understood

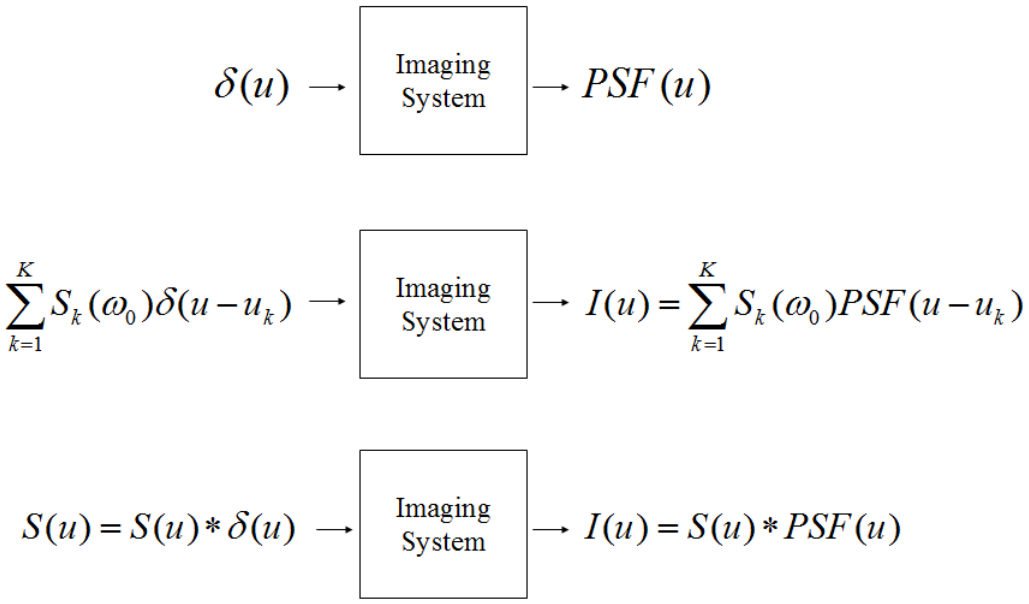

Figure 5.1: Block Diagram for Transmit/Receive Imaging System

if we write Equation 5.6 more carefully. Starting from Equation 5.3:

$$\begin{aligned} PSF(u) &= \sum_{n=1}^{N} w_{Tn} e^{-jk_0 u x_{Tn}} \sum_{m=1}^{M} w_{Rm} e^{-jk_0 u x_{Rm}} \\ &= \mathcal{F}[\{w_{Tn}\}]\mathcal{F}[\{w_{Rm}\}] \\ &= \mathcal{F}[\{w_{Tn}\} * \{w_{Rm}\}] \\ &= \sum_{l=1}^{L} \gamma_l e^{-jk_0 u y_l} \\ &= \mathcal{F}[\{\gamma_l\}] \end{aligned} \tag{5.7}$$

The coarray is the *convolution* of the sets of transmit and receive array weightings.

When there are multiple targets as in Equation 5.5, the image produced can be viewed as the superposition of many weighted and shifted point spread functions. Figure 5.1 illustrates this. The input is the target reflectivity distribution, here a sum of delta functions weighted by the complex target amplitudes, and the output is

the image. From linear system theory, we know that for a general target distribution $S(u)$, the image is given by the target distribution convolved with the point spread function.

By manipulating the coarray, the point spread function can be modified. As the number of coarray points L increases, the width of the mainbeam generally becomes narrower. This is related to the resolution capabilities of the imaging system, and will be our focus in this chapter.

5.2.3 Multi-Frequency Coarray

Multiple frequencies can be used to modify the coarray [26]. If we use Q frequencies, $\omega_q = \alpha_q \omega_0, q = 0, 1, ..., Q-1$ (where $\alpha_0 = 1$ corresponds to the reference frequency), by superposition, Equation 5.3 is now given by

$$I(u) = \sum_{q=0}^{Q-1} \sum_{m=1}^{M} \sum_{n=1}^{N} \sum_{k=1}^{K} S_k(\omega_q) w_{Tn} w_{Rm} e^{-jk_0(u-u_k)\alpha_q(x_{Tn}+x_{Rm})}, \tag{5.8}$$

and the coarray is the set of points

$$\begin{aligned} &\{\alpha_q(x_{Tn} + x_{Rm}) | m = 1, 2, ..., M, n = 1, 2, ..., N, q = 0, 2, ..., Q-1\} \\ &\qquad = \bigcup_{q=0}^{Q-1} \alpha_q \{x_{Tn} + x_{Rm} | m = 1, 2, ..., M, n = 1, 2, ..., N\}. \end{aligned} \tag{5.9}$$

The coarray is the union of narrowband coarray points dilated by the factors $\{\alpha_q\}$. We can re-index the coarray points such that z_l is the l^{th} multi-frequency coarray point. The weight ζ_l corresponding to the coarray point z_l now encompasses the sums of the product $w_{Tn} w_{Rm}$ over the element-pairs and frequency combinations contributing to

the l^{th} coarray point and is given explicitly by

$$\zeta_l = \sum_{(m,n,q)\in\mathcal{S}} w_{Tn} w_{Rm}, \tag{5.10}$$

where the set $\mathcal{S} = \{(q,m,n)|z_l = \alpha_q(x_{Tn} + x_{Rm})\}$.

The multi-frequency coarray may be denser and/or wider than single-frequency narrowband coarray. This modifies the point spread function and generally improves image quality in terms of resolution and/or sidelobe height.

The Fourier Transform relationship still holds for the point spread function when multiple frequencies are used:

$$PSF(u) = \sum_{l=1}^{L} \zeta_l e^{-jk_0 u z_l} = \mathcal{F}[\{\zeta_l\}] \tag{5.11}$$

5.3 Retransmission

For the retransmission scheme, we have the initial transmit array $\{x_{Tn}, n = 1, 2, ..., N\}$, an intermediate receive/transmit array $\{x_p, p = 1, 2, ..., P\}$ and the final receive array $\{x_{Rm}, m = 1, 2, ..., M\}$. These arrays may or may not be identical.

A narrowband signal is sent from a transmit element at x_{Tn}. The signal is reflected by the targets and received by the transmit/receive array. The complex amplitude of the intermediate received signal from x_{Tn} to x_p is

$$\tilde{w}_{p,n} = \sum_{k=1}^{K} S_k e^{jk_0 u_k (x_{Tn} + x_p)}. \tag{5.12}$$

This intermediate receive signal is transmitted back out into the scene from x_p, reflected by the targets and received at the receive array. The complex amplitude of

the final received signal at x_{Rm} is

$$\begin{aligned}\mathbf{X}_{m,p,n} &= \sum_{l=1}^{K} \tilde{w}_{p,n} S_l e^{jk_0 u_l (x_p + x_{Rm})} \\ &= \sum_{k=1}^{K} \sum_{l=1}^{K} S_k S_l e^{jk_0 u_k (x_{Tn} + x_p)} e^{jk_0 u_k (x_p + x_{Rm})}.\end{aligned} \tag{5.13}$$

In order to beamform, we compensate for the propagation delays from x_{Tn} to a pixel in direction u, u to x_p, x_p to u again, and u to x_{Rm}. Array weights w_{Tn}, w_p and w_{Rm} may be applied to the transmit, transmit/receive and receive arrays respectively. Applying the weights and compensating for the propagation delays yield the image:

$$\begin{aligned}I(u) &= \sum_{m=1}^{M} \sum_{p=1}^{P} \sum_{n=1}^{N} w_{Tn} w_p w_{Rm} \mathbf{X}_{m,p,n} e^{jk_0 u (x_{Tn} + 2x_p + x_{Rm})} \\ &= \sum_{m=1}^{M} \sum_{p=1}^{P} \sum_{n=1}^{N} \sum_{k=1}^{K} \sum_{l=1}^{K} S_k S_l w_{Tn} w_p w_{Rm} e^{-jk_0 (u - u_k)(x_{Tn} + x_p)} e^{-jk_0 (u - u_l)(x_p + x_{Rm})}\end{aligned} \tag{5.14}$$

The retransmission scheme can be interpreted as a single transmit/receive scheme. To see this, consider using the received complex amplitudes from the first transmit/receive step as transmit weights for the second transmit step. The total receive complex amplitude at the p^{th} intermediate receiver is

$$\tilde{w}_p = \sum_{n=1}^{N} w_{Tn} w_p \tilde{w}_{p,n} = \sum_{n=1}^{N} \sum_{k=1}^{K} w_{Tn} w_p S_k e^{jk_0 u_k (x_{Tn} + x_p)}. \tag{5.15}$$

Then Equation 5.14 can be rewritten as

$$I(u) = \sum_{m=1}^{M} \sum_{n=1}^{N} \sum_{l=1}^{K} S_l \tilde{w}_p w_{Rm} e^{jk_0 (u - u_l)(x_p + x_{Rm})}. \tag{5.16}$$

This has the same form as a single transmit/receive step with transmit weights $\tilde{w}_p$ and receive weights w_{Rm}.

5.3.1 Point Spread Function

If the only target in the scene is a target at broadside with unit reflectivity, the point spread function for retransmission becomes from Equation 5.14,

$$\begin{aligned} PSF_{RT}(u) &= \sum_{m=1}^{M}\sum_{p=1}^{P}\sum_{n=1}^{N} w_{Rm}w_p w_{Tn} e^{-jk_0 u(x_{Tn}+2x_p+x_{Rm})} \\ &= \sum_{l=1}^{L} \eta_l e^{-jk_0 u v_l}. \end{aligned} \tag{5.17}$$

where $\{v_l\} = \{x_{Rm} + 2x_p + x_{Tn} | m = 1, ..., M, p = 1, ..., P, n = 1, ..., N\}$ are the new coarray points and $\{\eta_l\}$ are the new weights. The point spread function of the retransmit scheme is given by the Fourier Transform of the coarray weights η_l at the coarray points v_l. Examining the point spread function more carefully, we see that it is a product of beampatterns:

$$\begin{aligned} PSF_{RT}(u) &= [\sum_{m=1}^{M} w_{Rm} e^{-jk_0 u x_{Rm}}][\sum_{p=1}^{P} w_p e^{-jk_0 u 2x_p}][\sum_{n=1}^{N} w_{Tn} e^{-jk_0 u x_{Tn}}] \\ &= [B_R(u)][B(2u)][B_T(u)] \end{aligned} \tag{5.18}$$

Here each function in square brackets corresponds to a beampattern. $B_R(u)$ is the receive array beampattern, $B_T(u)$ is the transmit array beampattern and $B(u)$ is the retransmit array beampattern. The beampatterns are the Fourier Transforms of the array weights at the array element positions. Notice that in the expression for the point spread function, the retransmit beampattern is evaluated at $2u$. This arises because we retransmit from this array.

Continuing with the analysis of the point spread function,

$$\begin{aligned} PSF_{RT}(u) &= \mathcal{F}[\{w_{Rm}\}]\mathcal{F}[\{w_p \uparrow_2\}]\mathcal{F}[\{w_{Tn}\}] \\ &= \mathcal{F}[\{w_{Rm}\} * \{w_p \uparrow_2\} * \{w_{Tn}\}] \\ &= \mathcal{F}[\{\eta_l\}] \\ &= \sum_{l=1}^{L} \eta_l e^{-jk_0 u v_l}. \end{aligned} \tag{5.19}$$

In this expression, $\uparrow_N$ represents the operation upsampling by a factor N. For an array, the upsampling operation stretches the array by a factor of N. The upsampled array has points at N times their original spacing each retaining their original weight and "array elements" with zero weight are inserted at the empty locations.

The coarray for retransmission is given by the convolution of the transmit array weights, receive array weights, and the retransmit array weights upsampled by a factor of two. Comparing the point spread function of the retransmit scheme to the point spread function of the standard scheme (Equation 5.6), we see that the coarray for retransmission has an additional convolution. This will yield a wider coarray than just the convolution of the transmit and receive elements. Thus, we expect the point spread function to have a narrower beam than conventional transmit/receive imaging. This yields finer location resolution for a single point target.

From this point forward, unless otherwise stated, it will be assumed that the transmit, retransmit and receive arrays are the same array which is uniformly spaced with spacing $\frac{\lambda_0}{2}$. λ_0 is the wavelength associated with the reference frequency ω_0. The array weighting is assumed to be uniform, i.e. $w_{Tn}, w_p, w_{Rm} = 1 \ \forall \ n, p, m$ unless stated otherwise.

As an example to illustrate how retransmission influences the point spread function, consider a uniformly spaced three element array, with unit weighting, where

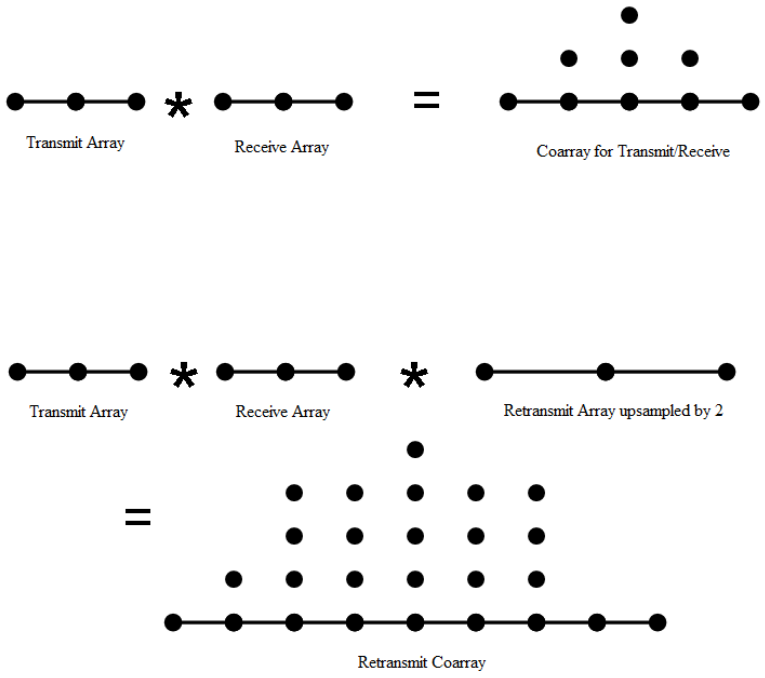

Figure 5.2: Example Coarrays for Transmit/Receive and Retransmit Imaging

the same array is used for all transmit and receive operations. In the conventional transmit/receive scenario, the coarray weighting is given by the convolution of the transmit and receive array weightings, $[1,1,1] * [1,1,1] = [1,2,3,2,1]$. The coarray, shown in Figure 5.2, consists of five uniformly spaced elements at the same spacing. The coarray has a triangular weighting.

When we consider the same array in a retransmission scheme, the coarray becomes $[1,1,1] * [1,0,1,0,1] * [1,1,1] = [1,2,4,4,5,4,4,2,1]$. The coarray has nine uniformly spaced elements and is shown in Figure 5.2. This will cause the beamwidth of the point spread function to be narrower than in conventional transmit/receive imaging. Note that the coarray weighting is no longer triangular.

The point spread functions corresponding to the coarrays in Figure 5.2 are plotted

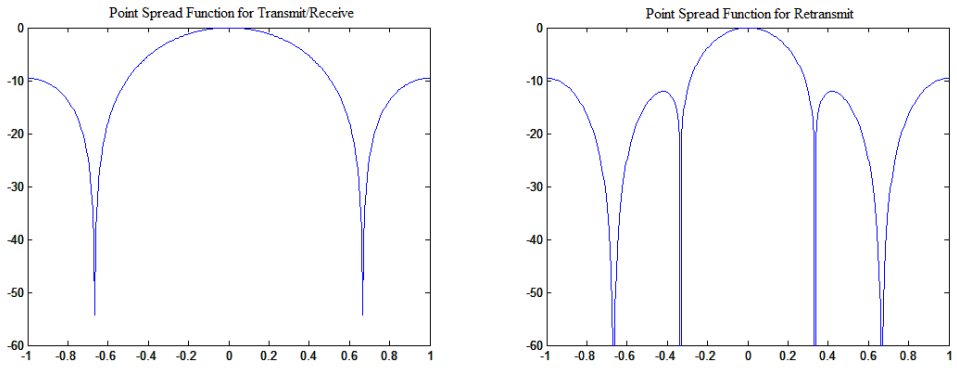

Figure 5.3: Example Point Spread Functions for Transmit/Receive and Retransmit Imaging

in Figure 5.3. The mainbeam of point spread function for the retransmission scheme is about half the width of the mainbeam for standard active imaging. Mainbeam width is the characteristic related to resolution, so it is reasonable to expect better resolution with retransmission.

The retransmission scheme seems to allow for an interesting coarray synthesis. With only a few real array elements, a relatively wide coarray can be synthesized. However, we will see that there are some problems for more than one target in the scene.

5.3.2 Retransmission with Two Coherent Point Targets

To examine the resolution capabilities of retransmission further, consider a scene which has two coherent point targets at u_1 and u_2 each with unit reflectivity. Assume

unit array weights, $w_{Tn} = w_p = w_{Rm} = 1$, for all n, m, p, then Equation 5.14 becomes

$$\begin{aligned} I(u) &= \sum_{m=1}^{M}\sum_{p=1}^{P}\sum_{n=1}^{N}\sum_{k=1}^{2}\sum_{i=1}^{2} e^{-jk_0(u-u_k)(x_{Tn}+x_p)} e^{-jk_0(u-u_i)(x_p+x_{Rm})} \\ &= \sum_{m=1}^{M}\sum_{p=1}^{P}\sum_{n=1}^{N} (e^{-jk_0(u-u_1)(x_{Tn}+x_p)} + e^{-jk_0(u-u_2)(x_{Tn}+x_p)}) \\ &\quad \times (e^{-jk_0(u-u_1)(x_{Tn}+x_p)} + e^{-jk_0(u-u_2)(x_{Tn}+x_p)}) \\ &= \sum_{m=1}^{M}\sum_{p=1}^{P}\sum_{n=1}^{N} [e^{-jk_0(u-u_1)(x_{Tn}+2x_p+x_{Rm})} + e^{-jk_0(u-u_1)(x_{Tn}+x_p)} e^{-jk_0(u-u_2)(x_{Rm}+x_p)} \\ &\quad + e^{-jk_0(u-u_1)(x_{Rm}+x_p)} e^{-jk_0(u-u_2)(x_{Tn}+x_p)} + e^{-jk_0(u-u_2)(x_{Tn}+2x_p+x_{Rm})}]. \end{aligned} \tag{5.20}$$

The first and fourth terms inside of the square brackets are the retransmit point spread functions with peaks at $u = u_1$ and $u = u_2$, respectively. This is what we want to see in our image. The second and third terms are *crossterms*; these are artifactual terms. We can rewrite Equation 5.20 as

$$I(u) = PSF_{RT}(u - u_1) + PSF_{RT}(u - u_2) + F(u) \tag{5.21}$$

where $F(u)$ contains the crossterms. Examining the crossterms,

$$\begin{aligned}
F(u) = &\sum_{m=1}^{M}\sum_{p=1}^{P}\sum_{n=1}^{N} e^{-jk_0(u-u_1)(x_{Tn}+x_p)}e^{-jk_0(u-u_2)(x_{Rm}+x_p)} \\
&\quad + e^{-jk_0(u-u_1)(x_{Rm}+x_p)}e^{-jk_0(u-u_2)(x_{Tn}+x_p)} \\
= &\sum_{m=1}^{M}\sum_{p=1}^{P}\sum_{n=1}^{N} e^{-jk_0(u-\frac{u_1+u_2}{2})(x_{Tn}+2x_p+x_{Rm})}\times \\
&\quad [e^{jk_0\frac{u_1-u_2}{2}(x_{Tn}+x_p)}e^{-jk_0\frac{u_1-u_2}{2}(x_p+x_{Rm})} + e^{-jk_0\frac{u_1-u_2}{2}(x_{Tn}+x_p)}e^{jk_0\frac{u_1-u_2}{2}(x_p+x_{Rm})}] \\
= &\sum_{m=1}^{M}\sum_{p=1}^{P}\sum_{n=1}^{N} e^{-jk_0(u-\frac{u_1+u_2}{2})(x_{Tn}+2x_p+x_{Rm})}[e^{jk_0\frac{u_1-u_2}{2}(x_{Tn}-x_{Rm})} + e^{-jk_0\frac{u_1-u_2}{2}(x_{Tn}-x_{Rm})}] \\
= &\sum_{m=1}^{M}\sum_{p=1}^{P}\sum_{n=1}^{N} e^{-jk_0(u-\frac{u_1+u_2}{2})(x_{Tn}+2x_p+x_{Rm})}2\cos[k_0\frac{u_1-u_2}{2}(x_{Tn}-x_{Rm})]
\end{aligned} \tag{5.22}$$

we see that the crossterm $F(u)$ looks very similar to a point spread function evaluated at $\frac{u_1+u_2}{2}$, however it is modified by the cosine factor which effectively gives an element weighting depending on the angular separation of the target locations. The peak of the crossterm appears at the average of the two target locations.

The image $I(u)$ has three potential peaks: two desired peaks near the target locations u_1 and u_2 and one undesired peak near $\frac{u_1+u_2}{2}$. Figure 5.4 illustrates this effect of the crossterm. This simulation was performed with a 9 element $\frac{\lambda_0}{2}$ uniformly-spaced array being used for transmission, retransmission and receiving, with targets at $u = \pm.15$. The simulation shows the correctly estimated target locations near $\pm.15$ and the crossterm is clearly present at $u = 0$.

To further examine the behavior of the crossterm, assume without loss of generality, that the array is symmetric about the origin. Then the sets $\{x_{Rm} + x_{Tn}\} = \{x_{Rm} - x_{Tn}\} = \{y_l\}$. If the arrays are uniformly spaced at $\frac{\lambda_0}{2}$, then $\{y_l\}$ has a trian-

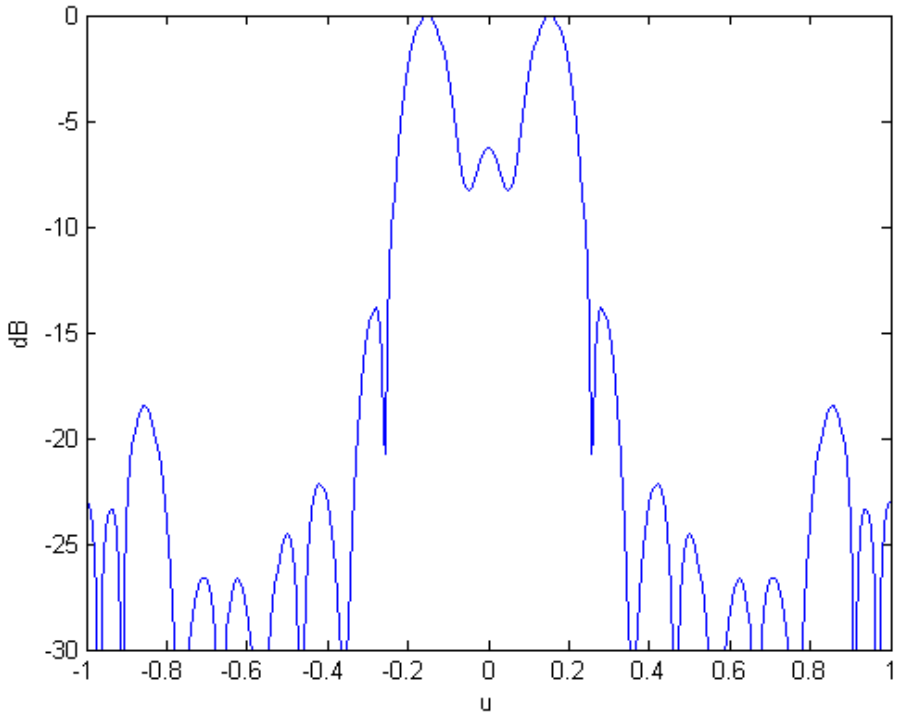

Figure 5.4: Illustration of the Crossterm appearing between Two Targets

gular weighting $\{\gamma_l\}$. Evaluating the crossterm, $F(u)$ at the peak crossterm location $u = \frac{u_1+u_2}{2}$ yields

$$\begin{aligned} F(\frac{u_1+u_2}{2}) =& 2\sum_{n=1}^{M}\sum_{m=1}^{M}\cos[k_0\frac{u_1-u_2}{2}(x_{Tn}-x_{Rm})]\sum_{p=1}^{M}e^{-jk_0(\frac{u_1+u_2}{2}-\frac{u_1+u_2}{2})(x_{Tn}+2x_p+x_{Rm})} \\ =& 2M\sum_{n=1}^{M}\sum_{m=1}^{M}\cos[k_0\frac{u_1-u_2}{2}(x_{Tn}-x_{Rm})] \\ =& 2M\sum_{l=-(M-1)}^{M-1}(M-|l|)\cos[l\pi\frac{u_1-u_2}{2}]. \end{aligned} \tag{5.23}$$

The last equation is true since we have assumed uniformly-spaced unit-weighted array centered at the origin.

For very separated targets, $u_1 \to 1$ and $u_2 \to -1$, so $\frac{u_1-u_2}{2} \to 1$. When M is even, $F(\frac{1+1}{2}) = F(1) = 0$. When M is odd, $F(\frac{1+1}{2}) = F(1) = 2M$. Comparing this to the power at an actual target, which is $PSF_{RT}(0) = M^3$, when the targets are far apart, the power at the crossterm location is small compared to the power at the actual target locations. The crossterm is not a major issue for separated targets. However, for very closely spaced targets, $u_1 \to u_2$ and $\frac{u_1-u_2}{2} \to 0$, $F(0) = 2M^3$ which is comparable to the power at the actual target locations. A large crossterm may appear.

The idea of increasing the diameter of the coarray by retransmission to increase resolution capabilities of the system creates an undesirable crossterm which is significant as the targets come closer together. This occurs because retransmission is not a linear operation. For multiple point targets, the image is not a superposition of the individual point spread functions as it is in standard active imaging.

5.4 Resolution Limits

In this section, we will analyze the beamwidth of the point spread functions for both transmit/receive and retransmit imaging to determine whether retransmit imaging with the crossterm present can provide better resolution.

In standard transmit/receive imaging, two targets are said to be resolvable if they are more than $2u_{3dB}$ apart. u_{3dB} is the 3 dB point of the mainlobe of the point spread function - the postive point closest to zero where $PSF(u_{3dB}) = \frac{1}{2}$, assuming the maximum of the point spread function has been normalized to unity.

Since in retransmission with two targets we have two mainbeams corresponding to the estimated target locations and then the crossterm halfway in between, the crossterm is distinguishable from the two mainbeams if it is at least $2u_{3dB}^{RT}$ from each target. u_{3dB}^{RT} is the positive point closest to zero where $PSF_{RT}(u_{3dB}^{RT}) = \frac{1}{2}$. This means that the targets must be at least $4u_{3dB}^{RT}$ away from each other. This is illustrated in Figure 5.5.

For retransmission where a crossterm is present, to be able to have better resolution capabilities than standard transmit/receive imaging, we need

$$4u_{3dB}^{RT} \leq 2u_{3dB}. \tag{5.24}$$

5.4.1 Analysis of Beamwidths

Assuming a uniform weighting on the M-element uniformly spaced array which is centered about the origin, the receive and transmit beampatterns for a target at

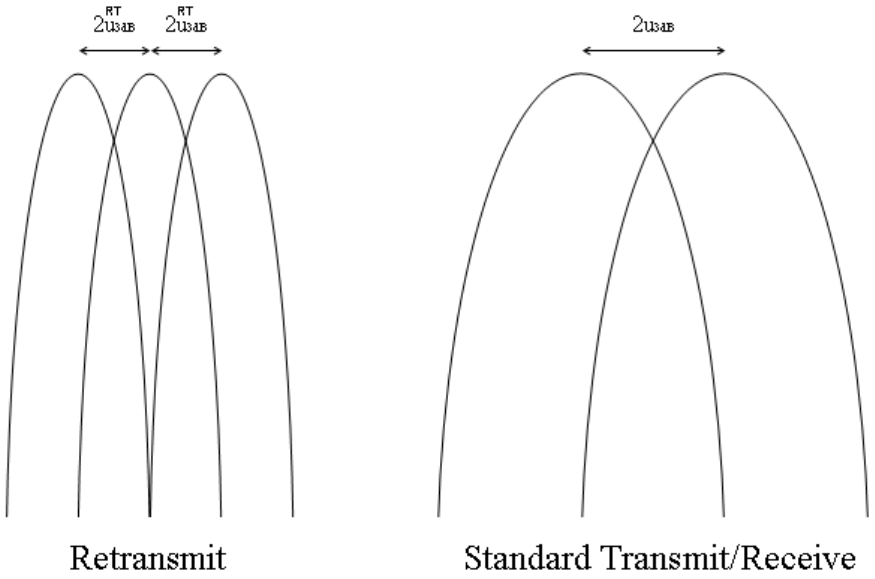

Figure 5.5: Illustration of Retransmit Imaging with the Crossterm vs. Standard Transmit/Receive Imaging Mainbeam Widths

broadside with unit reflectivity are given by their respective Fourier Transforms,

$$B_R(u) = \sum_{m=1}^{M} e^{-jk_0 u x_{Rm}} = \frac{\sin(\frac{M}{2}\pi u)}{\sin(\frac{1}{2}\pi u)},\ B_T(u) = \sum_{n=1}^{M} e^{-jk_0 u x_{Tn}} = \frac{\sin(\frac{M}{2}\pi u)}{\sin(\frac{1}{2}\pi u)}. \quad (5.25)$$

The point spread function is the product of the two beampatterns:

$$PSF(u) = B_T(u)B_R(u) = \sum_{m=1}^{M}\sum_{n=1}^{M} e^{-jk_0 u(x_{Rm}+x_{Tn})} = \frac{\sin^2(\frac{M}{2}\pi u)}{\sin^2(\frac{1}{2}\pi u)} \quad (5.26)$$

For the retransmit scheme where the M elements are used to transmit, retransmit and receive, the beampatterns for the transmit and receive stages are again given by Equation 5.25 and the retransmit stage is given by the upsampled version,

$$B(u) = \sum_{p=1}^{M} e^{-jk_0 u 2x_{Rm}} = \frac{\sin(M\pi u)}{\sin(\pi u)}. \quad (5.27)$$

M	u_{3dB}	u_{3dB}^{RT}	$4u_{3dB}^{RT} - 2u_{3dB}$
2	0.5	0.2880	0.1520
3	0.3106	0.1790	0.0948
4	0.2277	0.1313	0.0698
5	0.1804	0.1040	0.0552
6	0.1495	0.0863	0.0462
7	0.1277	0.0737	0.0394
8	0.1116	0.0644	0.0344
9	0.0990	0.0572	0.0308
10	0.0891	0.0514	0.0274
> 10	$\frac{.8858}{M}$	$\frac{.5108}{M}$	$\frac{.2716}{M}$

Table 5.1: 3 dB Beamwidths for Transmit/Receive and Retransmit Imaging for Various Array Sizes

The point spread function is given by the products of the three beampatterns (see Equation 5.18):

$$\begin{aligned} PSF_{RT}(u) &= B_T(u)B(2u)B_R(u) \\ &= \sum_{m=1}^{M}\sum_{n=1}^{M}\sum_{p=1}^{M} e^{-jk_0u(x_{Rm}+2x_p+x_{Tn})} = \frac{\sin^2(\frac{M}{2}\pi u)}{\sin^2(\frac{1}{2}\pi u)}\frac{\sin(M\pi u)}{\sin(\pi u)}. \end{aligned} \tag{5.28}$$

For the purpose of estimating the 3 dB point of the point spread function, we can approximate the mainbeam of the beampatterns with $\text{sinc}(.) = \frac{\sin(.)}{(.)}$ functions with reasonable accuracy for large enough M (approximately $M > 10$). This is because as M increases, the 3 dB point becomes smaller and the small angle approximation can be used, $\sin(\pi u) \approx \pi u$. Using these expressions, Table 5.1 summarizes the distance from the peak of the mainlobe to the 3 dB point of the mainlobe for transmit/receive (u_{3dB}) and retransmit cases (u_{3dB}^{RT}). The values were calculated numerically using MATLAB. Exact values are used for $M \leq 10$ and the sinc(.) approximation is used for $M > 10$.

Now that we have these exact beamwidth results, we can compare the beamwidths

of retransmit to standard transmit/receive. For retransmit imaging to have an advantage over standard transmit/receive imaging, the targets in the retransmit scheme should be able to be closer than in the standard scheme. As was stated in the beginning of this section, this condition is

$$4u_{3dB}^{RT} \leq 2u_{3dB}. \tag{5.29}$$

Based on this table, for any M, we see that this is not true since the difference (given in the last column of the table) is always positive. Thus, for any M we cannot achieve the resolution in retransmit with the crossterm present that we can in standard transmit receive. Thus the only way to make retransmission feasible is to consider means for eliminating or reducing the crossterm.

5.4.2 Crossterm Mitigation Schemes

Modifying Array Element Spacing

One approach to reducing the crossterm is to force $F(u)$ to zero at $u = \frac{u_1+u_2}{2}$ by choosing the array appropriately. This is equivalent to forcing the argument of the cosine factor in $F(u)$ to $\frac{\pi}{2}$ (modulus π) for all $\{x_{Tn} - x_{Rm}\}$. For this exercise, assume we know the separation $u_1 - u_2$, then the argument of the cosine factor should be chosen such that it is equal to $\frac{\pi}{2}$ modulus π, i.e.,

$$\begin{aligned} k_0 \frac{u_1 - u_2}{2}(x_{Tn} - x_{Rm}) &= l\pi + \frac{\pi}{2} \\ x_{Tn} - x_{Rm} &= \frac{(l + \frac{1}{2})\lambda_0}{u_1 - u_2} \\ x_{Tn} - x_{Rm} &= \frac{l\lambda_0}{u_1 - u_2} + \frac{\lambda_0}{2(u_1 - u_2)} \text{ for all } n, m \text{ and for some } l \end{aligned} \tag{5.30}$$

If we know the spacing of the targets, the above analysis simply says that in

order to reduce the crossterm, we must modify the spacing of the array elements. As the targets get closer together, the spacing of the elements must get further apart. However, if such a spacing is chosen, the targets might be able to be resolved without using retransmission because of the wider coarray. This approach also causes grating lobes due to undersampling. The spacing of targets is generally unknown, so this approach is not likely viable. However, this analysis provides some insight into other methods which may be useful. Essentially what is happening here is we are chosing the array elements so that the contributions from the crossterms add up out of phase. We can use this idea applied to other methods of crossterm reduction such as using aperiodic arrays or multiple frequencies as will be examined in the following sections.

Using an Aperiodic Array

In this section, we simulate examples of aperiodic arrays to observe the effect of the aperiodicity in the retransmission scheme. The hope is that the aperiodicity will help reduce the crossterm size while preserving the narrow shape of the retransmission beam to allow for higher resolution.

The first array we study is a 5-element array. We fix the length of the aperture at $2\lambda_0$, which is the length of the 5-element $\frac{\lambda_0}{2}$-uniformly-spaced array, so that the increase in resolution does not come from an increase in aperture size. The other three array element positions are variable. We will simulate many trials where each of the elements is uniformly randomly located within the aperture. We assume that we are observing two targets which are symmetric about broadside.

Quantities to be observed are the how close the estimated target locations are to the actual target locations, the power of the null between the two target locations ($u = 0$) and the peak sidelobe power. We will compare retranmission with standard transmit/receive imaging in each of these areas.

For our first examination, we have two targets at ± 0.19 and use frequency $\omega_0 = 1$ GHz. This separation is chosen because it is just barely resolvable by a uniformly spaced 5 element array, see Table 5.1. 100 trials are run, allowing the three variable array elements to be placed randomly within the aperture with a uniform probability density function over $[-\lambda_0, \lambda_0]$. The results of the trials are plotted in Figure 5.6. For standard transmit/receive imaging, the two targets were successfully resolved 100 out of 100 times. Retransmission imaging resolved the targets 83 out of 100 times. The times where the two targets were not resolved in retransmission, the crossterm at $u = 0$ dominated. When the targets were resolved, on average, standard transmit/receive imaging estimated the target locations to be at $u = \pm .2039$ and retransmission imaging estimated them to be at $u = \pm .2176$. For standard active imaging, the power between the targets $u = 0$ was -2.0025 dB while for retransmission it was slightly better at -2.8701 dB. The peak sidelobe level for standard active imaging was on average -1.3815 dB and for retransmission is was significantly better at -5.0224 dB.

For this experiment, it seems that standard active imaging provides a better chance of resolving the targets and gives better accuracy in estimating the target locations, but retransmit imaging gives a deeper null between targets when they are resolved and significantly lower peak sidelobe power.

One of the chosen random arrays which provided low crossterm and sidelobe levels for retransmission imaging will be examined. The array $[-.3, -.1365, -.1297, .1304, .3]$ provided good results. We will slightly modify this array for our simulations. The array elements $-.1365$ and $-.1297$ are too close to actually have two separate array elements there, so we will consider them one element. We will also enforce symmetry on the array. The array we use for simulations is $[-.3, -.1365, .1365, .3]$. We will compare this array for both standard transmit/receive imaging and retransmit imaging

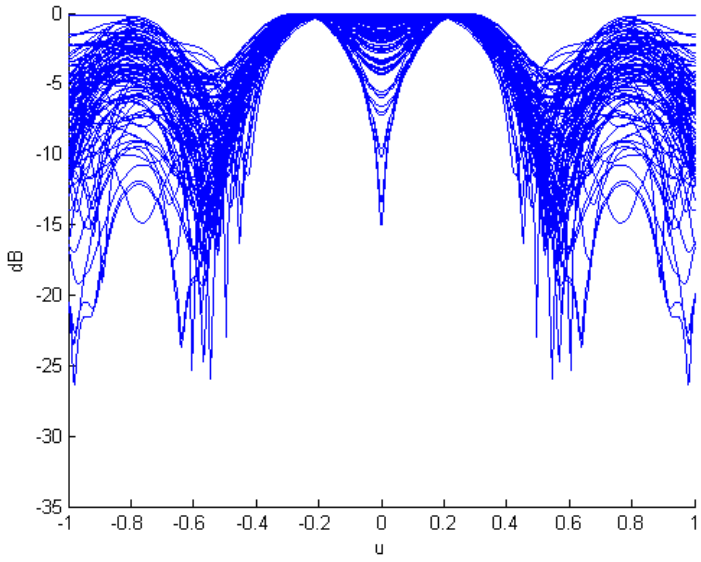

(a) Standard Transmit/Receive Imaging Trials

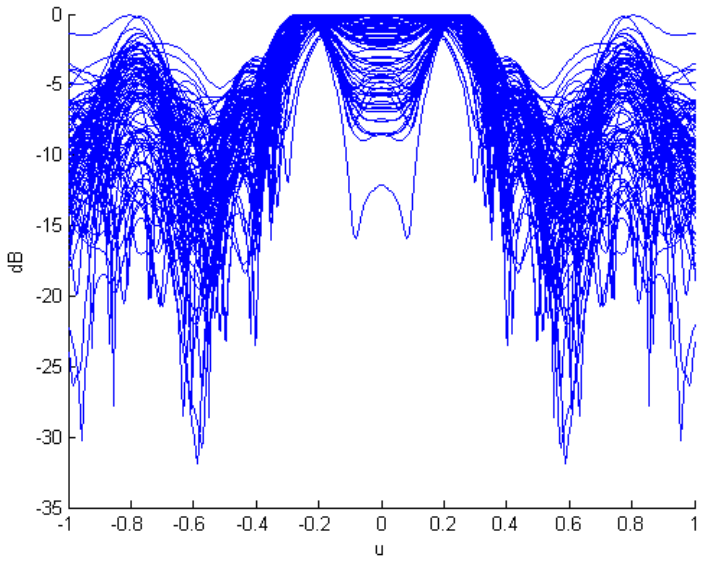

(b) Retransmit Imaging Trials

Figure 5.6: Random Array Trials

for various target separations. As is shown in Figure 5.7(a), for $u = \pm.19$, standard transmit/receive imaging estimated the targets to be at $\pm.22$, with a between target null of $-1.3848\ dB$ and peak sidelobe power of $-6.462\ dB$. Retransmit imaging also estimated the targets to be at $\pm.22$, with a between target null of $-2.1618\ dB$ and peak sidelobe power of $-8.4801\ dB$. This is shown in Figure 5.7(b). Retransmission for this case overall performs better than standard transmit/receive imaging.

If the targets are slightly more separated to $\pm.25$, standard transmit/receive imaging estimates the targets to be at $\pm.27$, with a between target null of $-6.2277\ dB$ and peak sidelobe power of $-6.3121\ dB$. Retransmit imaging estimated the targets to be at $\pm.265$, with a between target null of $-9.34\ dB$ and peak sidelobe power of $-9.303\ dB$. This simulation is shown in Figure 5.8. The retransmission scheme again outperforms standard transmit/receive imaging. Notice that there is an actual peak at the crossterm location. It is on the level of the sidelobes, so it is not prohibitively large.

If the targets are moved closer together to $\pm.165$, retransmission cannot resolve them, while standard transmit/receive can barely do so. See Figure 5.9. At $\pm.17$, they can be resolved by both schemes as is shown in Figure 5.10. Standard transmit/receive imaging estimats the targets to be at $\pm.165$, with a between target null of $-.3037\ dB$ and peak sidelobe power of $-6.3414\ dB$. Retransmit estimates the targets to be at $\pm.16$, with a between target null of $-.2475\ dB$ and peak sidelobe power of $-9.1282\ dB$. Now, in terms of target resolution, standard transmit/receive imaging is better in this case.

There are trade-offs between standard transmit/receive imaging and retransmission imaging. Retransmission does not appear to provide better resolution capabilities with an aperiodic array. Standard transmit/receive imaging may be able to resolve targets that retransmission cannot, and standard transmit/receive imaging seems

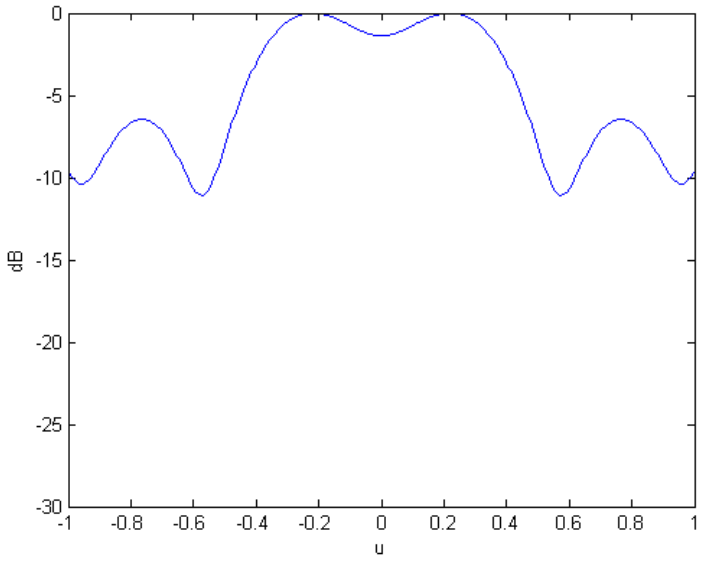

(a) Standard Transmit/Receive Imaging

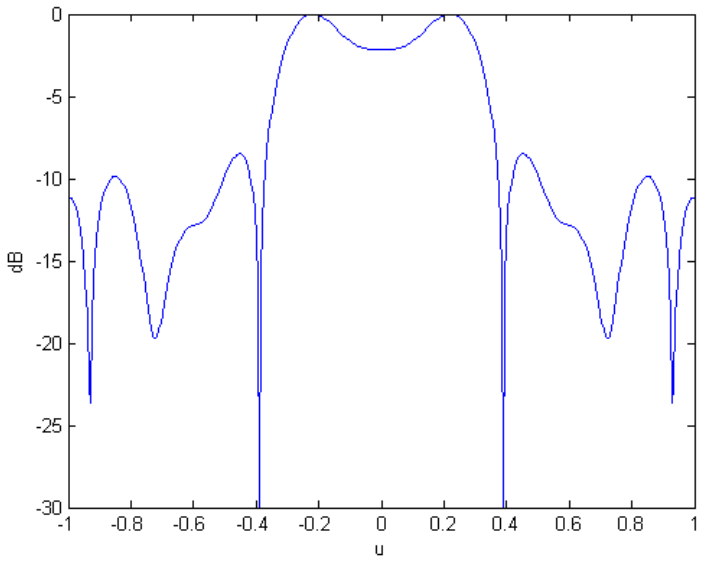

(b) Retransmit Imaging

Figure 5.7: 4-element Aperiodic Array, Targets at $\pm.19$

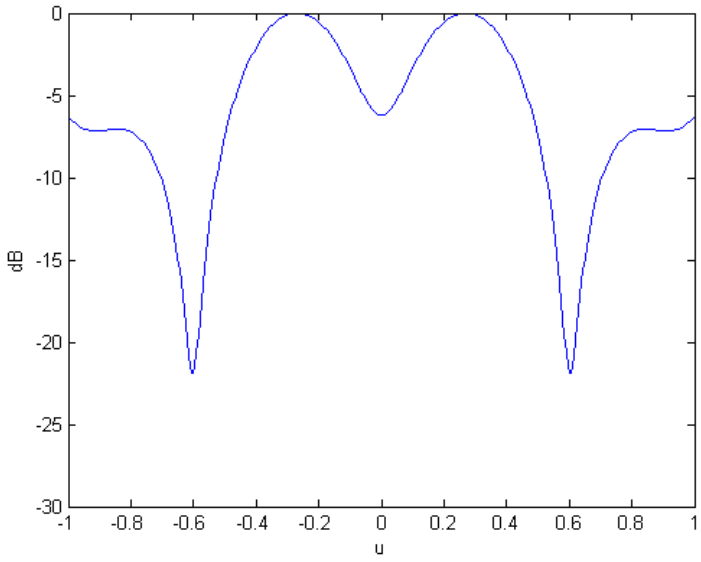

(a) Standard Transmit/Receive Imaging

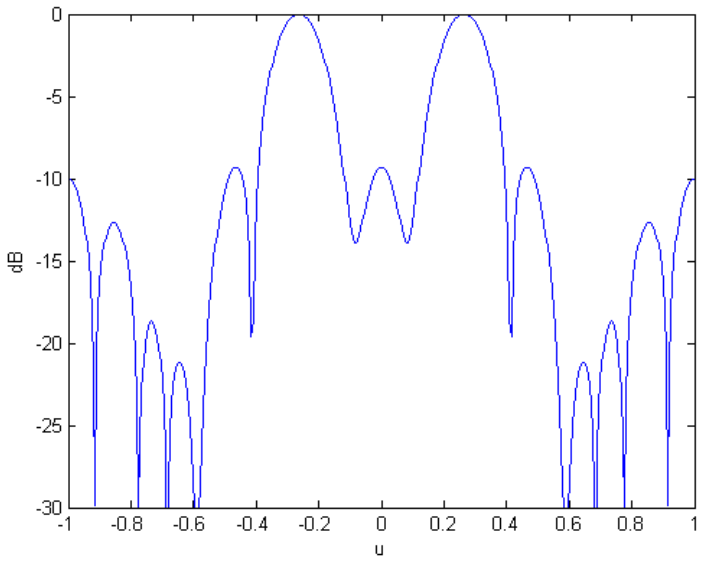

(b) Retransmit Imaging

Figure 5.8: 4-element Aperiodic Array, Targets at $\pm.25$

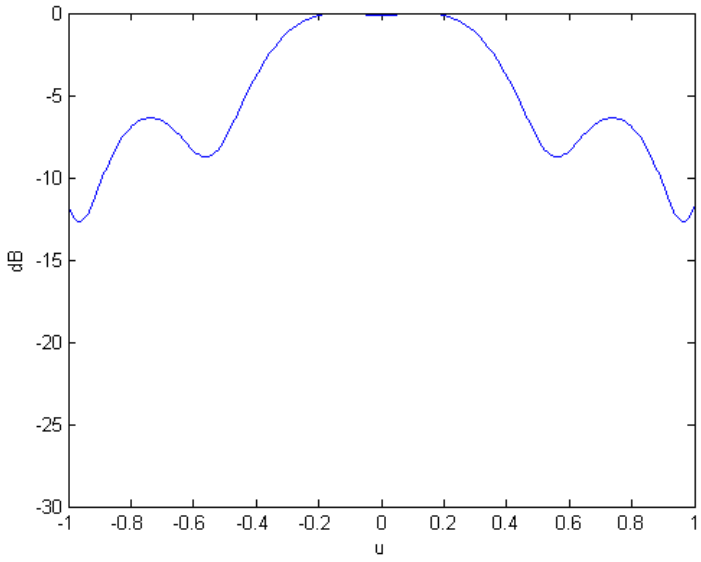

(a) Standard Transmit/Receive Imaging

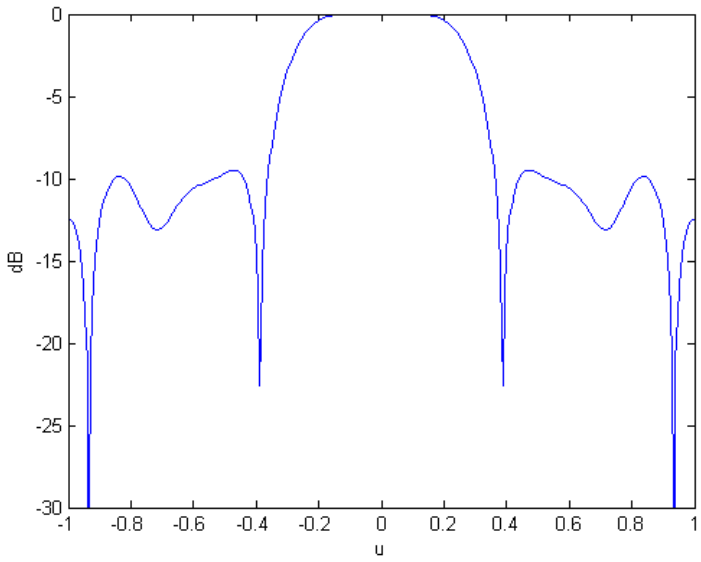

(b) Retransmit Imaging

Figure 5.9: 4-element Aperiodic Array, Targets at $\pm.165$

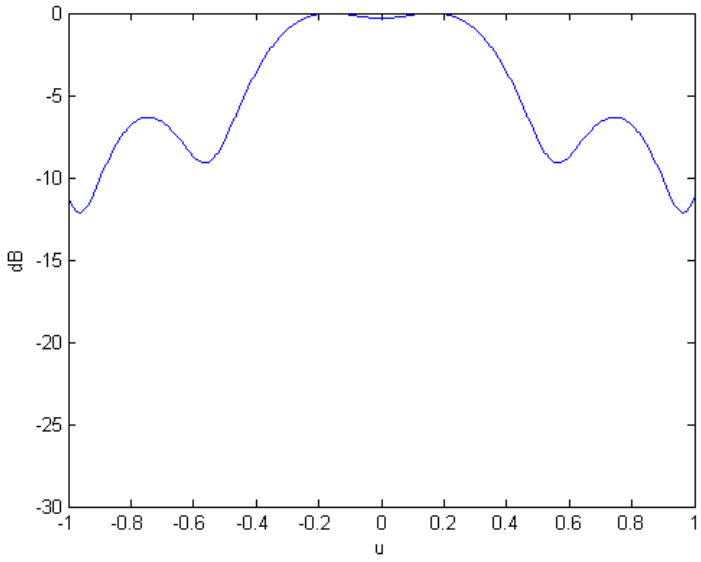

(a) Standard Transmit/Receive Imaging

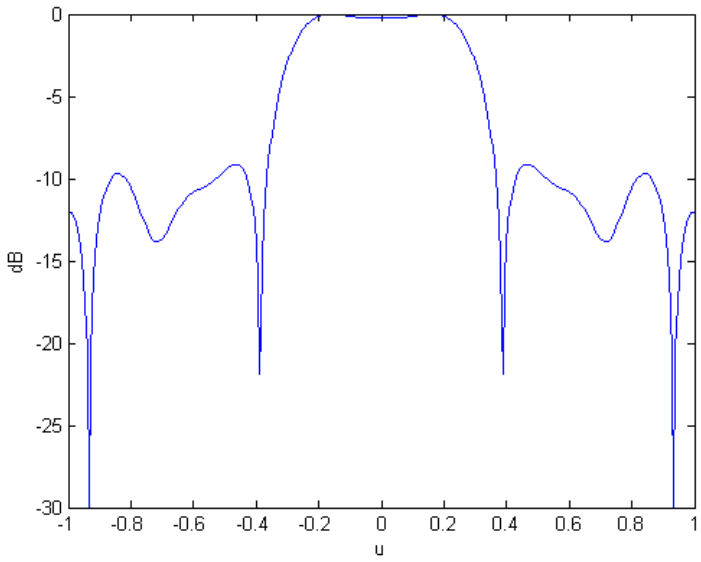

(b) Retransmit Imaging

Figure 5.10: 4-element Aperiodic Array, Targets at $\pm.17$

to provide better target accuracy. However, for targets that are not at the critical resolution capability, retransmission with an aperiodic array could provide slightly better imaging in terms of narrower beamwidth, depth of the null between the target locations and peak sidelobe power.

Using Multiple Frequencies

As has been shown, using multiple frequencies changes the coarray, [17]. In this section, we examine the effect of using multiple frequencies on retransmission imaging and compare it to standard transmit/receive imaging.

We assume we have a 5 element $\frac{\lambda_0}{2}$-uniformly spaced array. Radiation of various frequencies is transmitted and received (and retransmitted and received again for retransmission imaging). The image is formed by beamforming and summing over all of the returns at each frequency. The hope is that these returns will add up out of phase at the crossterm location.

For targets at $\pm.19$, which are barely resolvable for narrowband imaging at the reference frequency, we simulate the image at various frequencies. In Figure 5.11(a), the standard transmit/receive image from 20 equally spaced frequencies from 1 GHz to 2 GHz are individually plotted. The reference frequency is taken to be $\omega_0 = 1\,GHz$. We see that as frequency increases, the mainlobe width decreases, the null between the targets decreases and grating lobes appear. This is expected because as the frequency increases, the effective array spacing increases yielding higher resolution, but grating lobes appear because the spatial sampling separation is below the Nyquist spacing, [40]. Figure 5.11(b) shows the retransmit image from the same 20 equally spaced frequencies and the effects are the same. The power of the crossterm decreases as frequency increases.

In Figures 5.12(a) and 5.12(b), the average of the images from each of the fre-

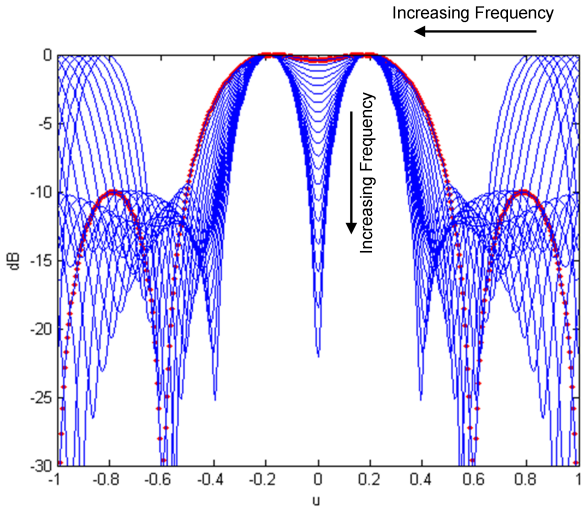

(a) Standard Transmit/Receive Imaging

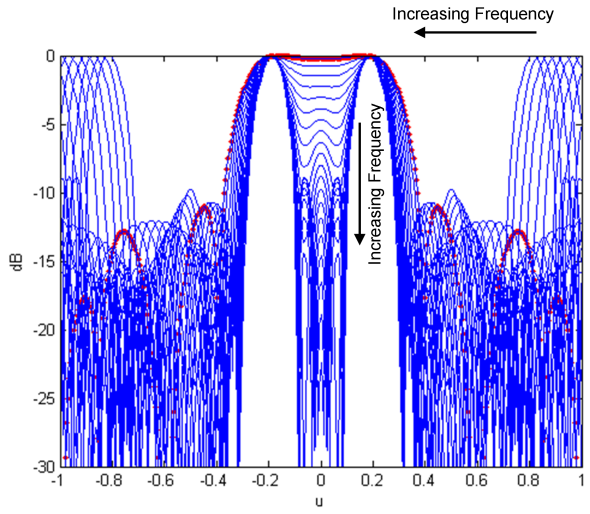

(b) Retransmit Imaging

Figure 5.11: 5-element Uniformly Spaced Array, Multiple Frequencies from 1-2 GHz

quencies is taken for standard transmit/receive and retransmit imaging, respectively. We see that with the use of multiple frequencies, the targets become more resolvable. Averaging over the frequencies controls grating lobes, as they add up out of phase, but preserves the increased resolution. The crossterm power is reduced because the cosine factors in $F(u)$ are adding up out of phase. In this example, both retransmit and standard transmit/receive imaging estimate the targets to be in the correct location, at $\pm.19$. Retransmission performs better in terms of between target null. For retransmission it is $-5.4909\ dB$ and for standard transmit/receive it is $-4.8280\ dB$. Retransmission also has lower peak sidelobe levels.

As happened with aperiodic arrays, as the targets become closer together, retransmission performance degrades compared to standard transmit/receive imaging. Figures 5.13(a) and 5.13(b) show the multi-frequency simulation for target at $u = \pm.15$. Here, retransmission still outperforms standard transmit/receive imaging in terms of peak sidelobe height and null depth between targets. When the targets are less separated at $u = \pm.12$, retransmission cannot resolve the two targets, while standard transmit/receive imaging can - the crossterm becomes too large. This is shown in Figures 5.14(a) and 5.14(b). For targets at $u = \pm.13$, retransmission can resolve them, but standard transmit/receive imaging performs better in terms of depth of null between the targets and accuracy of target location estimation. Retransmission still has better sidelobe characteristics. These simulations are shown in Figures 5.15(a) and 5.15(b).

Using multiple frequencies in retransmit imaging can help reduce the crossterm size, however, overall resolution capabilities do not appear to be improved compared to standard transmit/receive imaging. Retransmission imaging can yield improved image quality in terms of lower sidelobe levels and depth of between target null for sufficiently separated targets. This result is similar to using aperiodic arrays in

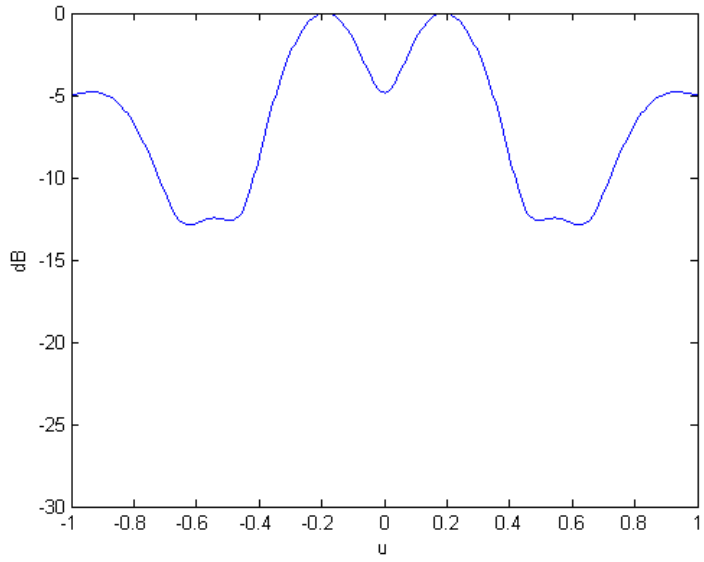

(a) Standard Transmit/Receive Imaging

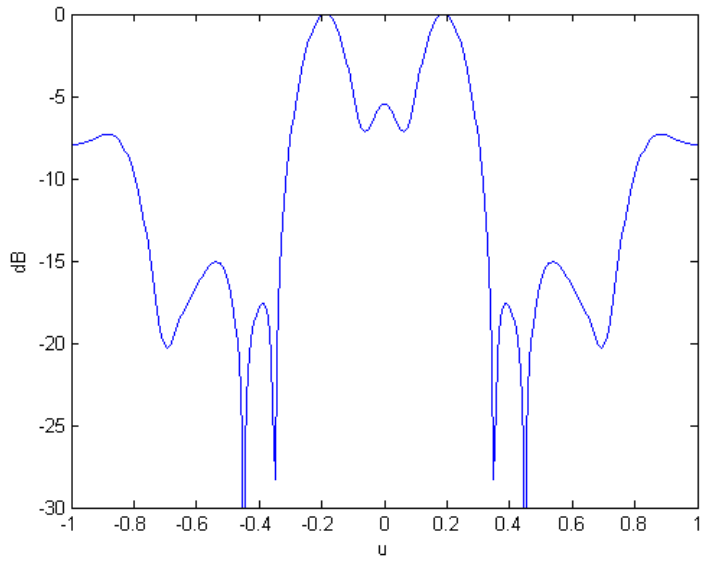

(b) Retransmit Imaging

Figure 5.12: 5-element Uniformly Spaced Array, Average over all Frequencies, Targets at $\pm.19$

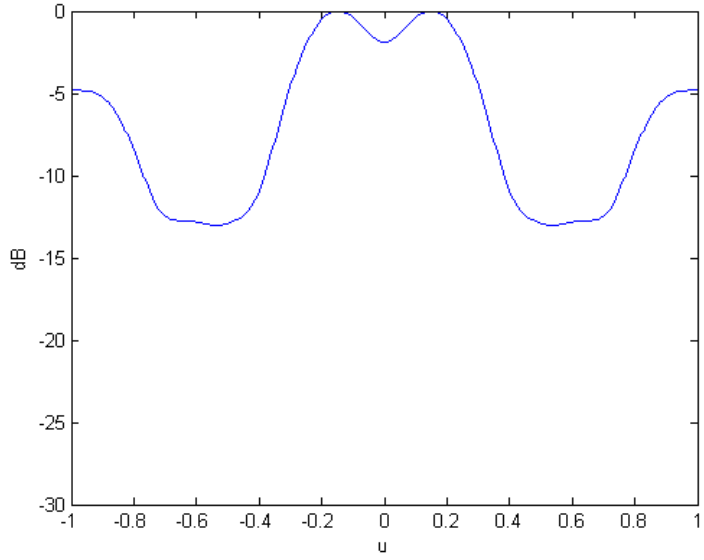

(a) Standard Transmit/Receive Imaging

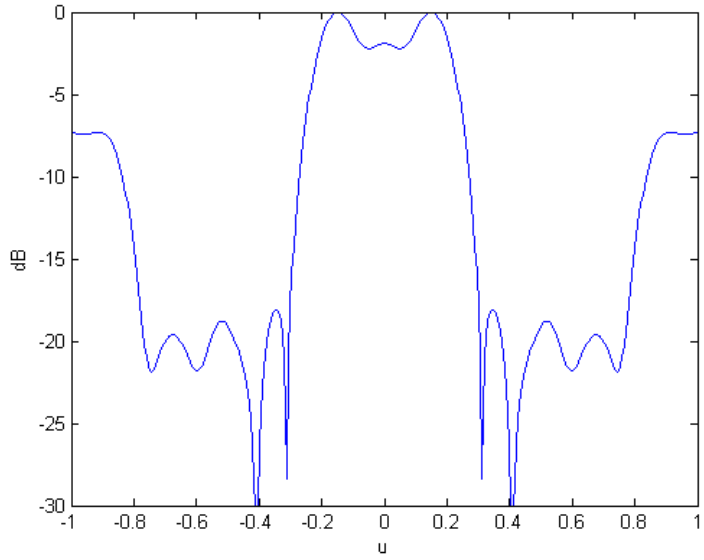

(b) Retransmit Imaging

Figure 5.13: 5-element Uniformly Spaced Array, Average over all Frequencies, Targets at $\pm.15$

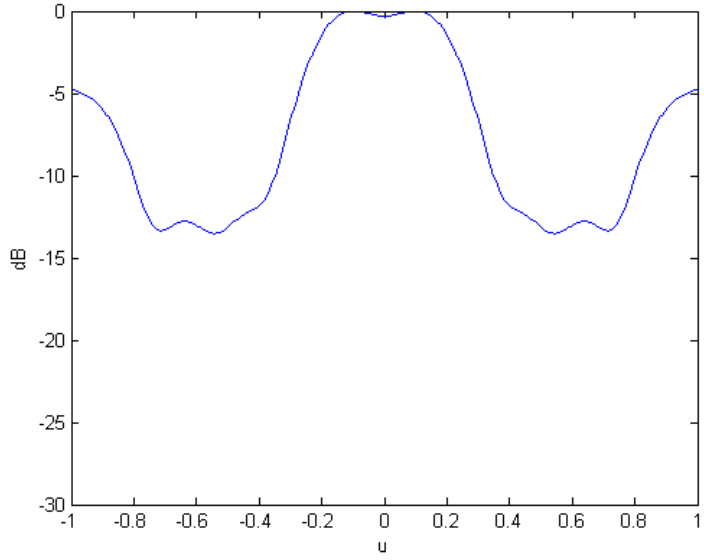

(a) Standard Transmit/Receive Imaging

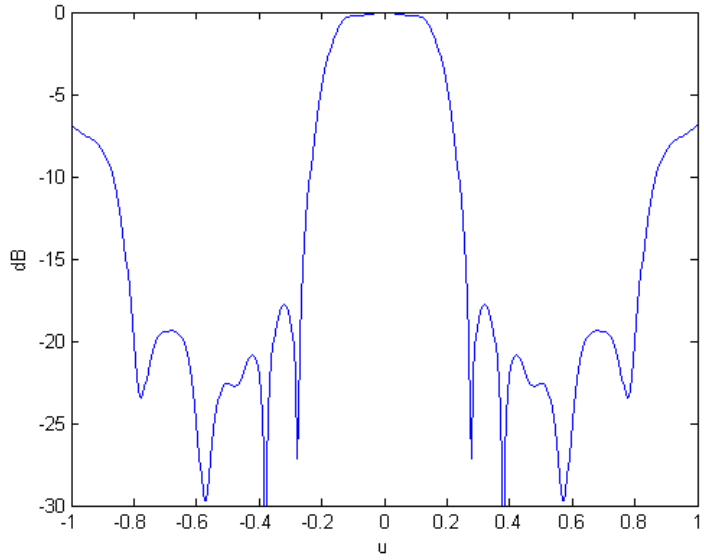

(b) Retransmit Imaging

Figure 5.14: 5-element Uniformly Spaced Array, Average over all Frequencies, Targets at $\pm.12$

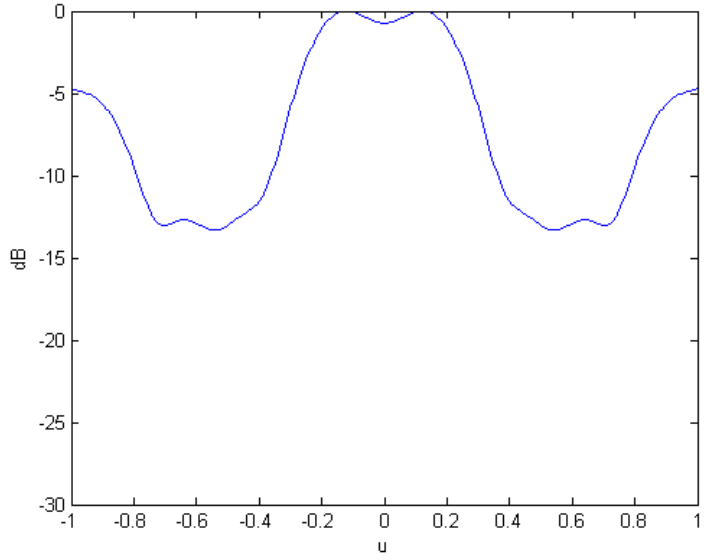

(a) Standard Transmit/Receive Imaging

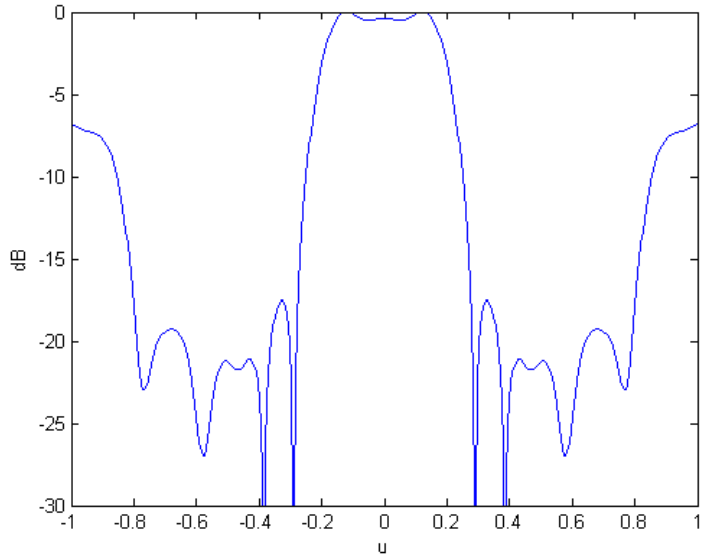

(b) Retransmit Imaging

Figure 5.15: 5-element Uniformly Spaced Array, Average over all Frequencies, Targets at $\pm.13$

retransmit imaging.

5.5 Retransmission with Incoherent Targets

So far, we have only considered coherent targets - targets that reflect with a fixed phase difference - and the reflectivities could be considered deterministic because of this fixed phase difference. In this section, we consider incoherent targets, which are targets that each reflect with an independent uniformly random phase. Now, we must consider taking the expection of the image given in Equation 5.14. The complex amplitude S_k can be modeled as a real, deterministic amplitude a_k and a uniformly random phase $\beta_k \in [-\pi, \pi]$. The phases for different targets are independent of each other. Since we are observing a random process, we take multiple snapshots of the scene and average the images of the snapshots. Over the snapshots, the relationship between the complex amplitudes is

$$\mathbb{E}[S_k S_i] = \begin{cases} \mathbb{E}[a_k e^{j\beta_k} a_i e^{j\beta_i}] = a_k a_i \mathbb{E}[e^{j\beta_k}]\mathbb{E}[e^{j\beta_i}] = 0 \text{ for } k \neq i \\ \mathbb{E}[a_k e^{j\beta_k} a_k e^{j\beta_k}] = a_k^2 \mathbb{E}[e^{j2\beta_k}] = 0 \text{ for } k = i \end{cases} \tag{5.31}$$

Because of this, when the targets are incoherent, Equation 5.14 becomes

$$I(u) = \sum_{m=1}^{M}\sum_{n=1}^{N}\sum_{p=1}^{P}\sum_{k=1}^{K}\sum_{i=1}^{K} \mathbb{E}[S_k S_i] e^{-jk_0(u-u_k)(x_{Tn}+x_p)} e^{-jk_0(u-u_i)(x_p+x_{Rm})} = 0 \tag{5.32}$$

and retransmit imaging with independent targets is rendered useless.

Since there is no conjugation involved, the expectation of the source reflectivities over the snapshots is zero. A popular method called Time Reversal Imaging is basically retransmission, except that in the retransmit stage the complex conjugate of the received data is used as weights, [27]. In this case where conjugation is performed,

the relationship between the target reflection amplitudes is

$$\mathbb{E}[S_k S_i^*] = \begin{cases} \mathbb{E}[a_k e^{j\beta_k} a_i^* e^{-j\beta_i}] = a_k a_i^* \mathbb{E}[e^{j\beta_k}]\mathbb{E}[e^{-j\beta_i}] = 0 \text{ for } k \neq i \\ \mathbb{E}[a_k e^{j\beta_k} a_k^* e^{-j\beta_k}] = |a_k|^2 \text{ otherwise.} \end{cases} \tag{5.33}$$

Then, if time reversal imaging is used, the image is

$$\begin{aligned} I(u) &= \sum_{m=1}^{M}\sum_{n=1}^{N}\sum_{p=1}^{P}\sum_{k=1}^{K}\sum_{i=1}^{K} \mathbb{E}[S_k^* S_i] e^{jk_0(u-u_k)(x_{Tn}+x_p)} e^{-jk_0(u-u_i)(x_p+x_{Rm})} \\ &= \sum_{m=1}^{M}\sum_{n=1}^{N}\sum_{p=1}^{P}\sum_{k=1}^{K} |a_k|^2 e^{jk_0(u-u_k)(x_{Tn}+x_p)} e^{-jk_0(u-u_k)(x_p+x_{Rm})} \\ &= \sum_{m=1}^{M}\sum_{n=1}^{N} P \sum_{k=1}^{K} |a_k|^2 e^{-jk_0(u-u_k)(x_{Rm}-x_{Tn})}. \end{aligned} \tag{5.34}$$

We see that the coarray for time reversal imaging is the *difference coarray*. For a uniformly spaced array, the difference coarray and the sum coarray seen in standard transmit/receive imaging are the same, [41]. Time reversal imaging does not provide increased resolution through coarray dilation, however, in the literature [27], time reversal imaging is shown to have increased resolution when clutter is present, but this is out of the scope of this chapter.

5.6 Retransmission with More than Two Targets

As the number of targets increases, the crossterms may become more of an issue - as there are multiple crossterms resulting from each pair of targets. Instead of examining the complicated imaging expressions for more than two targets, we can examine what happens by examining polynomial multiplication analogy.

The general image expression for more than two targets is given by

$$I(u) = \sum_{m=1}^{M}\sum_{p=1}^{P}\sum_{n=1}^{N}\sum_{k=1}^{K}\sum_{i=1}^{K} S_k S_i w_{Tn} w_p w_{Rm} e^{-jk_0(u-u_k)(x_{Tn}+x_p)} e^{-jk_0(u-u_i)(x_p+x_{Rm})}. \tag{5.35}$$

The crossterm arises because of the coupling of the factors containing i and k in the summations.

To understand how this is related to polynomial multiplication, we let everything in the expression involving target u_i be represented by v_i, then the image can roughly be written as

$$\sum_{k=1}^{K}\sum_{i=1}^{K} v_k v_i = (v_1 + v_2 + v_3 + ... + v_K)^2. \tag{5.36}$$

For the familiar case when there are two targets, $K = 2$, this is

$$(v_1 + v_2)^2 = v_1^2 + v_2^2 + 2v_1 v_2. \tag{5.37}$$

Comparing this to Equation 5.20, we see that there are two "pure" terms involving target u_1 and u_2 separately. These correspond to v_1^2 and v_2^2 in Equation 5.37. We know that there is one crossterm involving u_1 and u_2 jointly in Equation 5.20, corresponding to $2v_1v_2$ in Equation 5.37.

For three targets, the polynomial analogy becomes

$$(v_1 + v_2 + v_3)^2 = v_1^2 + v_2^2 + v_3^2 + 2v_1v_2 + 2v_1v_3 + 2v_2v_3 \tag{5.38}$$

and we see that there are three "pure" targets and three crossterms.

In general, for K targets, by the multi-nomial theorem, there will be K pure target locations and $\frac{K(K-1)}{2}$ crossterms. The number of crossterms grows quadratically in

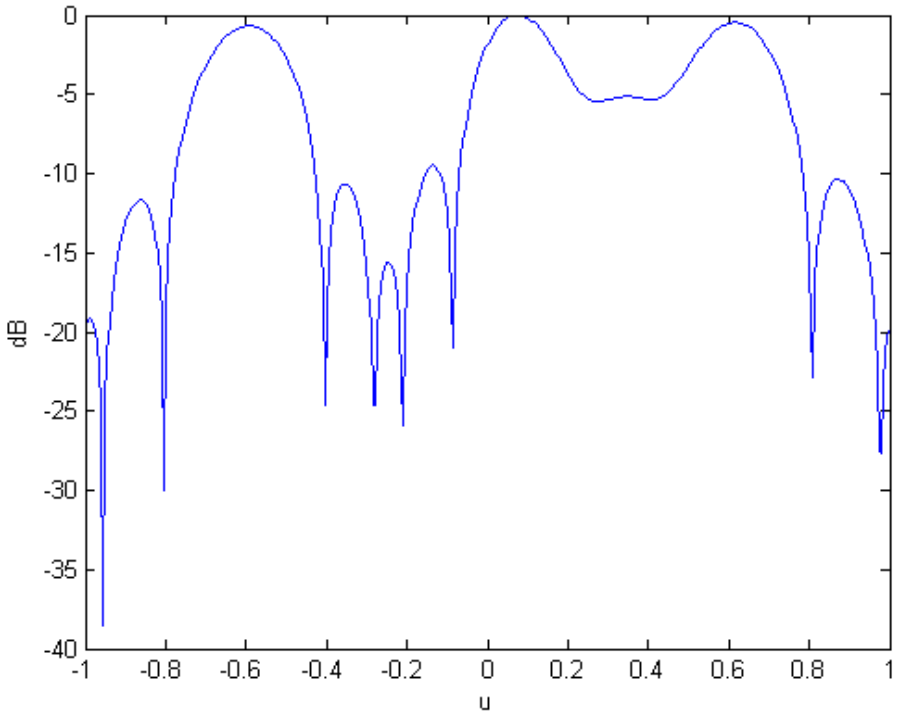

Figure 5.16: Retransmit Imaging with Three Targets at $u = [-.6, .1, .6]$

K.

This can potentially be a large number of crossterms. However, recall from Section 5.3.2 that as the targets become further apart, the strength of the crossterm decreases, so not every crossterm will appear above sidelobe levels. For example, a 5 element uniformly spaced array with three equal power targets at $u = [-.6, .1, .6]$ produces the image in Figure 5.16. Note that the only noticeable crossterm present is at $u = \frac{.1+.6}{2} = .35$.

5.7 Multiple Retransmissions

More than one retransmission can be used. For each retransmission, the received signal at each element is used as the weight for the next transmission. Multiple retransmissions would create an even larger coarray for a single target. The initial transmit array is denoted by $\{x_{Tn}, n = 1, 2, ..., N\}$. The i^{th} retransmit array is denoted by $\{x_{p(i)}, p(i) = 1, 2, ..., P(i)\}$ and the final receive array is $\{x_{Rm}, m = 1, 2, ..., M\}$

For L retransmit arrays, the image is

$$\begin{aligned} I(u) = &\sum_{n=1}^{N}\sum_{p(1)=1}^{P(1)}\sum_{p(2)=1}^{P(2)}...\sum_{p(L)=1}^{P(L)}\sum_{k(0)=1}^{K}\sum_{k(1)=1}^{K}...\sum_{k(L)=1}^{K}\sum_{m=1}^{M} S_{k(0)}S_{k(1)}...S_{k(L-1)}S_{k(L)}... \\ &\times e^{-jk_0(u-u_{k(0)})(x_{Tn}+x_{p(1)})}e^{-jk_0(u-u_{k(1)})(x_{p(1)}+x_{p(2)})}e^{-jk_0(u-u_{k(2)})(x_{p(2)}+x_{p(3)})}... \\ &\times ...e^{-jk_0(u-u_{k(L-1)})(x_{p(L-1)}+x_{p(L)})}e^{-jk_0(u-u_{k(L)})(x_{p(L)}+x_{Rm})} \end{aligned} \tag{5.39}$$

The polynomial analogy is now given by

$$\sum_{k(0)=1}^{K}\sum_{k(1)=1}^{K}...\sum_{k(L)=1}^{K} v_{k(0)}v_{k(1)}...v_{k(L)} = (v_1 + v_2 + ... + v_K)^{L+1} \tag{5.40}$$

As an example, for two targets and two retransmissions, polynomial multiplication is

$$(v_1 + v_2)^3 = v_1^3 + v_2^3 + 3v_1^2v_2 + 3v_1v_2^2. \tag{5.41}$$

From this, we would expect two crossterms to appear. This is supported by simulation in Figure 5.17. For a 5-element uniformly spaced array, performing two retransmission with two targets located at $u = \pm.33$, there are clearly two crossterms located at $u = \pm.0762$.

In general, for K targets and L retransmissions, by the multi-nomial theorem,

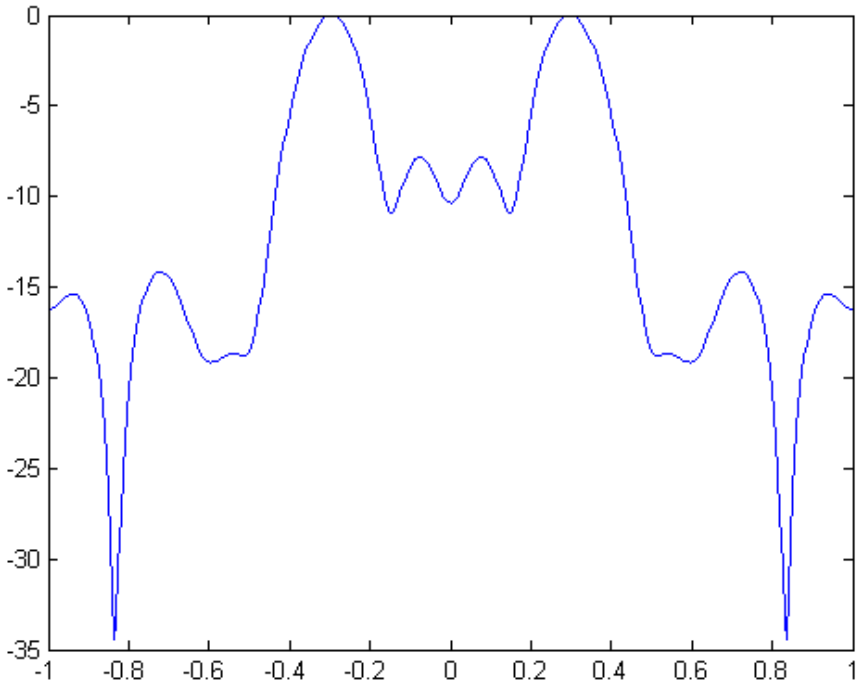

Figure 5.17: Two Retransmissions and Two Targets

there are K pure terms and $\frac{(K+L)!}{(K-1)!(L+1)!} - K$ crossterms. The number of crossterms now grows quickly in both K and L.

5.8 Conclusion

Retransmission was examined in this chapter with the hope for increasing resolution. In terms of the point spread function, the mainbeam is narrower than in standard transmit/receive imaging with the same array. The coarray length appears to approximately double. However, for retransmit imaging this does not translate to higher resolution when two targets are present. This is because retransmission is a nonlinear operation and the coarray analysis does not apply. When there are multiple targets present, the image is not the superposition of shifted point spread functions - crossterms can appear between actual target locations.

It was shown for two targets that as targets become closer together, in the image, the power of the crossterm between them becomes larger and can overpower the actual target location estimates. This thwarts any hope for resolution gain. As the targets become further apart, the crossterm power decreases.

A rough beamwidth analysis was performed on uniformly spaced array for both retransmit and standard transmit/receive imaging showing that, with the crossterm present, standard transmit/receive imaging provides better resolution.

It was demonstrated for some aperiodic arrays that retransmission can slightly outperform standard transmit/receive imaging in peak sidelobe power and in the depth of the null between the estimated target locations, provided that the targets were sufficiently separated. It does not appear to perform better in resolution or target location accuracy with aperiodic arrays. Retransmission may help provide a cleaner image, though not better resolution.

Likewise, multiple frequencies can be used to produce multiple images. In retransmission, if the images are summed together over frequency, they may add up out of phase at the crossterm, and thus reduce its power relative to the estimated target locations. Using multiple frequencies extends the coarray in standard transmit/receive imaging, so any reduction is crossterm power acheived is matched by increased resolution in transmit/receive imaging, but as with aperiodic array, retransmission may only help provide a slightly cleaner image in terms of sidelobe height and null depth between targets for sufficiently separated targets.

When more than two targets are present, additional crossterms arise between all possible target locations. For K targets, it was shown that $\frac{K^2-K}{2}$ crossterms are present, however, since the power of the crossterm decreases as target become further apart, for many targets spread over the scene, not all of them may be visable above sidelobe levels.

For multiple retransmissions, the number of crossterms present depends on the number of targets and the number of retransmissions used. For K targets and L retransmissions, it was shown that $\frac{(K+L)!}{(K-1)!(L+1)!} - K$ crossterms are present. For many targets and many retransmissions, this number could be quite large.

Overall, retransmission may not provide the resolution gain as hoped, but it may be a viable way to obtain clean-up of some image on an existing transmit/receive system.

Chapter 6

Conclusion

Using multiple frequencies in imaging yields additional information. In this dissertation, we researched ways to use this extra information to allow for better resolution capabilities. We considered both passive and active high-resolution techniques. By using multiple frequencies with existing techniques, we can resolve more point sources than the existing techniques alone permit. We also considered using multiple frequencies in a retransmission scheme to increase resolution for beamforming methods.

In Chapter 2, we showed that by using multiple frequencies, the effect of a larger, virtual array can be synthesized for passive imaging with line arrays. The effect of a larger, virtual array allowed for more points sources to be resolved using existing high-resolution techniques compared to using the existing techniques in their original narrowband form. It was shown that when the sources had proportional power spectra, our approach worked well. However, for sources with non-proportional power spectra, the source location estimation was skewed. Some methods were suggested to mitigate the effect of non-proportional sources in the context of a small example. One such method using array interpolation stood out as a possibility to extend this method to larger problems where sources with non-proportional spectra are present.

Chapter 3 presented a frequency-smoothing method similar to spatial-smoothing or pattern diversity to allow for coherent targets to be resolved with line arrays using Multiple Signal Classification [9, 10]. It was previously shown that using virtual arrays with active imaging, additional targets could be resolved at the expense of the ability to resolve coherent targets [13]. The key contribution in this chapter is that we showed by averaging the virtual correlation matrices over frequency, these targets could be coherent and still be successfully resolved.

The work done in the first two chapters was extended to planar arrays in Chapter 4. For active imaging, the extension was relatively straightforward. However, for passive imaging, it was not always possible to synthesize the effect of any virtual array with any physical array. A class of arrays that works for passive imaging was suggested, but shown to not perform as well as existing narrowband virtual array techniques.

Chapter 5 focused on increasing the length of the coarray to improve resolution in beamforming techniques by using a retransmission scheme. Previous work showed that when retransmission was used, artifactual peaks, called crossterms, arise in the image [26]. These crossterms counter any resolution gain when more than one target is present. We investigated this work further. A few techniques were employed in order to reduce or eliminate the crossterms, including using multiple frequencies, but it was shown that these provide very little, if any, gain in performance over standard transmit/receive imaging.

6.1 Possibilities for Future Research

In Chapter 2, we suggested ways to help combat the effect of non-proportional spectra. One of the more promising ways, which should be extendable to larger arrays and

more sources, is using array interpolation [19] to average the narrowband correlation matrices before forming the virtual correlation matrix. This averaging, in theory, causes each of the averaged narrowband correlation matrices to have the same source correlation matrix and thus is equivalent to having proportional spectra. This same averaging process could potentially allow for coherent sources to be resolved. This approach needs to be fully investigated, because it would be ideal for the multi-frequency high resolution techniques to be able to be applied to all types of sources.

The work done in Chapter 3 applies only to targets clustered together in a sufficiently small sector. If targets of comparable reflection power lie outside of the sector, this causes location estimation errors. We suggested an alternative way of finding the array interpolation matrices using a beamspace method that nulls out of sector targets, but it was not examined in detail. Similar techniques exist in the literature [47], and further research should be performed to see if similar beamspace techniques could work for our technique.

The main extension that should be examined for the work done in Chapter 4 is using a search-free technique, such as root-MUSIC, since two-dimensional MUSIC is computationally intensive. Also, for passive imaging, additional array and virtual array geometries which work could possibly be found that provide an advantage over the existing narrowband virtual array techniques for passive planar arrays.

In addition, it would be an interesting problem to try to find the minimum redundancy arrays when using multiple frequencies [28]. In theory, using multiple frequencies generates additional coarray points, so potentially, even more sparse arrays can be found when multiple frequencies are used [17]. This may also be an interesting exercise for retransmit imaging, though its effort may not have true practical value since crossterms arise.

Bibliography

[1] P. Darwood, P.N. Fletcher, G.S. Hilton, "Pattern synthesis in small phased arrays using adaptive array theory," *Electronics Letters*, vol. 33, pp. 254 – 255, Feb. 1997.

[2] J. Capon, "Multiple emitter location and signal parameter estimation," *IEEE Transactions on Antennas and Propagation*, vol. AP-34, Mar. 1986.

[3] ——, "High resolution frequency-wavenumber spectrum analysis," *Proc. IEEE*, vol. 57, Aug. 1969.

[4] V. F. Pisarenko, "The retrieval of harmonics from a covariance function," *Geophys. J. Royal Astron. SOC.*, vol. 33, pp. 374–366, 1973.

[5] S.M. Kay, S.L. Marple, Jr., "Spectrum analysis: A modern perspective," *Proceedings of the IEEE*, vol. 69, pp. 1380 – 1419, Nov. 1981.

[6] M. Gunsay, B.D. Jeffs, "A subspace decomposition method for point source localization in blurred images," *1994 IEEE International Conference on Acoustics, Speech, and Signal Processing*, vol. 5, pp. 469–472, 1994.

[7] D. Johnson, S. DeGraaf, "Improving the resolution of bearing in passive sonar arrays by eigenvalue analysis," *IEEE Transactions on Acoustics, Speech and Signal Processing*, vol. 30, pp. 638 – 647, Aug. 1982.

[8] D.V. Sidorovich, A.B. Gershman, J.F. Bohme, "Processing of experimental seismic army data using 2-D wideband interpolated root-MUSIC," *Proceedings of the 1998 IEEE International Conference on Acoustics, Speech and Signal Processing*, vol. 4, pp. 1985 – 1988, 1998.

[9] T.J. Shan, M. Wax, T. Kailath, "On spatial smoothing for direction-of-arrival estimation of coherent signals," *IEEE Transactions on Acoustics, Speech, and Signal Processing*, vol. 33, pp. 806–811, 1985.

[10] Y. Sun, S. Roy, S.A. Kassam, F. Haber, "Coherent source location using a pattern diversity technique," *Journal of the Acoustical Society of America*, vol. 92, pp. 3213–3220, Dec. 1992.

[11] K.W. Lo, "Adaptive array processing for wide-band active sonars," *IEEE Journal of Oceanic Engineering*, vol. 29, pp. 837 – 846, July 2004.

[12] Yeo-Sun Yoon, M.G. Amin, "High-resolution through-the-wall radar imaging using beamspace MUSIC," *IEEE Trans. Antennas Propag.*, vol. 56, pp. 1763 – 1774, 2008.

[13] R. T. Hoctor and S. A. Kassam, "High resolution coherent source location using transmit/receive arrays," *IEEE Trans. Image Proc.*, vol. 1, pp. 88–100, Jan. 1992.

[14] ——, "The unifying role of the coarray in aperture synthesis for coherent and incoherent imaging," *Proceedings IEEE*, vol. 78, pp. 735–752, Apr. 1990.

[15] S.U. Pillai et al, "A new approach to array geometry for improved spatial spectrum estimation," *Proceedings of the IEEE*, vol. 73, pp. 1522 – 1524, Oct. 1985.

[16] Wing-Kin Ma, Tsung-Han Hsieh, Chong-Yung Chi, "DOA estimation of quasi-stationary signals with less sensors than sources and unknown spatial noise covariance: A Khatri-Rao subspace approach," *IEEE Transactions on Signal Processing*, vol. 58, pp. 2168 – 2180, Apr. 2010.

[17] F. Ahmad and S. A. Kassam, "Coarray analysis of the wide-band point spread function for active array imaging," *Signal Process.*, vol. 81, pp. 99–115, Jan. 2001.

[18] H. Wang, M. Kaveh, "Coherent signal-subspace processing for the detection and estimation of angles of arrival of multiple wide-band sources," *IEEE Transactions on Acoustics, Speech and Signal Processing*, vol. 33, pp. 823 – 831, 1985.

[19] B. Friedlander and A.J. Weiss, "Performance analysis of wideband direction finding using interpolated arrays," *Proc. Acoustics, Speech and Signal Process.*, pp. 457–460, Mar. 1992.

[20] H. W. E. Doron, M.A. Doron, "Coherent wideband array processing for arbitrary array geometry," *IEEE Trans. SP*, vol. 41, pp. 414–417, Jan. 1993.

[21] Y.I. Abramovich et al., "Positive-definite Toeplitz completion in DOA estimation for nonuniform linear antenna arrays. I. Fully augmentable arrays," *IEEE Transactions on Signal Processing*, vol. 46, pp. 2458–2471, Sept. 1998.

[22] ——, "Positive-definite Toeplitz completion in DOA estimation for nonuniform linear antenna arrays. II. Partially augmentable arrays," *IEEE Transactions on Signal Processing*, vol. 47, pp. 1502 – 1521, June 1999.

[23] J. Odendaal , E. Barnard and C. Pistorius, "Two-dimensional superresolution radar imaging using the MUSIC algorithm," *IEEE Trans. Antennas Propag.*, vol. 42, pp. 1386 – 1391, 1994.

[24] A. Barabell, "Improving the resolution performance of eigenstructure-based direction-finding algorithms," *IEEE International Conference on Acoustics, Speech, and Signal Processing, ICASSP '83.*, vol. 8, pp. 336 – 339, 1983.

[25] F. Belloni, A. Richter, V. Koivunen, "DoA estimation via manifold separation for arbitrary array structures," *IEEE Transactions on Signal Processing*, vol. 55, pp. 4800 – 4810, Oct. 2007.

[26] F. Ahmad, *Analysis and Design of Wideband Imaging Arrays Based on the Coarray.* University of Pennsylvania: PhD Thesis, 1997.

[27] J. M. F. Moura, Y. Jin, "Time reversal imaging by adaptive interference canceling," *IEEE Trans. Signal Process.*, pp. 233–247, Jan. 2008.

[28] A. Moffet, "Minimum-redundancy linear arrays," *IEEE Transactions on Antennas and Propagation*, vol. 16, pp. 172–175, Mar. 1968.

[29] R.T. Hoctor, S.A Kassam, "Array redundancy for active line arrays," *IEEE Transactions on Image Processing*, vol. 5, pp. 1179 – 1183, July 1996.

[30] Y. I. Abramovich, N. K. Spencer, A. Y. Gorokhov, "Positive-definite Toeplitz completion in DOA estimation for partially-augmentable nonuniform linear antenna arrays," *Proc. 8th IEEE Statistical Signal Array Process. Workshop*, pp. 550–553, June 1996.

[31] S.U. Pillai and B.H. Kwon, "Forward backward spatial smoothing techniques for coherent signal identification," *IEEE Transactions on Acoustics, Speech, and Signal Processing*, vol. 37, pp. 8–15, Jan. 1989.

[32] A.B. Gershman, M. Rubsamen, M. Pesavento, "One- and two-dimensional direction-of-arrival estimation: An overview of search-free techniques," *Signal Process.*, vol. 90, pp. 1338–1349, May 2010.

[33] H.F. Gu, P. Wei, H.M. Tai, "2-D direction-of-arrival estimation of coherent signals using cross-correlation matrix," *Signal Process.*, vol. 88, pp. 75–85, Jan. 2008.

[34] J.L. Moulton, S.A. Kassam, "Resolving more sources with multi-frequency coarrays in high-resolution direction-of-arrival estimation," *43rd Annual Conference on Information Sciences and Systems, 2009*, pp. 772 – 777, Mar. 2009.

[35] ——, "High-resolution spectrum estimation for non-coherent source location using the multi-frequency virtual correlation matrix," *IEEE Pacific Rim Conference on Communications, Computers and Signal Processing, 2009*, vol. 88, pp. 843 – 848, Aug. 2009.

[36] ——, "High-resolution coherent reflector location with multi-frequency active virtual arrays," *44th Annual Conference on Information Sciences and Systems, 2010*, vol. 88, pp. 1–5, Aug. 2010.

[37] J. Moulton, S. Kassam, F. Ahmad, M. Amin, K. Yemelyanov, "Target and change detection in synthetic aperture radar sensing of urban structures," *IEEE Radar Conference, 2008*, pp. 1 – 6, Aug. 2008.

[38] J.L. Moulton, S.A. Kassam, "Multi-frequency MUSIC for passive imaging with line arrays," *in preparation.*

[39] ——, "Frequency smoothing with virtual arrays for active imaging," *in preparation.*

[40] B. D. Steinberg, *Principles of Aperture and Array System Design*. New York: John Wiley and Sons, 1976.

[41] R. T. Hoctor, *The Coarray Approach to Aperture Synthesis for Active and Passive Imaging*. University of Pennsylvania: PhD Thesis, 1990.

[42] S. M. Kay, *Modern Spectral Estimation: Theory and Application*. Englewood Cliffs, NJ: Prentice-Hall, 1988.

[43] E.M. Stein and Rami Shakarchi, *Complex Analysis*. Princeton, NJ: Princeton University Press, 2003.

[44] S. Boyd and L. Vandenberghe, *Convex Optimization*. Cambridge, UK: Cambridge University Press, 2004.

[45] K. B. Petersen and M. S. Pedersen, *The Matrix Cookbook*. http://matrixcookbook.com, Nov. 2008.

[46] B. Friedlander, "Direction finding using an interpolated array," *Proc. ICASSP, Albuquerque, NM*, pp. 2951–2954, Apr. 1990.

[47] A. Hassanien, S.A. Elkader, A.B. Gershman, K.M. Wong, "Beamspace preprocessing with an improved robustness against out-of-sector sources using second-order cone programming," *Sensor Array and Multichannel Signal Processing Workshop Proceedings*, pp. 347–351, 2004.